

**Characterization of DnaA mutant proteins from**  
*Bacillus subtilis*

**Novel insights into the initiation of replication**

INAUGURALDISSERTATION

zur Erlangung der Doktorwürde  
der Fakultät für Biologie an der  
Albert-Ludwigs Universität  
Freiburg im Breisgau



vorgelegt von

Marc Eisemann

geboren in Wriezen

Freiburg im Breisgau

2012

|                         |                           |
|-------------------------|---------------------------|
| Dekan:                  | Prof. Dr. Gunther Neuhaus |
| Promotionsvorsitzender: | Prof. Dr. Samuel Rossel   |
| Betreuer:               | Prof. Dr. Peter Graumann  |
| Kogutachter:            | PD Dr. Ivan Berg          |
| Drittprüfer:            | PD DR. Gerald Radziwill   |
| Tag der Prüfung:        | 11.05.2012                |

# Erklärung

1. Ich erkläre hiermit, dass ich die vorliegende Arbeit ohne zulässige Hilfe Dritter und ohne Benutzung anderer als der angegebenen Hilfsmittel angefertigt habe. Die aus anderen Quellen direkt oder indirekt übernommenen Daten und Konzepte sind unter Angabe der Quellen gekennzeichnet. Insbesondere habe ich hierfür nicht die entgeltliche Hilfe von Vermittlungs- beziehungsweise Beratungsdiensten (Promotionsberater oder anderer Personen) in Anspruch genommen. Niemand hat von mir unmittelbar oder mittelbar geldwerte Leistungen für Arbeiten erhalten, die im Zusammenhang mit dem Inhalt der vorgelegten Dissertation stehen.
2. Die Arbeit wurde bisher weder im In- noch im Ausland in gleicher oder ähnlicher Form einer anderen Prüfungsbehörde vorgelegt.
3. Die Bestimmung der Promotionsordnung der Fakultät für Biologie der Universität Freiburg ist mir bekannt, insbesondere weiß ich, dass ich vor Vollzug der Promotion zur Führung des Dokortitels nicht berechtigt bin.

(Marc Eisemann)

Für meine Eltern Frank und Sabine

“life is what happens to you while you´re busy making other plans”

John Lennon

## Zusammenfassung

Das Initiatorprotein der chromosomalen Replikation, DnaA, und dessen Regulation wurden in *Escherichia coli*, einem Modellorganismus Gram negativer Bakterien, intensiv untersucht. Daraus ergaben sich eine Reihe hoch konservierter funktionaler Charakteristika, wie die Fähigkeit ATP zu binden und zu hydrolysieren, zu oligomerisieren und spezifisch an DNA zu binden [1, 6-7]. Dennoch scheint der eigentliche Prozess und die Regulation der Initiation in Gram positiven Bakterien unterschiedlich abzulaufen [1, 4]. Die spezifischen Eigenschaften von DnaA und deren Implikation auf die Initiation von *Bacillus subtilis* wurden mithilfe von DnaA-Mutanten untersucht, welche durch Substitutionen bestimmter hochkonservierter Aminosäuren generiert wurden. Die Expression von DnaA in *B. subtilis* ist durch einen negativen Feedback-Loop autoreguliert, indem hohe DnaA-Mengen die Transkription von *dnaA* reprimieren und geringe DnaA-Mengen die Transkription induzieren [8-9]. Dieser Kontrollmechanismus scheint nicht ATP-abhängig zu sein, da Mutanten mit einem ATP-Bindedefekt (YFP-DnaAA163V, YFP-DnaAD214N) die *dnaA*-Transkription *in vivo* noch immer effizient reprimieren können. Die Aufreinigung und biochemische Charakterisierung rekombinanter (His)<sub>6</sub>-getaggtter Initiatorproteine machte deutlich, dass DnaA-Moleküle mit ihren jeweiligen Domänen I interagieren, um native Dimere oder Trimere zu konstituieren. Dies konnte für (His)<sub>6</sub>-wtDnaA und alle Mutanten, mit Ausnahme von (His)<sub>6</sub>-DnaAA163V und (His)<sub>6</sub>-DnaAW8A gezeigt werden, welche imperativisch konstitutive Multimere beziehungsweise Monomere bilden. Anzunehmen ist, dass der größte Teil aller DnaA-Protomere durch die extrem hohe Affinität zu ATP Kofaktor-gebunden vorliegt [1, 11-12]. Der Replikationsursprung (*oriC*) von *B. subtilis* enthält zahlreiche Hochaffinitätsboxen, die eine Interaktion mit ATP-DnaA erlauben, was wiederum zur Konstituierung des bakteriellen ORC (origin recognition complex, Replikationsursprungs-Erkennungskomplex) führt, gefolgt von einer Multimerisierungs-abhängigen Bildung des pre-RC (prereplication complex, Prä-Replikationskomplex) [1, 8, 11-15]. Es konnte klar gezeigt werden, dass (His)<sub>6</sub>-DnaAW8A, trotz seiner uneingeschränkten ATP-Binde- und ATP-Hydrolyse-Aktivität, nicht in der Lage war, höhermolekulare DNA-bindende Komplexe zu bilden. Demnach scheint es, dass eine Domäne I vermittelte Dimerisierung zweier *B. subtilis* DnaA-Protomere einer koordinierten AAA+ Domäne III-Interaktion notwendig zu Grunde liegt, die wiederum zu funktionalen initiationskompetenten Multimeren führt. Darüber hinaus konnte gezeigt werden, dass die defekte Kofaktor-abhängige differentielle *oriC*-DNA-Bindeaktivität von (His)<sub>6</sub>-DnaAE183Q hauptsächlich auf dessen stark reduzierte ATPase-Aktivität zurückzuführen war. Dies führte zu der Annahme, dass im Gegensatz zu *E. coli*, bei dem die induzierte ATP-Hydrolyse die Dissoziation eines Multimers zur Folge hat, die kooperative Multimerisierung, die notwendig ist für eine effiziente DNA-Interaktion, individuelle ATP-Hydrolyse-Reaktionen der DnaA-Protomere erfordert. Gestützt

wird diese These erstens dadurch, dass (His)<sub>6</sub>-DnaAE183Q keine stabilen höhermolekularen Multimere konstituiert und zweitens, dass PY79 *in vivo* scheinbar keine höheren Mengen an YFP-DnaAE183Q toleriert. Die Analyse der ektopischen Expression von funktionalem YFP-DnaA und DnaA-Mutanten in lebenden *B. subtilis*-Zellen mithilfe der Fluoreszenzmikroskopie zeigte darüber hinaus, dass die Initiationsfrequenz der Replikation und die eigentliche Zelllänge charakteristisch betroffen waren. Auffallend war, dass beide ATP-bindedefizienten DnaA-Stämme, *B. subtilis* PY79-YFP-DnaAA163V/D214N eine erhöhte Initiationsfrequenz aufwiesen. PY79-YFP-DnaAE183Q, das eine DnaA-Variante mit stark reduzierter ATP-Hydrolyse-Aktivität enthält, zeigte ebenfalls eine geringfügig verstärkte Initiationsfrequenz, die jedoch auf den erhöhten DNA-Gehalt in anormal verlängerten Zellen zurückzuführen war. *B. subtilis* PY79-YFP-DnaAR260A war stark beeinträchtigt in der zeitlichen Zellzyklus-Regulation, indem es verfrüht die Replikation bzw. die Zellteilung initiierte. Sowohl der Stamm mit einer konditionalen dimerisierungsdefizienten DnaA-Mutante, *B. subtilis* PY79-YFP-DnaAW8A, als auch derjenige mit einer DNA-bindedefizienten DnaA-Mutante, PY79-YFP-DnaAR387C, konnten erwartungsgemäß keine distinkten YFP-DnaA Foci assemblieren.

## Summary

The initiator protein of chromosomal replication, DnaA, and its regulation have intensively been studied in *Escherichia coli*, a model organism of Gram negative bacteria. A variety of functional capacities, such as ATP-binding and hydrolysis, oligomerization and specific DNA-binding, have been discovered and appear to be highly conserved in bacteria [1, 6-7]. Nevertheless, the process of initiation and its regulation seem to work differently in Gram positive bacteria [1, 4]. Specific DnaA activities and their implication in the initiation of *Bacillus subtilis* were investigated by generating several DnaA mutants, each carrying single substitutions of highly conserved amino acids. The expression of DnaA in *B. subtilis* is autoregulated by a negative feedback loop, i.e. high DnaA levels repress and low levels derepress *dnaA* transcription [8-9]. This control mechanism does not seem to require ATP-bound DnaA, since both ATP-binding defective mutant proteins (YFP-DnaAA163V, YFP-DnaAD214N) could still efficiently repress *dnaA* transcription *in vivo*. The purification and biochemical characterization of recombinant (His)<sub>6</sub>-tagged initiator proteins revealed that DnaA molecules interact via their respective domain I to form native dimeric or trimeric constitutions, which has been shown for (His)<sub>6</sub>-wtDnaA and all other mutant forms, except (His)<sub>6</sub>-DnaAA163V and (His)<sub>6</sub>-DnaAW8A that imperatively establish constitutive multimers or monomers, respectively. Presumably, most of the DnaA protomers are present in a cofactor-bound state since they have an extremely high affinity to ATP [1, 11-12]. *B. subtilis oriC* contains several high-affinity boxes allowing ATP-DnaA interaction, which leads to the constitution of the bacterial ORC (origin recognition complex) prior to self-multimerization dependent pre-RC (prereplication complex) formation [1, 8, 11-15]. It was clearly demonstrated that (His)<sub>6</sub>-DnaAW8A, despite its unaffected ATP-binding and ATPase activity, was unable to form DNA-binding proficient high-molecular weight complexes. Thus, it seems that domain I mediated dimerization of two *B. subtilis* DnaA protomers is required for coordinated AAA+ domain III interactions leading to functionally initiation competent multimers. Furthermore, it was shown that the abrogated cofactor-dependent differential *oriC*-DNA-binding activity of (His)<sub>6</sub>-DnaAE183Q could mainly be attributed to its strongly reduced ATPase activity. This led to the hypothesis that unlike in *E. coli* where ATP-hydrolysis is induced to disassemble an established multimer, cooperative multimerization, essential for efficient DNA-binding, requires individual ATP-hydrolysis events of the DnaA protomers. In support of this assumption, (His)<sub>6</sub>-DnaAE183Q does not constitute stable higher-order multimers and PY79 does not seem to tolerate high amounts of YFP-DnaAE183Q *in vivo*. The analysis of the effect of expressing functional YFP-DnaA and mutant forms from an ectopic locus on the chromosome in live *B. subtilis* cells using fluorescence microscopy further showed that the consequences on cell cycle specific parameters, like the frequency of initiation of replication and cell length were characteristically affected. Strikingly,

both ATP-binding deficient DnaA-strains, *B. subtilis* PY79-YFP-DnaAA163V/D214N displayed an increased replication initiation frequency. PY79-YFP-DnaAE183Q, which bears a DnaA variant with a strongly reduced ATP-hydrolysis activity, also showed a slightly enhanced initiation frequency, but which could be attributed to a greater DNA-content in abnormally elongated cells. *B. subtilis* PY79-YFP-DnaAR260A has an affected cell-cycle timing and prematurely initiates replication or rather induces cell division. Dimerization defective DnaA-strain *B. subtilis* PY79-YFP-DnaAW8A and DNA-binding deficient DnaA-strain PY79-YFP-DnaAR387C, as expected, did not assemble distinct YFP-DnaA foci.

# Table of contents

|  |    |
|--|----|
| 1. Introduction  | 1  |
| 1.1. Initiation of bacterial DNA replication                                 | 2  |
| 1.2. Initiation control mechanisms   | 3  |
| 1.3. Organization of the origin of replication ( <i>oriC</i> )               | 7  |
| 1.4. The molecular structure of DnaA   | 9  |
| 1.5. Specific <i>E. coli</i> DnaA allele <i>dnaAcos</i>                      | 12 |
| 1.6. Cell cycle dependent localization of DnaA in <i>B. subtilis</i>         | 13 |
| 1.7. Aims of research  | 15 |
| 2. Materials and Methods   | 16 |
| 2.1. Chemicals and Kits for DNA-purification purposes                        | 17 |
| 2.2. Bacterial strains   | 17 |
| 2.2.1. <i>Escherichia coli</i>   | 17 |
| 2.2.2. <i>Bacillus subtilis</i>  | 17 |
| 2.3. Growth media and complements  | 18 |
| 2.4. Preparation and transformation of electrocompetent <i>E. coli</i> cells | 19 |
| 2.5. Preparation and transformation of competent <i>B. subtilis</i> cells    | 19 |
| 2.6. DNA extraction and quantification                                       | 20 |
| 2.7. Principles of vector construction                                       | 20 |
| 2.7.1. Polymerase chain reaction (PCR)                                       | 21 |
| 2.7.2. Digestion of DNA-molecules with restriction endonucleases             | 23 |
| 2.7.3. Ligation of linearized DNA-molecules                                  | 23 |
| 2.7.4. Agarose gel electrophoresis   | 23 |
| 2.8. Protein analysis  | 23 |
| 2.8.1. Protein purification  | 23 |
| 2.8.2. SDS-polyacrylamide gel electrophoresis (SDS-PAGE)                     | 25 |
| 2.8.3. Immunoblotting  | 25 |
| 2.8.4. Protein extracts from <i>B. subtilis</i>                              | 26 |
| 2.9. Determination of ATP-binding and ATPase activities                      | 26 |
| 2.10. Electrophoretic mobility shift assays (EMSA)                           | 27 |
| 2.11. Surface plasmon resonance experiments                                  | 28 |
| 2.12. DSS-crosslink assays   | 28 |

|  |    |
|--|----|
| 2.13. Fluorescence microscopy  | 29 |
| 2.14. Software   | 29 |
| 3. Results   | 31 |
| 3.1. Sequence Alignment of <i>E. coli</i> DnaA and <i>B. subtilis</i> DnaA   | 32 |
| 3.2. Purification of recombinant (His) <sub>6</sub> -wtDnaA/(His) <sub>6</sub> -mutDnaA  | 33 |
| 3.3. ATP-binding activity of recombinant (His) <sub>6</sub> -wtDnaA/(His) <sub>6</sub> -mutDnaA determined by filter binding assays using [ $\alpha$ - <sup>32</sup> P]-ATP                    | 34 |
| 3.3.1. (His) <sub>6</sub> -wtDnaA exhibits a very strong temperature independent ATP-binding activity  | 34 |
| 3.3.2. (His) <sub>6</sub> -DnaAA163V and (His) <sub>6</sub> -DnaAD214N do not or poorly bind ATP, respectively   | 34 |
| 3.3.3. (His) <sub>6</sub> -DnaAE183Q and (His) <sub>6</sub> -DnaAR260A show an approximately 2-fold reduced ATP-binding capacity   | 35 |
| 3.3.4. (His) <sub>6</sub> -DnaAW8A and (His) <sub>6</sub> -DnaAR387C are not significantly affected in their ATP-binding activity  | 36 |
| 3.4. ATPase activity of recombinant (His) <sub>6</sub> -wtDnaA/(His) <sub>6</sub> -mutDnaA determined by filter binding assays using [ $\gamma$ - <sup>32</sup> P]-ATP                         | 36 |
| 3.4.1. (His) <sub>6</sub> -wtDnaA exhibits a weak temperature dependent ATPase activity  | 36 |
| 3.4.2. (His) <sub>6</sub> -DnaAA163V and (His) <sub>6</sub> -DnaAD214N do not hydrolyze ATP  | 37 |
| 3.4.3. (His) <sub>6</sub> -DnaAE183Q ATPase activity is strongly reduced, whereas (His) <sub>6</sub> -DnaAR260A shows a 2-fold reduced ATPase activity   | 38 |
| 3.4.4. (His) <sub>6</sub> -DnaAW8A and (His) <sub>6</sub> -DnaAR387C are not significantly affected in their respective ATPase activities  | 39 |
| 3.5. DNA-binding activity of recombinant (His) <sub>6</sub> -wtDnaA/(His) <sub>6</sub> -mutDnaA determined by electrophoretic mobility shift assays (EMSA) and surface plasmon resonance (SPR) | 40 |
| 3.5.1. (His) <sub>6</sub> -wtDnaA exhibits a cofactor-dependent sequence specific DNA-binding activity   | 40 |
| 3.5.2. (His) <sub>6</sub> -DnaAR387C displays a strongly reduced DNA-binding activity  | 42 |
| 3.5.3. (His) <sub>6</sub> -DnaAA163V exhibits a stable cofactor-independent DNA-binding activity   | 43 |
| 3.5.4. (His) <sub>6</sub> -DnaAE183Q has an abrogated cofactor-dependent differential DNA-binding activity   | 44 |
| 3.5.5. (His) <sub>6</sub> -DnaAD214N displays a strongly reduced cofactor-dependent differential DNA-binding activity  | 46 |
| 3.5.6. (His) <sub>6</sub> -DnaAR260A exhibits a cofactor-dependent DNA-binding activity  | 47 |

|  |    |
|--|----|
| 3.5.7. (His) <sub>6</sub> -DnaAW8A exhibits a cofactor-independent strongly reduced capacity in the formation of DNA-binding competent high-molecular weight complexes | 48 |
| 3.6. Multimer formation capacity of recombinant (His) <sub>6</sub> -wtDnaA/(His) <sub>6</sub> -mutDnaA determined by disuccinimidyl suberate crosslinking assays       | 50 |
| 3.6.1. (His) <sub>6</sub> -wtDnaA exhibits a cofactor-dependent self-oligomerization capacity  | 50 |
| 3.6.2. (His) <sub>6</sub> -DnaAA163V forms stable HMWCs in the absence of ATP  | 51 |
| 3.6.3. (His) <sub>6</sub> -DnaAE183Q does not constitute stable higher-order multimers   | 52 |
| 3.6.4. (His) <sub>6</sub> -DnaAD214N has a reduced capacity in constituting stable higher-order multimers  | 53 |
| 3.6.5. Self-multimerization capacity of (His) <sub>6</sub> -DnaAR260A is not affected  | 54 |
| 3.6.6. (His) <sub>6</sub> -DnaAW8A displays a conditional dimerization deficiency in the absence of ATP  | 54 |
| 3.6.7. Self-multimerization capacity of (His) <sub>6</sub> -DnaAR387C is irresponsive to linear <i>oriC</i> -DNA   | 55 |
| 3.7. Growth of <i>B. subtilis</i> PY79 expressing N-terminal YFP-fusions of wtDnaA/mutDnaA from an ectopic site <i>in vivo</i>   | 56 |
| 3.8. Transcriptional regulation of the <i>dnaA-dnaN</i> operon by ectopically expressed N-terminal YFP-fusions of wtDnaA/mutDnaA <i>in vivo</i>                        | 60 |
| 3.8.1. Moderate ectopic expression of YFP-wtDnaA <i>in vivo</i> does not affect the transcriptional regulation of <i>dnaA-dnaN</i>                                     | 60 |
| 3.8.2. Overexpression of YFP-DnaAA163V, YFP-DnaAD214N, YFP-DnaAR260A and YFP-DnaAW8A outcompetes DnaA in regulating <i>dnaA-dnaN</i> transcription <i>in vivo</i>      | 61 |
| 3.8.3. Ectopic expression of YFP-DnaAE183Q does not reach sufficient protein levels to repress <i>dnaA-dnaN</i> transcription <i>in vivo</i>                           | 62 |
| 3.8.4. Overexpression of YFP-DnaAR387C does not interfere with the transcriptional regulation of <i>dnaA-dnaN</i> by DnaA <i>in vivo</i>                               | 62 |
| 3.9. Fluorescence microscopy of <i>B. subtilis</i> PY79 expressing N-terminal YFP-fusions of wtDnaA/mutDnaA from an ectopic site <i>in vivo</i>                        | 63 |
| 3.9.1. <i>B. subtilis</i> PY79- <i>oriC</i> -CFP   | 63 |
| 3.9.2. <i>B. subtilis</i> PY79-YFP-wtDnaA  | 65 |
| 3.9.3. <i>B. subtilis</i> PY79-YFP-DnaAA163V displays a strong overinitiation phenotype <i>in vivo</i>   | 68 |
| 3.9.4. <i>B. subtilis</i> PY79-YFP-DnaAD214N displays an increased replication initiation frequency <i>in vivo</i>   | 71 |
| 3.9.5. <i>B. subtilis</i> PY79-YFP-DnaAR260A prematurely initiates replication <i>in vivo</i>  | 73 |

|  |     |
|--|-----|
| 3.9.6. <i>B. subtilis</i> PY79-YFP-DnaAW8A does not assemble distinct YFP-DnaAW8A foci <i>in vivo</i>                  | 76  |
| 3.9.7. <i>B. subtilis</i> PY79-YFP-DnaAE183Q cells are significantly elongated <i>in vivo</i>                          | 78  |
| 3.9.8. <i>B. subtilis</i> PY79-YFP-DnaAR387C does not assemble distinct YFP-DnaAR387C foci <i>in vivo</i>              | 81  |
| 4. Discussion  | 84  |
| 4.1. Recapitulatory overview   | 85  |
| 4.2. <i>B. subtilis</i> wild type DnaA characteristics   | 86  |
| 4.3. ATP-binding and ATPase deficient DnaAD214N  | 87  |
| 4.4. ATPase deficient DnaAE183Q  | 88  |
| 4.5. Prematurely initiating DnaAR260A  | 90  |
| 4.6. Conditionally dimerization deficient DnaAW8A  | 92  |
| 4.7. DNA-binding deficient DnaAR387C   | 93  |
| 4.8. Specific <i>B. subtilis</i> mutant DnaAA163V (“DnaAcos”)  | 95  |
| 4.9. Functional dissection and mechanistic implications of DnaA in the initiation of replication in <i>B. subtilis</i> | 97  |
| 5. Bibliography  | 99  |
| 6. Acknowledgements  | 105 |

## Abbreviations

|                     |   |
|---------------------|---|
| A                   | absorption  |
| aa                  | amino acid(s)   |
| AAA+                | ATPases associated with diverse cellular activities                             |
| ADP (ATP)           | adenosine diphosphate (adenosine triphosphate)                                  |
| AMP-PCP             | 5'-adenylyl methylenediphosphonate  |
| ATP $\gamma$ S      | adenosine 5'-O-(3-thio)triphosphate   |
| BLAST               | basic local alignment search tool   |
| bp                  | base pair(s)  |
| BSA                 | bovine serum albumin  |
| <i>B. subtilis</i>  | <i>Bacillus subtilis</i>  |
| bzw.                | beziehungsweise   |
| c                   | concentration   |
| CFP (GFP/YFP)       | cyan fluorescent protein (green fluorescent protein/yellow fluorescent protein) |
| cm ( $\mu$ m/mm/nm) | centimeter (micrometer/millimeter/nanometer)                                    |
| CTP                 | cytidine triphosphate   |
| d                   | width   |
| DAPI                | 6', 4-diamidino-2-phenylindole  |
| DARS                | DnaA-reactivating sequence  |
| DBC(s)              | DnaA-box cluster(s)   |
| DBD                 | DNA-binding domain  |
| $^{\circ}$ C        | degree Celsius  |
| DMSO                | dimethyl sulfoxide  |
| DNA                 | deoxyribonucleic acid   |
| dNTP                | deoxyribonucleoside triphosphate  |
| DSS                 | disuccinimidyl suberate   |
| DTT                 | dithiothreitol  |
| DUE                 | DNA-unwinding element   |
| $\epsilon$          | extinction coefficient  |
| <i>E. coli</i>      | <i>Escherichia coli</i>   |

|                        |   |
|------------------------|---|
| EDTA                   | ethylenediaminetetraacetate   |
| EMSA                   | electrophoretic mobility shift assay(s)   |
| et al.                 | et alii   |
| Fig(s).                | figure(s)   |
| FM 4-64                | N-(3-triethylammoniumpropyl)-4-(4-diethylaminophenylhexatrienyl) pyridinium dibromide |
| HEPES                  | 4-(2-hydroxyethyl)-1-piperazineethanesulfonic acid                                    |
| (His) <sub>6</sub>     | hexahistidine   |
| HMWC(s)                | high-molecular weight complex(es)   |
| i.e.                   | id est  |
| IgG                    | immunoglobulin G  |
| IPTG                   | isopropyl β-D-1-thiogalactopyranoside   |
| $K_{app}$              | apparent binding constant   |
| kb                     | kilobase  |
| $K_d$                  | dissociation constant   |
| kDa (MDa)              | kilo Dalton (mega Dalton)   |
| LB                     | Luria Bertani   |
| mem.                   | membrane  |
| mA                     | milliampere   |
| μg (mg/ng)             | microgram (milligram/nanogram)  |
| μM (mM)                | micromolar (millimolar)   |
| μl (ml)                | microliter (milliliter)   |
| min                    | minute  |
| MOPS                   | 3-(N-morpholino) propanesulfonic acid   |
| <i>M. tuberculosis</i> | <i>Mycobacterium tuberculosis</i>   |
| mut                    | mutant  |
| MW                     | molecular weight  |
| NEB                    | New England Biolabs   |
| nt                     | nucleotide(s)   |
| OD <sub>600</sub>      | optical density at 600 nm   |
| <i>oriC</i>            | (chromosomal) origin of replication   |
| ORC                    | origin recognition complex  |

|            |  |
|------------|--|
| PCR        | polymerase chain reaction                                    |
| %          | percent  |
| PhD        | Doctor of Philosophy   |
| pmol       | picomol  |
| pre-RC     | prereplication complex                                       |
| psi        | pound per square inch  |
| ret.vol.   | retention volume   |
| RIDA       | regulatory inactivation of DnaA                              |
| rpm        | rounds per minute  |
| RU         | response/resonance units                                     |
| SDS(-PAGE) | sodium dodecyl sulfate (-polyacrylamide gel electrophoresis) |
| SPR        | surface plasmon resonance                                    |
| subsp.     | subspecies   |
| TEMED      | tetramethylethylenediamine                                   |
| Tris       | tris (hydroxymethyl) aminomethane                            |
| U          | unit(s)  |
| UV         | ultraviolet  |
| V          | volt   |
| v/v        | volume per volume  |
| wt         | wild type  |

# INTRODUCTION

---

# 1. Introduction

The genetic information of each cell encoding for all relevant compounds of the cellular blueprint lies within its genome. Therefore, accurate replication of genomic DNA is a key element for proper reproduction. Each cell cycle, both in prokaryotes and eukaryotes, requires the duplication (and segregation) of the chromosome(s) prior to cell division [1]. Although the regulation of chromosomal replication is very distinct between prokaryotes and eukaryotes, its overall cycle is rather similar and can be subdivided into three consecutive processes: the coordinated constitution of the replisome at the origin of replication upon open complex formation by the initiator protein (initiation), the subsequent phase of elongation comprising bidirectional fork progression in conjunction with simultaneous DNA synthesis and the fusion of the two replication forks at the terminus (termination) [1, 4, 16]. The process of DNA replication is highly regulated in all cells so as to occur only once per cell cycle [1, 4]. Malfunction in replication control leads to asynchronous initiation, aberrant chromosome segregation and defects in cytokinesis [17].

## 1.1. Initiation of bacterial DNA replication

Most of the insight into bacterial replication has been obtained by studies on the  $\gamma$ -proteobacterium *Escherichia coli*, a model organism of Gram negative bacteria. The *E. coli* chromosome contains one origin of replication, referred to as *oriC*, that is organized into several clusters of consensus sequences that promote the coordinated assembly of the replisome [7]. The main characteristics of this region are: 1. an accumulation of DnaA boxes, which are short DNA sequences that allow for specific binding of the initiator protein DnaA with variable affinity and 2. the presence of an AT-rich region, where the local unwinding of the DNA takes place and which represents the site of replication fork formation [6]. DnaA has a very high affinity both for ATP and ADP, but only in the ATP-bound form DnaA is capable of binding to the high- and low-affinity DnaA binding sites of the *oriC* [6]. In *E. coli*, DnaA forms a stable complex (bacterial origin recognition complex, ORC) with the high-affinity binding sites in the *oriC* during most of the cell cycle [18-21]. Replication initiation begins with cooperative binding of additional DnaA-monomers to low-affinity sites (prereplication complex, pre-RC), directed by the ORC [19-20, 22]. DnaA-multimerization is triggered by DnaA initiator-associating protein (DiaA) and integration host factor (IHF) on the DNA, a process that is believed to execute torsional stress on the AT-rich region leading to duplex unwinding [4, 23-24]. The exact molecular mechanism underlying open complex formation remains to be elucidated [2, 4, 7, 25-26]. Subsequently, ATP-DnaA binds to single-stranded DNA (that is further stabilized by single-strand binding proteins, SSBs) and recruits two DnaB-DnaC

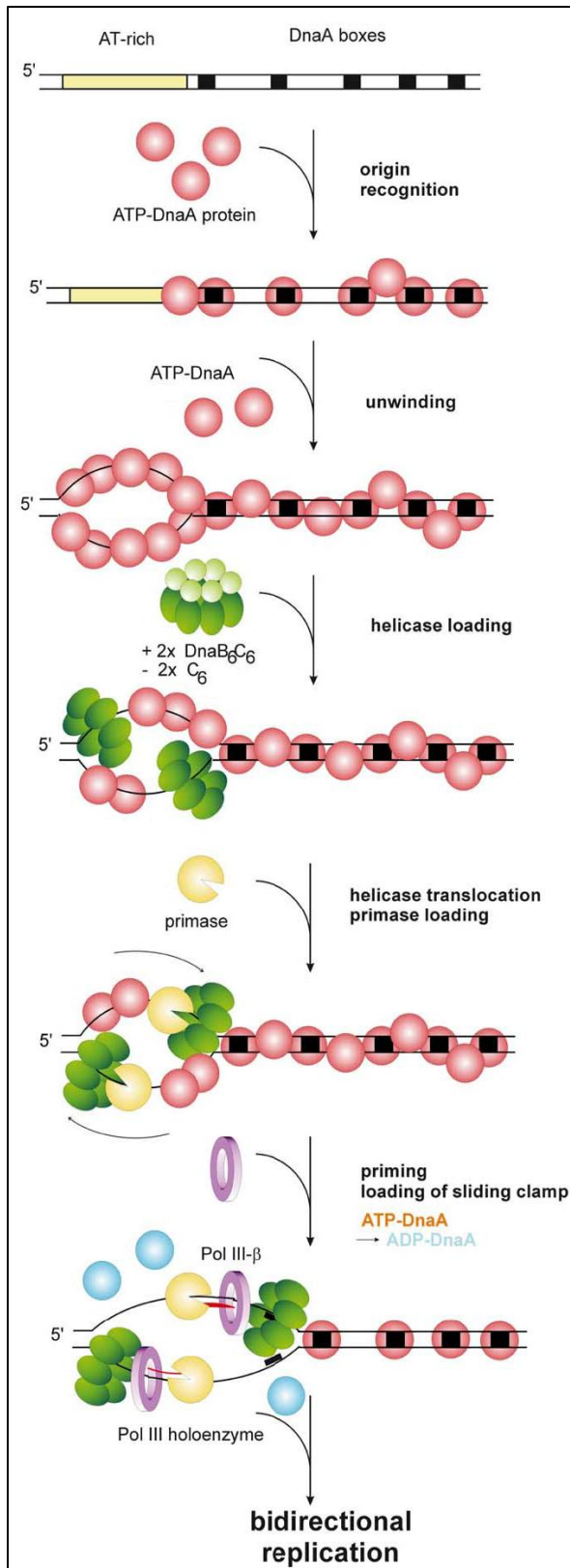


**Fig. 1.1.:** Initiation of DNA replication in *E. coli*. Modified after Messer W 2002 [1]. Courtesy of John Wiley and Sons (publisher).

complexes, one on each strand, whereby helicase loader DnaC represses the ATPase and helicase activity of DnaB [26-27]. Primase DnaG associates with the prepriming complex synthesizing the RNA-primers mandatory for proper release of DnaC and DnaA, which allows for activation and direct interaction of DnaB with DNA polymerase III holoenzyme that duplicates the leading and lagging strand of the chromosomal DNA-template in a continuous and discontinuous manner, respectively (Fig. 1.1.) [4, 26, 28]. It has been proposed that DnaC implication constitutes a checkpoint that allows for entry into elongation phase [26, 28]. This probably occurs by a DnaG induced conformational change of DnaB, which leads to DnaC release from the complex [26, 28]. Both replicative helicase DnaB and helicase loader DnaC belong, such as DnaA, to the AAA+ protein family (ATPases associated with diverse cellular activities) [26, 28].

## 1.2. Initiation control mechanisms

The mechanism of initiation of replication in *E. coli* presumably represents a rather general principle in all bacteria [1]. This assumption is based on the existence of the highly conserved initiator protein DnaA, its sequence specific DNA binding sites and an AT-rich region within the *oriC* [1]. But how the precisely timed mechanism of initiation

is controlled seems to be diverse among different bacterial phyla. In *E. coli*, the total protein level of DnaA does not change during the cell cycle, but the amount of DnaA bound to ATP or

ADP at specific times is crucial, i.e. most of initiation competent ATP-DnaA accumulates prior to the onset of replication and leads to an ORC dependent formation of the pre-RC [29-31]. This specific variation is achieved mainly by *de novo* DnaA-synthesis (binding immediately to ATP) and DnaA reactivation at specific DNA sequences termed DARS (DnaA-reactivating sequence) from ADP-DnaA to ATP-DnaA [4, 31-32]. After initiation, ATPase activity of DnaA is induced by interaction with regulatory proteins Hda and DnaN resulting in a reduced ATP-DnaA level [33-34]. The *dnaA* transcription is negatively regulated by ATP-bound DnaA protein that interacts with binding sites in the *dnaA* promoter and represses *dnaA* overexpression, what would lead to improper overinitiation events [4, 35-37]. Initiation frequency must tightly be coupled to growth, so that daughter cells receive the entirely duplicated chromosome [38]. Under optimal growth conditions, *E. coli* upregulates its *dnaA* expression to counterbalance the titration of ATP-DnaA molecules by additional *oriC* as a result of overlapping rounds of replication [38-39]. This mechanism is primarily important as the time of DNA replication exceeds the doubling time of cells under these conditions [38-40]. On the contrary, initiation-inhibitory regulation is enabled in slowly growing cells, in which DNA replication is accomplished long before the cells divide to prevent inappropriate reinitiation [38, 40].

For *E. coli* three principles of negative regulation of DNA replication are described, generally affecting the availability and activity of the initiator protein DnaA (Fig. 1.2.) [1, 4, 25, 41]:

### **Regulatory inactivation of DnaA (RIDA) via Hda and DnaN**

Active ADP-bound Hda protein (homologous to DnaA) induces the ATPase activity of DnaA right after initiation of replication through the interaction of the AAA+ modules of both proteins, thereby lowering the reinitiation potential of converted ATP-DnaA [33-34]. This mechanism is tightly linked to replication by the indispensable involvement of the sliding-clamp DnaN ( $\beta$ -subunit of DNA polymerase III) [33-34]. Upon DnaN loading onto the DNA, associated Hda stimulates the ATP-hydrolysis of DnaA resulting in initiation-inactive ADP-DnaA molecules [34].

### **SeqA binding to hemimethylated *oriC*-DNA**

The initiation of replication takes place at the *oriC*, which therefore represents the site that is replicated first. *E. coli* possesses a DNA adenine methylase (Dam), methylating the adenine deoxyribonucleotides within GATC-sequences on the DNA [4, 42-43]. Due to semiconservative DNA-replication, newly synthesized duplex DNA contains only one methylated strand (template) [42-43]. Hemimethylated GATC-sequences within the low-affinity DnaA-binding sites of the *oriC* are bound by SeqA (sequestration protein) with high affinity, which effectively prevents ATP-bound DnaA from rebinding to these sites crucial for initiation [19, 42]. Additionally, several GATC-sequences are present within the *dnaA*-gene, which is located

around 42 kb downstream of the *oriC* [44]. Those sequences are targeted by SeqA right after replication resulting in blocked *dnaA* transcription [4, 45-46].

### **Titration of ATP-DnaA to the *datA*-site**

Functional pre-RC formation at *oriC* comprises nearly 20 initiation-competent DnaA protomers out of the total cellular DnaA-pool that is estimated between 1000 and 2000 monomers [18, 25, 47-48]. The *datA* (DnaA titration)-locus is a 1 kb DNA-region containing five DnaA-boxes with an eightfold higher capacity of binding DnaA (up to 370 molecules) than *oriC* and that lies around 500 kb away from the origin of replication [4, 41, 49-51]. Thus, *datA* duplication occurs rather early during chromosome replication, what increases the capacity of binding and through titrating active DnaA-molecules upon initiation, which consequently prevents them from re-initiation at *oriC* [4, 41, 49-51].

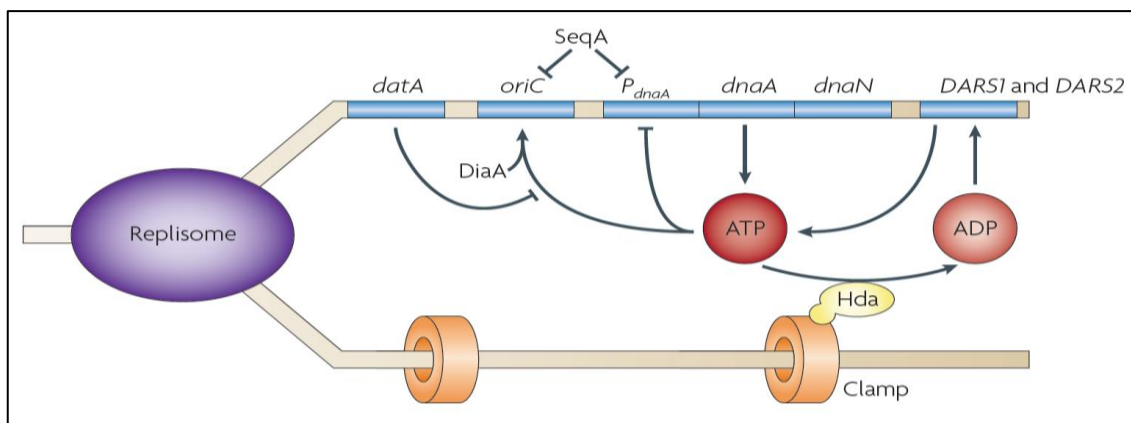


**Fig. 1.2.:** Schematic summary of initiation control mechanisms in *E. coli*. Modified after Katayama T et al. 2010 [4]. Courtesy of Nature Publishing Group.

These mechanistic regulatory pathways evolved within the family of *Enterobacteriaceae* and do not exist in Gram positive bacteria [16]. Hence, the regulation of initiation is different in *Bacillus subtilis*. Several proteins involved in these control mechanisms have been identified, such as YabA, Soj, Spo0J, Spo0A, SirA and DnaA itself.

### **YabA prevents cooperative binding of DnaA at *oriC***

YabA-protein negatively regulates DnaA-activity by repressing its cooperative binding at the origin [40]. Release of DnaN from the replisomal factory (which disassembles after termination) and direct interaction with YabA probably leads to a dislocation of YabA from the *oriC*, allowing pre-RC assembly only after completion of an ongoing replication cycle [40]. It has previously been proposed that YabA tethers DnaA to the replication machinery via DnaN right after the beginning of replication [10]. Consequently, DnaA is sequestered from the *oriC*, while the two origins of replication are directed to the cell poles during ongoing elongation [10]. This model implies DnaN to assist YabA in lowering the initiation potential and is primarily based

on the observation that during ongoing replication functional GFP-fusions of YabA colocalize with the replication machinery as does DnaA [10, 40, 52]. Moreover, DnaA loses its distinct localization in a *yabA* null mutant in addition to an overinitiation phenotype [10, 40, 52]. Very recently published studies indicate that YabA interacts with DnaA directly on the *oriC* (DnaA dependent association of YabA with *oriC*), thus preventing conversion from the ORC to the pre-RC by inhibiting cooperative DnaA multimerization required for DNA unwinding [40]. This negative regulation is independent of nucleotide-bound cofactors and ATP-hydrolysis [40]. Elevated DnaN levels lead to reduced YabA association with *oriC* on one hand and increased DnaA binding to *oriC* on the other hand, indicating that DnaN represses YabA after replisome disassembly [40]. These data provide a molecular mechanism of YabA-DnaA interaction on *oriC*, but lack explanation of DnaA titration to the replication machinery (see chapter 1.6.).

### **Soj modulates DnaA activity in accordance to its oligomeric conformation which in turn is regulated by Spo0J**

Soj-dependent regulation of DnaA activity occurs by direct interaction of both proteins [53-54]. Apo-form of Soj or ADP-Soj exclusively exists as a monomer, which is unable to bind DNA, and inhibits DNA replication, whereas ATP-Soj dimerizes, binds DNA (unspecifically) and promotes DnaA activity [54]. The DNA-binding capacity of Soj seems to be essential for this positive DnaA regulation [54]. Soj ATP-hydrolysis is induced by Spo0J thereby inhibiting the dimeric constitution of Soj [54]. Spo0J, generally bound to specific binding sites in close proximity to the *oriC* (*parS*-sites), only interacts with ATP-bound Soj [53]. Unpublished data of Scholefield G. and Murray H. indicate that Soj interacts with the AAA+ domain of DnaA and regulates its oligomerization capacity and consequently its active or inactive conformation. Soj and Spo0J both belong to the widely conserved partitioning protein family and are *B. subtilis* orthologues for ParA and ParB, respectively and encoded in the *par* operon [53].

### **Spo0A directly inhibits open complex formation by binding to *oriC* during sporulation**

Spo0A prevents replication events during sporulation, a typical cell differentiation process in *B. subtilis*, by directly inhibiting open complex formation at the *oriC* [55]. This occurs through binding to specific DNA sequences that partly coincide with DnaA-boxes, therefore preventing DnaA dependent duplex unwinding [55]. Additionally, SirA, induced during sporulation by Spo0A, directly binds to DnaA [56-57]. This interaction leads to a dislocation of DnaA from the *oriC* and results in the repression of DNA replication [57]. The molecular basis of the interaction between DnaA and SirA remains unclear due to the insolubility of recombinant SirA *in vitro* [57].

### Autoregulation of *dnaA* transcription

Genes *dnaA* and *dnaN* form an operon and are located at 0° on the *B. subtilis* chromosome, partially overlapping with the bipartite *oriC* [8-9, 58]. High levels of DnaA repress the transcription of the operon, whereas low amounts of DnaA lead to increased transcription [9]. Replication initiation is linked to a specific cell mass that has been termed as the initiation mass and defined as the cell mass per *oriC* at the time of initiation [9, 38, 59]. In cells containing low amounts of DnaA, the initiation mass is increased signifying late induction of initiation in the cell cycle, whereas high DnaA levels lead to decreased initiation mass values [9]. This led to the assumption, that the amount of DnaA molecules represents a factor that controls the rate of replication initiation and thus the rate of the cell cycle [9]. Interestingly, the transcription of the *dnaA-dnaN* operon is reversibly repressed in the presence of temperature sensitive helicase loader mutants at nonpermissive conditions resulting in stalled replication initiation [9, 60-61]. Together with the observation that the operon transcription cannot be forced by artificial titration of DnaA molecules after introduction of additional DnaA-box containing DNA into the cells, this indicates that the operon is transcribed once initiation is triggered and transcription stops through a DnaA mediated negative feedback-loop accompanied by yet unknown mechanisms that keep transcription repressed until a new replication cycle starts [8-9].

### 1.3. Organization of the origin of replication (*oriC*)

The origin of replication (*oriC*) represents the site on the chromosome where replication begins and has been described as the minimal region of autonomous replication [8]. It contains specific DnaA-boxes and a DNA unwinding element (DUE), but the organization of the *oriC* is strongly variable between different groups of bacteria [8]. The *E. coli oriC* is a 245 bp DNA region, composed of a DUE (three AT-rich 13-mer repeats with consensus sequence: GATCTNTTNTTTT) and high-affinity DnaA boxes as well as ATP-DnaA low-affinity sites, which allow for a coordinated assembly of DnaA (Fig. 1.3.1.) [1, 6, 24]. The high-affinity DnaA boxes promote DnaA-binding of both ATP- and ADP-bound DnaA [6, 62]. On the contrary, the low-affinity sites comprising DnaA boxes (9-mer consensus sequences: TTATNCACA), I-sites, C-sites (9-mer DnaA box consensus sequences with up to 4 mismatches) and  $\tau$ -sites (6-mer consensus sequences: TGATCC) poorly bind to ADP-DnaA, whereas binding of initiation competent ATP-DnaA is favoured and allows for its oligomerization required for duplex unwinding at the DUE [3, 6, 62-64]. However, heterogeneous complexes are still able to initiate replication *in vivo* when containing a limited amount of incorporated ADP-DnaA molecules [31]. This feature is particularly dependent on the arrangement of low-affinity I-sites that connect initiation sufficient ATP-DnaA levels to pre-RC formation [31]. Furthermore, single

high-affinity sites serve as nucleation centers for ordered and cooperative DnaA-multimerization towards proximal low-affinity sites at the time of initiation [20]. These high-affinity sites, termed R1, R2 and R4, are arranged in a symmetrical manner and it has very recently been proposed that *oriC* architecture provides a mechanism according to which two DnaA oligomers, anchored each at the distal R1 and R4 sites, extend towards the central R2 [3]. This assumption is supported by the presence of two oppositely-orientated low-affinity clusters that reside each between R1 and R2 and R2 and R4, respectively [3]. Their precise local arrangement allows for a physically possible interaction of two emerging helical filaments constituted of DnaA-monomers [3].

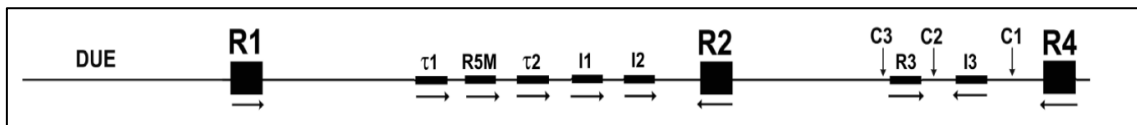


**Fig. 1.3.1.:** Illustration of *oriC* arrangement of the *E. coli* chromosome. DUE (DNA unwinding element), high- and low affinity sites are shown as large black squares and small black rectangles respectively. Modified after Rozgaja TA et al. 2011 [3]. Courtesy of John Wiley and Sons (publisher).

*B. subtilis oriC* comprises two noncoding DnaA box containing DNA sequences both upstream and downstream of *dnaA* referred to as *oriC1* and *oriC2*, respectively (Fig. 1.3.2.) [11, 14-15, 44]. The 5'-terminal region (*oriC1*) contains three AT-rich 16mer tandem repeats, three DnaA boxes with perfect match of the consensus sequence TTATCCACA and eleven DnaA boxes with one or two mismatches [11, 13]. The 3'-terminal region (*oriC2*, between *dnaA* and *dnaN*) includes one perfect consensus DnaA box and six boxes with one or two mismatches [11]. Additionally, a 27mer AT-rich sequence is present at this locus and has been shown to be close to the site of duplex unwinding [8, 13]. DNase I footprinting analysis with purified *B. subtilis* DnaA and the DnaA box clusters resulted in a highly coordinated manner of protection of the DnaA-boxes according to their degree of consensus [11]. Moreover, ATP, and not APD or any other nucleotide, has been shown to stimulate DnaA-binding to DnaA boxes *in vitro*, but it is still not clear if ATP-bound DnaA also represents the initiation competent constitution in *B. subtilis* like in *E. coli* [4, 11]. Both DnaA box containing regions are indispensable for replication initiation and form a loop structure upon addition of DnaA *in vitro* [8, 13]. The *oriC* region, precisely the number of DnaA boxes, in *B. subtilis* seem to participate in the initiation control to a much higher degree than it does in *E. coli* [4, 8]. Introduction of plasmids carrying *oriC* regions, unlike in *E. coli*, results in strong incompatibility with the chromosomal *oriC* leading to decreased initiation frequency and loss of such plasmids [8, 15, 65]. Corresponding to their location at *oriC*, these incompatible regions are referred to as *incA*, *incB* and *incC* [15].

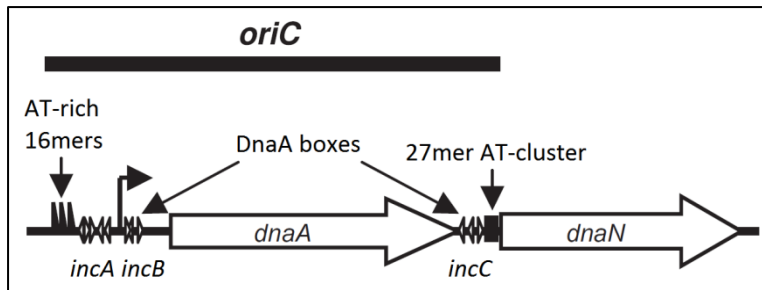


**Fig. 1.3.2.:** Organization of the origin of replication in *B. subtilis*. Modified after Berkmen MB and Grossman AD 2007 [5]. Courtesy of John Wiley and Sons (publisher).

DnaA does not exclusively bind to the origin, but to six additional DnaA-box clusters (DBC) in proximity to *oriC* [44, 66]. *B. subtilis* cells lacking these DBCs show an overinitiation phenotype and initiate earlier than wild type cells [44]. Interestingly, complementation of these effects can be achieved by reinsertion of particular DBCs into the chromosome [44]. Moreover, when further challenged by deleting *spo0J*, these DBC-lacking cells exhibit a strongly abnormal morphology and DNA segregation capacity resulting in an important reduction of the growth rate [44]. All of these defects can be rescued by an additional deletion of *soj* suggesting a synergistic regulatory interaction of Spo0J, Soj and these DnaA-box clusters [44].

Beside its function in DNA replication, *oriC* has also been proposed to be involved in chromosome segregation. Intriguingly, the 27mer AT-cluster of the intergenic *oriC*-region between *dnaA* and *dnaN* participates together with a 3'-coding sequence of *dnaA* in proper segregation of the replicated chromosomes into the daughter cells [67]. However, there is no *cis*-acting element within *oriC* that seems to be involved in its subcellular positioning required for accurate placement of the replisomal factory at the onset of initiation [5, 68]. Furthermore, *oriC* displacement leads to strong replication control defects, such as asynchronous and elevated initiation [58]. It has been speculated that formation of specific DNA-structures in close proximity to *oriC*, namely by interaction of Spo0J with its binding sites, might inhibit origin firing prior to the stimulation of initiation [58].

#### 1.4. The molecular structure of DnaA

DnaA belongs to the AAA+ family of ATPases all of which share common motifs for ATP binding, ATP-hydrolysis and ATP-sensing residues responsible for oligomerization and conformational change [23]. *B. subtilis* DnaA is a 50.7 kDa (*E. coli* DnaA: 52.6 kDa) protein that consists of 446 amino acids (*E. coli* DnaA: 467 aa). It shows sequence identity of 42% and sequence similarity of 63% with its *E. coli* homolog (sequence alignment results using ClustalW algorithm, <http://www.genome.jp/tools/clustalw/>).

DnaA from *E. coli* contains four functional domains each responsible for specific properties of the protein (Fig. 1.4.1.) [2, 6-7, 69].

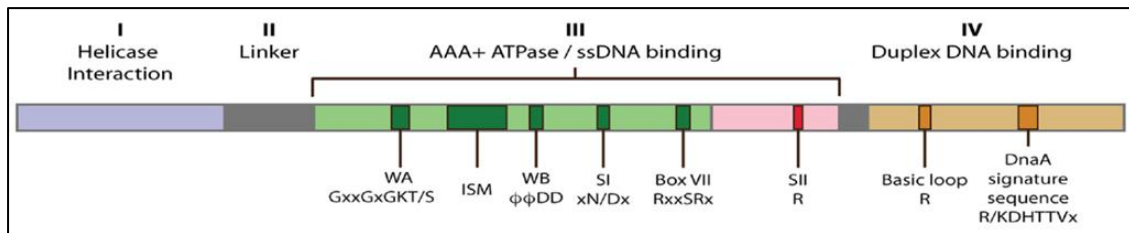


**Fig. 1.4.1.:** The functional domains of DnaA in their primary structure arrangement. Modified after Duderstadt KE et al. 2010 [2]. Courtesy of ASBMB (publisher); copyright agreement: “This research was originally published in *The Journal of Biological Chemistry*. Duderstadt KE, Mott ML, Crisona NJ, Chuang K, Berger JM. Origin remodeling and opening in bacteria rely on distinct assembly states of the DnaA initiator. *The Journal of Biological Chemistry*. 2010; 285(36): p. 28229-39. © the American Society for Biochemistry and Molecular Biology.”.

**Domain I** is essential for self-oligomerization of DnaA by binding to domain I of other DnaA molecules [6-7, 70]. The conserved hydrophobic residue W6 has been identified to be required for this property [6, 70]. Moreover, DnaA domain I allows for binding to DnaB helicase and DiaA [6, 71-73].

**Domain II** represents a linker between domain I and III without any other specific function than preventing steric constraints in the arrangement of the other domains [6-7].

**Domain III** includes several AAA+ protein specific motifs, such as Walker-type motifs for ATP binding and hydrolysis, sensor I motif responsible for its strong affinity to ATP and ADP, the Box VII arginine finger (R285) required for initiation competent ATP-dependent oligomer assembly stabilized by arginine residue R281 (needed for proper DnaB loading) and the Box VIII sensor II necessary for the ATPase activity involved in RIDA [6-7, 23, 64, 74]. Moreover, domain III has been described to be involved in binding of single-stranded DNA [2, 62]. Structural studies of *Aquifex aeolicus* DnaA bound to the non-hydrolyzable ATP analog AMP-PCP revealed, that the oligomer forms a helical filament (Fig. 6C), whereas ADP-DnaA remains monomeric [2, 7, 23].

**Domain IV** mediates specific recognition through its DnaA signature sequence located within a helix-turn-helix motif (DNA major groove interaction) and binding to the DnaA boxes through its basic loop (DNA minor groove interaction) with its essential residue R399 [6, 75]. It is proposed that the DNA interaction with the right-handed spiral-shaped DnaA-assembly occurs on the outside, suggesting a positive supercoiling of the DNA, which in turn needs to be counterbalanced at the proximal site of the filament by the introduction of negative supercoils [23]. This event is believed to occur at the AT-rich DNA unwinding element (DUE) leading to open complex formation [23].

Structural, mutational and biochemical approaches on DnaA function recently showed that ATP-DnaA assembles in two distinct multimeric constitutions dependent on the interaction with its DNA substrate (Fig. 1.4.2.) [2]. According to these observations, direct interaction of domain III and IV of two DnaA protomers are required for binding of single-stranded DNA and absolutely essential for pre-RC formation [2]. Structural modeling of such DnaA oligomeric interactions revealed that this “compact” conformational state is not competent in binding double-stranded DNA due to the fact that the helix-turn-helix motifs of domain IV face towards the inner surface of the filament [2]. Therefore, it has been postulated that ATP-DnaA, while bound to high-affinity sites constituting the bacterial ORC, adopts a second “extended” conformation, in which the position of domain IV is rearranged (through a linker helix between domain III and IV) such that the DNA-binding motifs are orientated towards the filament exterior [2].

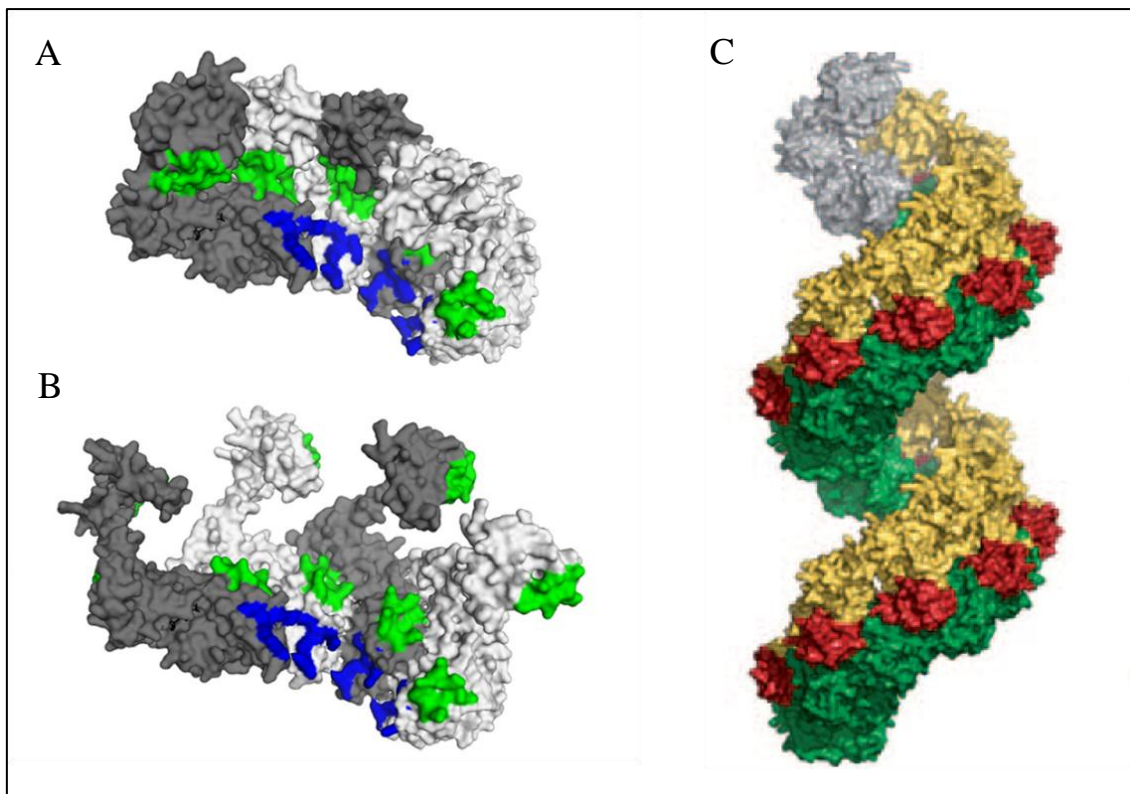


**Fig. 1.4.2.:** A and B, structures of oligomerized DnaA tetramers. A, “compact” conformation state of AMP-PCP-bound DnaA from *Aquifex aeolicus*. B, modeled “extended” conformation of ATP-bound DnaA. Adjacent protomers are shown in dark and light grey, DNA-binding domain (DBD, domain IV)/AAA+ domain (domain III) interaction sites are colored in green and single-stranded DNA binding sites shown in blue. Modified after Duderstadt KE et al. 2010 [2]. Courtesy of ASBMB (publisher); copyright agreement: “This research was originally published in *The Journal of Biological Chemistry*. Duderstadt KE, Mott ML, Crisona NJ, Chuang K, Berger JM. Origin remodeling and opening in bacteria rely on distinct assembly states of the DnaA initiator. *The Journal of Biological Chemistry*. 2010; 285(36): p. 28229-39. © the American Society for Biochemistry and Molecular Biology.”.

C, Higher-order structure of 16 oligomerized AMP-PCP-bound DnaA molecules (“compact” conformation) forming a helical filament with right-handed orientation. The first protomer of the multimer is shown in grey. Green, yellow and red illustrate the AAA+ domain (except for sensor II), AAA+ motif sensor II and DNA-binding domain IV respectively. Modified after Mott ML and Berger JM 2007 [7]. Courtesy of Nature Publishing Group.

Some of the assigned molecular features, specifically within the conserved AAA+ module do not seem to be involved in the same functional mechanisms in different bacteria. One such example is the intrinsic ATPase activity of DnaA that has been proposed to be essential in inactivating DnaA after initiation in the Gram negative  $\gamma$ -proteobacterium *E. coli* [33-34]. However, studies of bacterial initiation of replication in the Gram positive *Mycobacterium tuberculosis*, the pathogenic agent of human tubercule disease, suggest an implication of both ATP-binding and ATP-hydrolysis in efficient cooperative binding and multimerization of DnaA at the origin [76]. DnaA mutant protein of *M. tuberculosis* unable to hydrolyze ATP does not associate on *oriC* as fast as wild type DnaA *in vitro* and its expression is lethal for replicating cells [76]. The ATPase activity is stimulated by supercoiled DNA-templates independently of the presence of specific DnaA binding sites [77]. Moreover, DnaA bound to the non-hydrolyzable ATP analogue ATP $\gamma$ S is deficient in open complex formation *in vitro* [77]. Thus, ATP-hydrolysis is mechanistically required for pre-RC formation in *M. tuberculosis* which lies in sharp contrast to the molecular mode of operation of *E. coli* DnaA that can still assemble a functional pre-RC when associated with ATP $\gamma$ S or CTP [24, 77]. Another observation for a distinct molecular property in different organisms is the interaction of DnaA with factors that promote association of DnaA. As mentioned above, DiaA represents one of such factors in *E. coli* and interacts with the C-terminal part of DnaA domain I that lies in opposite orientation to the site responsible for self-oligomerization [72-73]. Unpublished results from Scholefield G. and Murray H. show that the initiation promoting capacity of Soj on *B. subtilis* DnaA results from a direct stimulation of DnaA oligomerization. But in contrast to DiaA, Soj does not interact with domain I but seems to dock on domain III, the AAA+ module, thereby promoting or preventing its oligomerization, dependent on its own molecular conformation [54].

### 1.5. Specific *E. coli* DnaA allele *dnaAcos*

Mutational analyses of DnaA both *in vivo* and *in vitro* are highly informative in terms of understanding the molecular mode of operation and the principles of regulation of the initiation of replication. A particular mutant allele in *E. coli*, termed *dnaAcos*, shows a striking heat resistance and cold sensitivity in colony formation as a result of DNA overproduction due to hyperinitiation [78-82]. The *dnaAcos* allele contains four amino acid substitutions, Q156L, A184V, H252Y and Y271H, but the cold sensitivity phenotype is mainly correlated to the A184V and Y271H substitutions that could be dissected to be relevant in hyperinitiation and stabilization of the replication at high temperatures, respectively [78-82]. *In vitro* data of purified DnaAcos revealed a significant ATP-binding defect (A184 lies proximal to a specific Walker A motif), but interestingly DnaAcos does not show reduced affinity for DnaA box containing double-stranded DNA and obviously provides an initiation competent constitution

that allows for pre-RC formation [79, 82]. Introduction of plasmids carrying the *dnaAcos* allele under a native *dnaA* promoter into strains that still contain functional *dnaA* leads to a strong reduction in transformation efficiency both at permissive (42°C) and nonpermissive temperatures (30°C and below), thus results in a dominant negative effect of *dnaAcos* over chromosomal *dnaA* [79]. This effect results from *oriC* dependent overinitiation events through regulation irresponsive DnaAcos [79-80]. Recent reports support the assumption that DnaAcos is insensitive to inhibitory control mechanisms *in vivo* [79-80]. Hence, DnaAcos can neither be inactivated by the interaction with Hda and DnaN (RIDA) nor sufficiently titrated to *datA* once replication has initiated [80]. It is noteworthy to mention that studies on Soj-mediated DnaA regulation in *B. subtilis* revealed that the inhibition of replication initiation by a DNA-binding deficient Soj mutant (SojG12V) can be suppressed by spontaneous point mutations in *dnaA* leading to overinitiation, among amino acid substitution H162Y which lies adjacent to the corresponding *dnaAcos* phenotype determining residue substitution A184V (A163V in *B. subtilis*) [53].

## 1.6. Cell cycle dependent localization of DnaA in *B. subtilis*

*In vivo* studies of *B. subtilis* analyzing the subcellular localization of DnaA revealed a distinct and cell cycle coupled pattern of DnaA fused to fluorescent proteins [10]. Previous data based on immunofluorescence microscopy for DnaA visualization suggested that DnaA is distributed all over the cytoplasm throughout the cell cycle in exponentially growing cells (after methanol fixation) with elevated protein concentrations at the cell poles compared to reduced DnaA amounts around the nucleoid [83]. However, corresponding to a later report, DnaA localizes as a discrete focus at the origin of replication at the beginning of the cell cycle in live cells (see Fig. 1.6.A) [10]. Upon assembly of the replication machinery (represented as a fusion of a fluorescent protein to DnaX, the  $\tau$ -subunit of DNA polymerase III), which is generally located at the cell center during slow growth, DnaA seems to be spatially sequestered from the origins (that move towards the cell poles throughout replication elongation) to midcell and presumably tightly associated to the stationary replication machinery through a mechanism that involves YabA regulatory protein and DnaN, the sliding clamp of the DNA polymerase (see chapter 1.2.) [10]. This cell-centered co-accumulation of both DnaA and the subunits of the replication machinery persists until the cell cycle is completed (see Fig. 1.6.B/C) [10]. Colocalization of origin regions and DnaA-foci has again only been observed at the time of replication machinery disassembly, thus suggesting a specific cell cycle coupled control mechanism of replication initiation that spatially prevents DnaA from rebinding and reinitiating at origin regions and thereby inhibiting cell damaging overinitiation events [10]. This specific localization pattern of DnaA during replication is abolished in *yabA* null mutants or *yabA* mutants lacking the capacity

to interact with either DnaA or DnaN [10]. Such cells overinitiate and YFP-DnaA is distributed all over the cytoplasm, probably masking discrete foci of DnaA interaction at the origins (see Fig. 1.6.E/F) [10]. In support of these observations, DnaA and YabA interdependently constitute a high molecular weight complex (> 1 MDa) *in vivo* [10]. This complex can only be detected in cells that already entered elongation phase of replication, but not before [10]. Nevertheless, the exact molecular basis of a proposed protein network that acts in order to titrate DnaA during replication and thereby negatively regulating initiation frequency has yet to be elucidated. Recent findings focused on the molecular interaction between DnaA and YabA revealed the mechanism of the inhibitory regulation through YabA, but do not explain the considerable amount of DnaA molecules retained at the replication machinery right after initiation (see chapter 1.2.) [10, 40]. Furthermore, till now, there is no provided evidence for a molecular means that induces the release of DnaA from *oriC* and thus inactivates an operative and potentially still functional pre-RC after the onset of replication in *B. subtilis*.

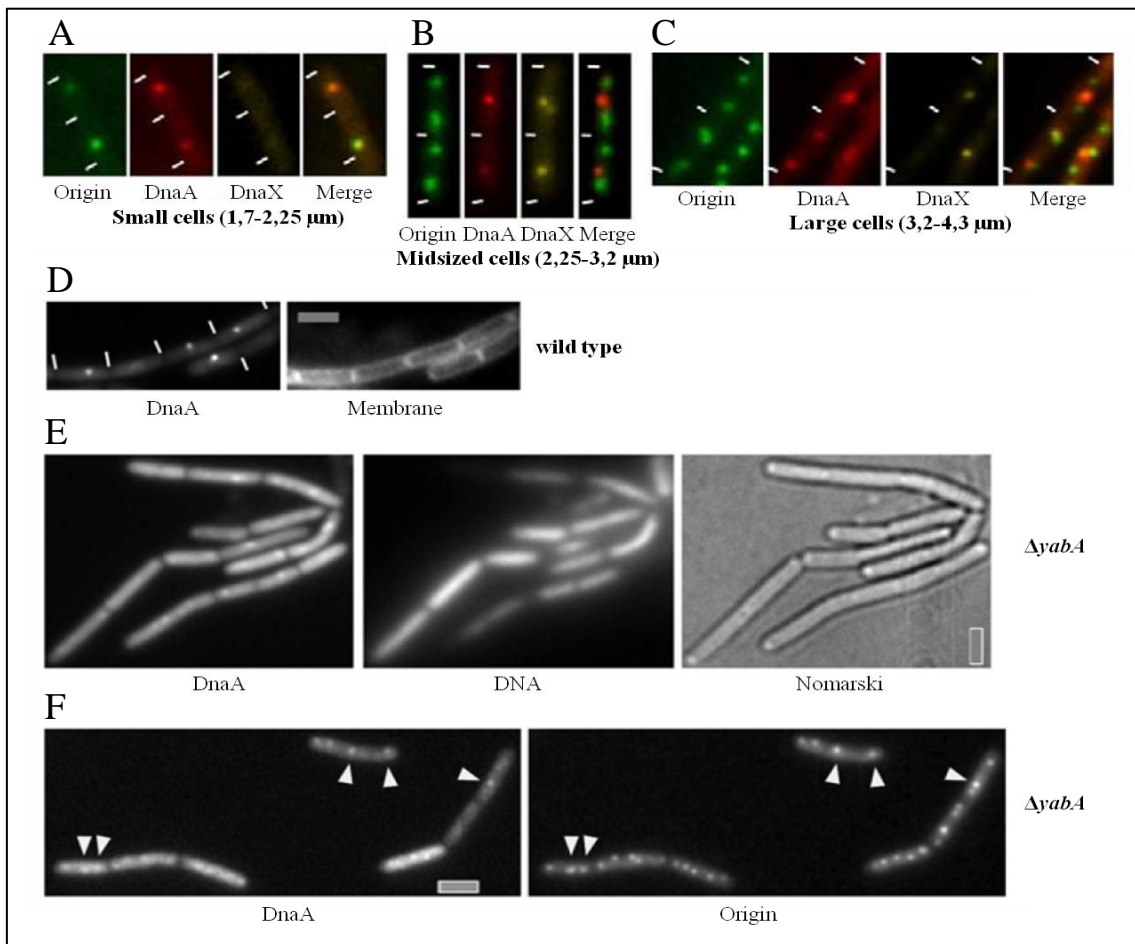


**Fig. 1.6.:** YabA dependent cell cycle coupled localization pattern of DnaA in live *B. subtilis* cells, using fluorescent proteins fused to proteins of interest (YFP-DnaA, DnaX-mCherry, origins were visualized using LacI-CFP binding to an array of *lacO* integrated close to *oriC*). A-C, localization of DnaA in correlation to the subcellular positions of origins of replications and the replication machinery (DnaX-mcherry) shown in cells that belong to different cell cycle specific stages that correspond to the cell size. D-F, localization of YFP-DnaA in differing genetic backgrounds. D, wild type cells (visualized YFP-DnaA and membrane). E, *yab-4* null mutant (visualized YFP-DnaA, and DNA). F, *yab-4* null mutant (visualized YFP-DnaA and origins of replication). White lines: ends of cells. White arrows: colocalized foci. Grey bars: 2 μm. Modified after Soufo CD et al. 2008 [10]. Courtesy of Elsevier (publisher).

## 1.7. Aims of research

The initiator protein of chromosomal replication, DnaA, and its regulation have intensively been studied in *E. coli*, a model organism of Gram negative bacteria. A variety of functional capacities, such as ATP-binding and hydrolysis, oligomerization and specific DNA binding, have been discovered and appear to be highly conserved in bacteria, thus are also valid for *B. subtilis* [1, 6-7]. Nevertheless, the process of initiation and its regulation seem to work differently in Gram positive bacteria [1, 4]. This study focused on the question of how DnaA initiates chromosomal DNA replication in *B. subtilis* by mutational approach using cytological and biochemical techniques. Specific DnaA activities and their implication in the initiation were investigated by analyzing several *B. subtilis* DnaA mutants each carrying single substitutions of highly conserved amino acids that have previously been reported for *E. coli* to be involved in the activities mentioned above. It has recently been observed that an ectopically expressed ATP-hydrolysis deficient *dnaA* mutant (*dnaAE183Q*) in *B. subtilis* displayed a dominant negative effect over chromosomal *dnaA* *in vivo* and was lethal for the cells that were highly elongated and showed abnormally decondensed nucleoids (PhD thesis of Clarisse Defeu Soufo, University of Freiburg, Institute of Biology, 2009). According to this observation, the particular interest of this study was to understand how ATP-binding and ATP-hydrolysis are involved in pre-RC assembly in *B. subtilis*. Thus, the two principal objectives of this work were:

1. Purification and biochemical characterization of recombinant (His)<sub>6</sub>-DnaA and several mutant forms of DnaA among (His)<sub>6</sub>-DnaAA163V (predicted ATP-binding deficient mutant carrying the corresponding amino acid substitution that causes the *dnaAcos* mutant phenotype in *E. coli*), (His)<sub>6</sub>-DnaAE183Q (predicted ATP-hydrolysis deficient), (His)<sub>6</sub>-DnaAD214N (predicted ATP-binding deficient), (His)<sub>6</sub>-DnaAR260A (predicted decrease in oligomerization stability), (His)<sub>6</sub>-DnaAW8A (predicted self-association deficient) and (His)<sub>6</sub>-DnaAR387C (predicted DNA-binding deficient).
2. Analysis of the effect of expressing YFP-DnaA and mutant forms from an ectopic locus on the chromosome in live *B. subtilis* cells. This was achieved using fluorescence microscopy with particular interest on the consequences on cell cycle specific parameters, such as the frequency of initiation of replication, DNA compaction, chromosomal segregation, septum formation and cell length.

# MATERIALS AND METHODS

---

## 2. Materials and Methods

### 2.1. Chemicals and Kits for DNA-purification purposes

The chemical substances and components for buffers, reaction solutions and growth media were purchased from VWR (Darmstadt, Germany), Roth (Karlsruhe, Germany), AppliChem (Darmstadt, Germany) and Sigma-Aldrich (Seelze, Germany). Enzymes and respective buffers are products from New England Biolabs, NEB (Frankfurt/Main, Germany) and Thermo Fisher Scientific/Fermentas (St. Leon-Rot, Germany). DNA-purification generally has been achieved using appropriate Kits for different types of DNA (chromosomal DNA, plasmid-DNA, linear DNA) from Qiagen (Hilden, Germany), ZYMO Research (Freiburg, Germany) and Analytik Jena (Jena, Germany).

### 2.2. Bacterial strains

#### 2.2.1. *Escherichia coli*

In this work, three *E. coli* strains with different genetic backgrounds were used either for vector construction and amplification (DH5 $\alpha$ , XL-1 blue) or heterologous protein overexpression (Rosetta (DE3) pLysS).

| Strain              | Relevant genotype  | Reference  |
|---------------------|--|------------|
| DH5 $\alpha$        | F <sup>-</sup> $\Phi$ 80lacZ $\Delta$ M15 $\Delta$ (lacZYA-argF) U169 <i>recA1 endA1 hsdR17</i> (rK <sup>-</sup> , mK <sup>+</sup> ) <i>phoA supE44 <math>\lambda</math><sup>-</sup> thi-1 gyrA96 relA1</i>                    | Invitrogen |
| XL-1 blue           | <i>recA1 endA1 gyrA96 thi-1 hsdR17 supE44 relA1 lac</i> [F' <i>proAB lacIqZ <math>\Delta</math>M15 Tn10 Tet<sup>R</sup></i> ]  | Stratagene |
| Rosetta (DE3) pLysS | F <sup>-</sup> <i>ompT hsdS<sub>B</sub></i> (R <sub>B</sub> <sup>-</sup> m <sub>B</sub> <sup>-</sup> ) <i>gal dcm <math>\lambda</math></i> (DE3 [ <i>lacI lacUV5-T7 gene 1 ind1 sam7 nin5</i> ]) pLysSRARE (Cam <sup>R</sup> ) | Novagen    |

**Table 2.2.:** *E. coli* strains used in this work.

#### 2.2.2. *Bacillus subtilis*

In this work, the prototroph wild type strain *B. subtilis* subsp. *subtilis* PY79 was used [84].

### 2.3. Growth media and complements

Growth conditions of liquid *E. coli* cultures generally were 37°C, 200 rpm, LB-medium (pH 7 ± 0.2) (see table 2.3.) supplemented with appropriate antibiotics or inducers. For growth on plates, LB-medium (pH 7 ± 0.2) was solidified by addition of agar (15 mg/ml). *B. subtilis* cultures were cultivated under similar conditions, but at 30°C. For fluorescence microscopy, *B. subtilis* cultures were grown in S750 minimal medium (pH 7 ± 0.2) (see table 2.3.). Selection of *B. subtilis* strains carrying constructs that provide resistance against spectinomycin was performed on DSM agar plates (see table 2.3.). All media were sterilized prior to use either by sterile filtration (pore size 0.2 µm, Filtropur S, Sarstedt) or autoclaving (121°C, 30 minutes).

| Medium                   | Composition |   |
|--------------------------|-------------|---|
| LB-medium (pH 7 ± 0.2)   | 5 mg/ml     | yeast extract                                   |
|                          | 10 mg/ml    | trypton   |
|                          | 10 mg/ml    | NaCl  |
| LB-agar (pH 7 ± 0.2)     | 5 mg/ml     | yeast extract                                   |
|                          | 10 mg/ml    | trypton   |
|                          | 10 mg/ml    | NaCl  |
|                          | 15 mg/ml    | agar  |
| S750 medium (pH 7 ± 0.2) | 55.6 mM     | fructose  |
|                          | 29.6 mM     | NaCl  |
|                          | 0.04 mg/ml  | casamino acids                                  |
|                          | 50 mM       | MOPS  |
|                          | 10 mM       | (NH <sub>4</sub> ) <sub>2</sub> SO <sub>4</sub> |
|                          | 5 mM        | KH <sub>2</sub> PO <sub>4</sub>                 |
|                          | 2 mM        | MgCl <sub>2</sub>                               |
|                          | 0.7 mM      | CaCl <sub>2</sub>                               |
|                          | 20 µM       | HCl   |
|                          | 5 µM        | MnCl <sub>2</sub>                               |
|                          | 5 µM        | FeCl <sub>3</sub>                               |
|                          | 3.3 µM      | thiamin   |
|                          | 1 µM        | ZnCl <sub>2</sub>                               |
| DSM-agar (pH 7 ± 0.2)    | 8 mg/ml     | nutrient broth                                  |
|                          | 13.4 mM     | KCl   |
|                          | 10 mM       | Ca(NO <sub>3</sub> ) <sub>2</sub>               |
|                          | 1 mM        | MgSO <sub>4</sub>                               |
|                          | 1 mM        | NaOH  |
|                          | 0.1 mM      | MnCl <sub>2</sub>                               |
|                          | 0.01 mM     | FeSO <sub>4</sub>                               |
|                          | 15 mg/ml    | agar  |

**Table 2.3.:** Composition of growth media used in this work.

Antibiotics used in this work were ampicillin (100 µg/ml), chloramphenicol (5 µg/ml), spectinomycin (100 µg/ml), erythromycin (1 µg/ml) and lincomycin (25 µg/ml). Gene expression controlled by inducible promoters required 1 mM IPTG or xylose (5 mg/ml). Transcription of xylose inducible gene constructs was repressed by glucose (5 mg/ml).

## 2.4. Preparation and transformation of electrocompetent *E. coli* cells

*E. coli* cells were cultivated in LB medium (400 ml) under continuous shaking (200 rpm, Infors HT) at 37°C till log phase ( $OD_{600} \sim 0.6$ ). The cells were kept on ice for 30 minutes prior to centrifugation (10 minutes, 4°C, 5000 rpm, Sorvall RC6+/Thermo Fisher Scientific [centrifuge], FiberLite F14/Pinamoon Technologies [rotor]). The pellet was resuspended in ice-cold deionized water (400 ml) and again centrifuged (see above). To concentrate the cells, this step was repeated with 200 ml ice-cold water, 8 ml ice-cold glycerol (10%, v/v) and finally 800  $\mu$ l ice-cold glycerol (10%, v/v). Aliquots (50  $\mu$ l) of concentrated electrocompetent cells were promptly frozen in liquid nitrogen and stored at -80°C. *E. coli* cells (50  $\mu$ l) were transformed with appropriate amounts of plasmid-DNA (10-500 ng), which has previously been dialyzed (pore-size 0.025  $\mu$ m, MF-membrane filters, Millipore) against deionized water. Electroporation of the *E. coli* cells was carried out in electroporation cuvettes (2 mm, Eurogentech) using 2500 V (Easyject Prima, Equibio). Subsequently, cells were carefully resuspended in 1 ml LB-medium and incubated at 37°C with vigorous shaking (200 rpm, Infors HT) for 1 hour followed by selective screening. For this purpose, cells were streaked on antibiotic containing LB-agar plates and grown for ~14 hours at 37°C.

## 2.5. Preparation and transformation of competent *B. subtilis* cells

*B. subtilis* cells were cultivated in SpC-medium (20 ml, see table 2.5.) under continuous shaking (200 rpm, Infors HT) at 37°C till stationary phase ( $OD_{600} \sim 3-5$ ). Subsequently, the cells were transferred in SpII-medium (100 ml, see table 2.5.) and incubated for 90 minutes at 37°C and vigorous shaking (200 rpm, Infors HT) prior to centrifugation (15 minutes, 25°C, 4000 rpm, Megafuge 1.0/Heraeus Sepatech [centrifuge], BS4402-A/Heraeus Sepatech [rotor]). The pellet was resuspended in a mixture of supernatant (9 ml) and glycerol (5%, v/v). Aliquots (500  $\mu$ l) of concentrated competent cells were rapidly frozen and stored at -80°C (adapted from [85], [86]). *B. subtilis* cells (125  $\mu$ l) were transformed with appropriate amounts of plasmid-DNA (100-500 ng) or chromosomal DNA (10-100 ng). Cells and DNA were incubated for 30 minutes at 37°C with vigorous shaking (200 rpm, Infors HT) followed by selective screening. For this purpose, cells were streaked on antibiotic containing LB/DSM-agar plates and grown for ~36 hours at 30°C. Double cross-over events provoked by gene insertion in the chromosomal *amyE* site of *B. subtilis* using the suicide vector pSG 1729 were screened for the incapacity of amylose catabolism. *B. subtilis* transformants were streaked on starch (15 mg/ml) containing LB-agar plates and incubated overnight at 30°C. Subsequently, a starch staining solution containing elemental iodine and potassium iodide (Lugol's iodine) was added on top of the colonies.

Successful gene integration disrupts *amyE*, thus inactivates metabolic starch processing. Hence, colonies without non-stained halos were qualified positive for gene integration [87].

| Medium      | Composition |   |
|-------------|-------------|---|
| SpC medium  | 2 mg/ml     | yeast extract                                   |
|             | 0.3 mg/ml   | casamino acids                                  |
|             | 80 mM       | K <sub>2</sub> HPO <sub>4</sub>                 |
|             | 50 mM       | KH <sub>2</sub> PO <sub>4</sub>                 |
|             | 27.75 mM    | glucose   |
|             | 13 mM       | (NH <sub>4</sub> ) <sub>2</sub> SO <sub>4</sub> |
|             | 4 mM        | tri-sodium-citrate                              |
|             | 1.66 mM     | MgSO <sub>4</sub>                               |
| SpII medium | 1 mg/ml     | yeast extract                                   |
|             | 27.75 mM    | glucose   |
|             | 0.1 mg/ml   | casamino acids                                  |
|             | 80 mM       | K <sub>2</sub> HPO <sub>4</sub>                 |
|             | 50 mM       | KH <sub>2</sub> PO <sub>4</sub>                 |
|             | 13 mM       | (NH <sub>4</sub> ) <sub>2</sub> SO <sub>4</sub> |
|             | 8.31 mM     | MgSO <sub>4</sub>                               |
|             | 4 mM        | tri-sodium-citrate                              |
|             | 0.5 mM      | CaCl <sub>2</sub>                               |

**Table 2.5.:** Composition of *B. subtilis* competence media used in this work.

## 2.6. DNA extraction and quantification

Extraction and purification of plasmid-DNA from *E. coli* was performed applying the principle of alkaline lysis using kits from ZYMO Research (ZR Plasmid Miniprep Classic-Kit) and Qiagen (QIAprep Spin Miniprep Kit) [88]. Isolation of chromosomal DNA from *B. subtilis* requires lysozyme treatment of a cell pellet prior to DNA extraction. For this purpose, an overnight culture (3 ml) was pelleted, resuspended in 200 µl TE-buffer (10 mM Tris-HCl (pH 8), 1 mM EDTA) containing lysozyme (1 mg/ml) and incubated for 30 minutes at 37°C. Subsequently, the bacterial DNA purification kit protocol, which is based on the ethanol precipitation method, was followed (innuPREP Bacteria DNA kit, Analytik Jena). DNA concentrations were measured using Implen NanoPhotometer. Sequencing of DNA-samples (PCR products or plasmid-DNA) was sourced out to GATC (Konstanz, Germany).

## 2.7. Principles of vector construction

All transgenic manipulations in this work required plasmid-DNA vectors as a vehicle. Specific vectors were constructed and applied for heterologous overexpression of recombinant proteins

(pETDuet-1, Novagen), N-terminal YFP-fusions of wt/mutDnaA and site-directed mutagenesis (pSG 1729) [89-90].

### 2.7.1. Polymerase chain reaction (PCR)

PCR was used for the amplification of linear DNA-molecules and site-directed mutagenesis. All oligonucleotides used in this work (see table 2.7.1.) were obtained from MWG Eurofins/Operon (Ebersberg, Germany). A standard PCR reaction mixture with a reaction volume of 50  $\mu$ l contained 32.25  $\mu$ l deionized water, 10  $\mu$ l 5xHF Phusion reaction buffer, 1  $\mu$ l DNA-template (1-100 ng), 2  $\mu$ l dNTP-mix (10 mM), 2  $\mu$ l of each oligonucleotide (12 mM) and 0.75  $\mu$ l Phusion DNA polymerase (1.5 U). PCR reactions were done in a programmable thermocycler (Mastercycler personal, Eppendorf). The settings were adapted to the length of the amplifiable DNA-fragment and the calculated annealing temperatures of the respective oligonucleotides to the DNA-template. A default setting for the amplification of a linear wild type or mutant *dnaA* fragment:

| Number of cycles | Temperature | Time       |
|------------------|-------------|------------|
| 10 cycles        | 95°C        | 2 minutes  |
|                  | 95°C        | 30 seconds |
|                  | 55°C        | 30 seconds |
|                  | 72°C        | 90 seconds |
| 25 cycles        | 95°C        | 30 seconds |
|                  | 60°C        | 30 seconds |
|                  | 72°C        | 90 seconds |
|                  | 72°C        | 2 minutes  |

The relative amount and the size of linear PCR products were verified by (agarose) gel electrophoresis prior to purification (QIAquick PCR Purification Kit, Qiagen).

A default setting for site-directed mutagenesis of *dnaA* inserted in vector pSG 1729:

| Number of cycles | Temperature | Time       |
|------------------|-------------|------------|
| 25 cycles        | 95°C        | 2 minutes  |
|                  | 95°C        | 30 seconds |
|                  | 45-60°C     | 30 seconds |
|                  | 72°C        | 8 minutes  |

The plasmid-DNA template was eliminated directly after the PCR reaction by addition of 5  $\mu$ l enzyme buffer 4 (NEB) and 1  $\mu$ l of DpnI (20 U). The solution was incubated for 120 minutes at 37°C, subsequently dialyzed against deionized water and transformed into electrocompetent *E. coli* XL-1 blue cells.

| Oligonucleotide    | Sequence                                 |
|--------------------|--|
| DnaA_A163V_up      | 5'-ACACACTTAATGCATGTGATCGGCCATTATGTA-3'  |
| DnaA_A163V_reverse | 5'-TACATAATGGCCGATCACATGCATTAAGTGTGT-3'  |
| DnaA_D214N_up      | 5'-GATGTGCTTTTGATAAACGATATTCAATTTTTA-3'  |
| DnaA_D214N_reverse | 5'-TAAAAATTGAATATCGTTTATCAAAAGCACATC-3'  |
| DnaA_R260R_up      | 5'-CCGACACTTGAAGACGCGTTGCGCTCACGTTTT-3'  |
| DnaA_R260R_reverse | 5'-AAAACGTGAGCGCAACGCGTCTTCAAGTGTCGG-3'  |
| DnaA_W8A_up        | 5'-AATATATTAGACCTGGCGAACCAAGCCCTTGCT-3'  |
| DnaA_W8A_reverse   | 5'-AGCAAGGGCTTGGTTCGCCAGGTCTAATATATT-3'  |
| dnaAE183Qup        | 5'-GTTTATCTGTCTTCTCAGAAATTTACAAACGAA-3'  |
| dnaAE183Qdw        | 5'-TCGTTTGTAATTTCTGAGAAGACAGATAAAC-3'    |
| dnaAR387Cup        | 5'-TCAGTAGCTTTTCCGTGTCAAATCGCCATGTAC-3'  |
| dnaAR387Cdw        | 5'-GTACATGGCGATTTGACACGGAAAAGCTACTGA-3'  |
| BamHI DnaA up      | 5'-ACTGGATCCTATGGAAAATATATTAGACCTG-3'    |
| NotI DnaA reverse  | 5'-ACTGCGGCCGCTCATTAAAGCTGTTCTTTAATTC-3' |
| oriC_up            | 5'-ATCATGACACCTCCCTCGAG-3'               |
| oriC_dw            | 5'-ATCCTTCCGGCACGTCCC-3'                 |
| oriC_up_Biotin     | 5'-ATCATGACACCTCCCTCGAG-3'               |
| oriC_dw_Biotin     | 5'-ATCCTTCCGGCACGTCCC-3'                 |
| dnaAbp801up        | 5'-GGGACTTATTACAGATATCAC-3'              |
| dnaAbp1333dw       | 5'-GCTGTTCTTTAATTTCTTTTAC-3'             |
| dnaASeq.primers    | 5'-GGCTTAGGGAAAACACACTTA-3'              |
| dnaAup pstI        | 5'-TCACTGCAGATGGAAAATATATTAGACCTG-3'     |
| 1729XbaI+AmyE5dw   | 5'-GACATGGCCTGCCCCGG-3'                  |
| 1729XbaI+AmyE5up   | 5'-CCGGGCAGGCCATGTC-3'                   |
| YFP@bp641 up       | 5'-AGAGAGACCACATGGTCC-3'                 |
| DnaA upstream up   | 5'-GGTAAGCGCCATTTGCTC-3'                 |
| DnaA downstream dw | 5'-GACAGGAAACACAGCCTATC-3'               |

**Table 2.7.1.:** Oligonucleotides and their respective sequences used in this work.

### 2.7.2. Digestion of DNA-molecules with restriction endonucleases

Digestion of linear or plasmid-DNA at defined restriction sites in order to create compatible fragments was carried out using specific restriction endonucleases and provided buffers (NEB). According to the instructions of NEB, a standard reaction mixture with a reaction volume of 50  $\mu\text{l}$  contained 28  $\mu\text{l}$  deionized water, 5  $\mu\text{l}$  10xNEB reaction buffer, 15  $\mu\text{l}$  DNA (0.1-2  $\mu\text{g}$ ), 1  $\mu\text{l}$  endonuclease (I), 1  $\mu\text{l}$  endonuclease (II) and was incubated for 90 minutes at the indicated temperature. The relative amount and the size of linearized DNA were verified by (agarose) gel electrophoresis prior to purification using a specific kit (QIAquick PCR Purification Kit, Qiagen).

### 2.7.3. Ligation of linearized DNA-molecules

Ligation of linearized DNA-molecules in order to create transferable constructs, thus vectors with an additionally integrated DNA-fragment, generally required a molar ratio of 1(vector):3(insert). The respective amounts were estimated using (agarose) gel electrophoresis. A standard reaction mixture with a reaction volume of 20  $\mu\text{l}$  contained 5  $\mu\text{l}$  deionized water, 2  $\mu\text{l}$  10xT4 ligation buffer (NEB), 12  $\mu\text{l}$  linearized DNA (both fragments in appropriate moieties), 1  $\mu\text{l}$  T4 DNA ligase (NEB) and was incubated overnight at 16°C. Subsequently, the reaction mixture was dialyzed against deionized water and transformed into electrocompetent *E. coli* XL-1 blue cells (see chapter 2.4.).

### 2.7.4. Agarose gel electrophoresis

Agarose gel electrophoresis (constant 100 mA, PHEROstab 500, Biotec Fisher) has been carried out in order to estimate relative amounts and sizes of DNA-molecules (PCR-products and linearized DNA-fragments). Specific electrophoretic migration in an agarose gel matrix allows separation of distinct DNA-fragments with particular sizes. Generally, the gel contained 10 mg/ml agarose, 50 mM boric acid, 50 mM Tris and was immersed in the running buffer (50 mM boric acid and 50 mM Tris). The DNA was mixed with 6xDNA loading buffer (30% glycerol (v/v), 300 mM boric acid, 300 mM Tris, 0.5 mg/ml bromphenol blue, GelRed nucleic acid gel stain [Biotium] 1:60000). DNA-visualization was achieved by ultraviolet light (UV Transilluminator, UVP).

## 2.8. Protein analysis

### 2.8.1. Protein purification

Protein purification was performed in two consecutive steps. The purification of (His)<sub>6</sub>-wild type/mutant DnaA initially began with affinity chromatography using an ÄKTA Prime

apparatus (GE Healthcare) and Nickel-Sepharose columns (HisTrap HP 1 ml, GE Healthcare) and was continued by size-exclusion chromatography using an ÄKTA FPLC apparatus (GE Healthcare) and a gelfiltration column (Superdex 200 10/300 GL, GE Healthcare). Prior to purification, the respective proteins were overexpressed in *E. coli* Rosetta (DE3) pLysS cells carrying a pETDuet-1 vector (Novagen) with an IPTG inducible T7 promoter, six encoded histidines and the full gene sequence of the *dnaA* variants. Transformant cells were grown under vigorous shaking (200 rpm, Infors HT) in LB-medium (1000 ml) at 37°C to exponential phase (OD<sub>600</sub> 0.8) and induced for 60 minutes with 1 mM IPTG. Subsequently, the cells were centrifuged (20 minutes, 4°C, 5000 rpm, Sorvall RC6+/Thermo Fisher Scientific [centrifuge], FiberLite F9S-4x1000y/Pinamoon Technologies [rotor]) and the pellet was resuspended in 30 ml HEPES A (50 mM HEPES, 300 mM NaCl, pH 7.5). To prevent protein degradation a protease inhibitor was added (Complete, Roche). Afterwards, the cells were french pressed (AMINCO French Press, Laurier Research Instrumentation) in two consecutive cycles at approximately 20000 psi and the lysate was centrifuged (30 minutes, 4°C, 16000 rpm, Sorvall RC6+/Thermo Fisher Scientific [centrifuge], SS-34/Du Pont Instruments [rotor]). The clear supernatant was passed through a filter (pore-size 0.45 µm, Filtropur S, Sarstedt) before injection into the loop of the ÄKTA Prime apparatus (preequilibrated with HEPES A and HEPES B [50 mM HEPES, 300 mM NaCl, 500 mM imidazole, pH 7.5]). The proteins were loaded onto the Nickel-Sepharose column, the column was washed with 25% HEPES B and the protein eluted with 100% HEPES B (exception: (His)<sub>6</sub>-DnaAW8A eluted as a shoulder of the wash peak with 25% HEPES B) in fractions of 1 ml and checked by SDS-PAGE (see chapter 2.8.2.). Fractions containing significant amounts of the desired protein were assembled and loaded into the loop of the ÄKTA FPLC apparatus (preequilibrated with HEPES A). The proteins were separated by molecular weight and fractionated in 0.5 ml samples. The peak fractions were analyzed by SDS-PAGE and only pure protein fractions were assembled and stored at 4°C. The described procedure has been carried out for all DnaA variants, except (His)<sub>6</sub>-DnaAA163V, which required slightly different purification conditions. Instead of 1000 ml of overexpressing cell culture, 2000 ml were pelleted and lysed, since the overexpression efficiency for this specific mutant protein was significantly reduced. Moreover, both HEPES buffers contained 500 mM NaCl instead of 300 mM. The determined concentration of the fractionated protein after gelfiltration was very low and, thus, needed to be further concentrated. Protein centrifugal concentrator columns (Vivaspin 6, Sartorius Stedim Biotech) were loaded with 6 ml of the assembled protein fractions and centrifuged (4°C, 3500 rpm, Sorvall RC6+/Thermo Fisher Scientific [centrifuge], SS-34/Thermo Fisher Scientific [rotor]) to decrease the volume and increase the concentration. The molar protein concentrations (c) were calculated with the equation of Lambert and Beer ( $c=A/\epsilon \times d$ ), describing the quotient of the

absorption at 280 nm (A) divided by the product of the extinction coefficient of the protein ( $\epsilon$ ,  $\epsilon_{(\text{His})6\text{DnaA}} = 38390$ ) and the path length of the used quartz cuvette (d, 1 cm).

### 2.8.2. SDS-polyacrylamide gel electrophoresis (SDS-PAGE)

SDS-PAGE (constant 25 mA, Power source, VWR) has been carried out in order to visualize relative amounts and to estimate molecular weight and purity of denatured proteins. Specific electrophoretic migration in a polyacrylamide gel matrix allows separation of distinct proteins with a particular molecular weight. Generally, a discontinuous gel was prepared according to the protocol of Laemmli [91] and contained a stacking gel (4% acrylamide (v/v), 0.11% N-N'-methylenebisacrylamide (v/v), 250 mM Tris-HCl (pH 6.8), 1 mg/ml SDS, 1 mg/ml  $(\text{NH}_4)_2\text{S}_2\text{O}_8$ , 0.07% TEMED (v/v)) and a variable running gel (8%/12% acrylamide (v/v), 0.21%/0.32% (8%/12% gel) N-N'-methylenebisacrylamide (v/v), 375 mM Tris-HCl (pH 8.8), 1 mg/ml SDS, 1 mg/ml  $(\text{NH}_4)_2\text{S}_2\text{O}_8$ , 0.07% TEMED (v/v)). The electrophoresis was performed in a running buffer (25 mM Tris-HCl (pH 8.3), 250 mM glycine, 1 mg/ml SDS). The protein sample was mixed with 4xSDS loading buffer (100 mM Tris-HCl (pH 6.3), 10% glycerol (v/v), 2 mg/ml SDS, 3%  $\beta$ -mercaptoethanol (v/v), 1 mg/ml bromphenol blue) and denatured at 95°C for 5 minutes prior to SDS-PAGE. Subsequently, the gel was either applied to a nitrocellulose membrane for further electrophoretic transfer of the proteins (see chapter 2.8.3.) or the immobilized proteins incorporated within the gel-matrix were stained with Coomassie brilliant blue R250. For this purpose, the gel was placed in a beaker containing a staining solution (2.5 mg/ml Coomassie brilliant blue R250, 20% acetic acid (v/v), 25% ethanol (v/v)) and rotated for 20 minutes. Afterwards, the staining solution was exchanged for a destaining solution (10% acetic acid (v/v), 30% ethanol (v/v)) and further rotated until the stained proteins were visible.

### 2.8.3. Immunoblotting

Proteins separated in acrylamide gels (see chapter 2.8.2) were transferred (constant 60 mA, 90 minutes, Power source, VWR) onto a nitrocellulose membrane (pore size 0.45  $\mu\text{m}$ , Protran, Whatman) and in order to detect particular proteins specific antibodies were applied. Three layers of Whatman paper were presoaked with transfer buffer (48 mM Tris, 38 mM glycine, 0.35 mg/ml SDS, 20% methanol (v/v)) and placed in the blotting apparatus (SV20-SDB, Sigma-Aldrich). Subsequently, the nitrocellulose membrane was activated by immersion with deionized water and placed on top of the Whatman papers. Prior to the electrophoretic transfer, the acrylamide gel was positioned above and covered by another three layers of Whatman paper presoaked with transfer buffer. Thereafter, the membrane was rotated overnight in a blocking solution (50 mg/ml skimmed milk powder, 0.8 mM  $\text{Na}_2\text{HPO}_4$ , 2 mM  $\text{NaH}_2\text{PO}_4$ , 10 mM NaCl, 0.1% Tween 20 (v/v)) and subsequently washed three times in PBST (0.8 mM  $\text{Na}_2\text{HPO}_4$ , 2 mM  $\text{NaH}_2\text{PO}_4$ , 10 mM NaCl, 0.1% Tween 20 (v/v)). The first antibody (anti-DnaA) was diluted to a

freshly prepared blocking solution to a final ratio of 1:500 and added to the membrane (rotation at room temperature for 1 hour). Afterwards, the membrane was washed again three times with PBST and the second horseradish peroxidase coupled antibody (goat anti-rabbit, Bio-Rad) was diluted with blocking solution to a final ratio of 1:3000, added to the membrane and incubated for 1 hour at room temperature. Upon three more washing steps with PBST, the proteins on the membrane were visualized by chemiluminescence, as a consequence of enzymatic luminol oxidation in the presence of hydrogen peroxide by the IgG coupled horseradish peroxidase. In order to initiate this reaction, the membrane was placed for approximately one minute in a beaker that contains freshly prepared immunodetection solution (2.5 mM luminol, 0.4 mM coumaric acid (stock dissolved in DMSO), 100 mM Tris-HCl (pH 8.5), 0.02% H<sub>2</sub>O<sub>2</sub> (v/v)). The emitted light was detected by a CCD-camera (Fujifilm LAS-3000 imager, Fujifilm).

#### 2.8.4. Protein extracts from *B. subtilis*

*B. subtilis* cells were grown in LB-medium or S750 minimal medium at 30°C under continuous shaking (200 rpm, Infors HT) till exponential phase (OD<sub>600</sub> ~0.6) and 2 ml of the cell culture were centrifuged (Centrifuge 5415R, Eppendorf [centrifuge], F45-24-11, Eppendorf [rotor]). The pelleted cells were resuspended in lysis buffer (100 mM NaCl, 50 mM EDTA, 0.05 mg/ml lysozyme, pH 7.6) and incubated for 20 minutes at 37°C. The lysate was mixed with 4xSDS loading buffer (100 mM Tris-HCl (pH 6.3), 10% glycerol (v/v), 2 mg/ml SDS, 3% β-mercaptoethanol (v/v), 1 mg/ml bromphenol blue) and denatured at 95°C for 5 minutes prior to SDS-PAGE and immunoblotting (see chapters 2.8.2. and 2.8.3.).

## 2.9. Determination of ATP-binding and ATPase activities

The ATP-binding and ATPase activity of recombinant *B. subtilis* (His)<sub>6</sub>-wild type/mutant DnaA was examined using filter binding assays with radioactive [ $\alpha$ -<sup>32</sup>P]-ATP and [ $\gamma$ -<sup>32</sup>P]-ATP (500  $\mu$ Ci, SRP-207 and SRP-301, Hartmann Analytic), respectively. ATP-binding experiments were performed as follows, the reaction mixture with a final volume of 350  $\mu$ l contained nucleotide binding buffer (40 mM HEPES (pH 7.6), 100 mM potassium glutamate, 10 mM magnesium acetate, 500  $\mu$ M EDTA, 1 mM DTT, 0.75  $\mu$ M BSA), (His)<sub>6</sub>-wild type/mutant DnaA or BSA (1.6  $\mu$ M) and [ $\alpha$ -<sup>32</sup>P]-ATP (4  $\mu$ M). Directly upon addition of [ $\alpha$ -<sup>32</sup>P]-ATP, 50  $\mu$ l of the reaction solution were passed through a nitrocellulose filter (pore size 0.45  $\mu$ m, diameter 25 mm, Protran, Whatman) preincubated with wash buffer (40 mM HEPES (pH 7.6), 10 mM magnesium acetate, 500  $\mu$ M EDTA) mounted on top of a filtration flask setup connected to a vacuum pump (self-construction). The filter was washed three times with 5 ml ice-cold wash buffer and placed in a scintillation counter vial (volume 6 ml, Mini-vial, Sarstedt). The remaining reaction mixture was incubated at either 0°C, 25°C or 37°C and samples (50  $\mu$ l)

filtrated after 2, 5, 10, 30 and 60 minutes. Subsequently, 2 ml of scintillation solution (Ultima Gold, PerkinElmer) were added to each filter prior to scintillation counter analysis (TRI-Carb 2900 TR, Packard Bioscience). The stoichiometry of bound ATP per DnaA monomer were indirectly determined from the measured counts per minute detected on the filter and a reference value of the initially employed molar amount of radiolabeled ATP per reaction. The ATPase activity was investigated in a similar way to ATP-binding, but with use of [ $\gamma$ - $^{32}$ P]-ATP. Only single cycles of ATP-hydrolysis were measured, i.e. the protein was first incubated with 4  $\mu$ M [ $\gamma$ - $^{32}$ P]-ATP and right afterwards treated with a 500-fold molar excess of non-radiolabeled ATP (2 mM) prior to sample filtration. This prevents rebinding to [ $\gamma$ - $^{32}$ P]-ATP during the measurement and allows to track only one hydrolysis cycle. The ATPase rates (hydrolyzed mol ATP/mol protein/minute) were indirectly determined from the fastest decrease of detected counts per minute at the beginning of the reaction on the respective filters and a reference value of the initially employed molar amount of radiolabeled ATP per reaction.

## 2.10. Electrophoretic mobility shift assays (EMSA)

Electromobility shift assays were performed with increasing amounts (0-80 pmol) of (His)<sub>6</sub>-wild type/mutant DnaA and either DnaA-box containing *oriC*-DNA (0.9 pmol, linear DNA-fragment, 624 nt, amplified with primers *oriC\_up* /*oriC\_dw* [see chapter 2.7.1.]) or control DNA without DnaA-boxes (0.9 pmol, linear DNA-fragment, 532 nt, amplified with primers *dnaAbp801up*/*dnaAbp1333dw* [see chapter 2.7.1.]) under ATP-containing (2.5 mM) and ATP-free conditions. The reaction mixture with a final volume of 20  $\mu$ l (27.5 mM HEPES (pH 7.6), 0.25 mM EDTA, 1.25 mM magnesium acetate, 2.5% glycerol (v/v), 0.025 mg/ml BSA, 135 mM NaCl) was incubated for 30 minutes at room temperature with either type of linear DNA (43.5 nM), concentration of purified (His)<sub>6</sub>-wild type/mutant DnaA (0-4  $\mu$ M) and with or without ATP (2.5 mM). Subsequently, the protein-DNA samples were mixed with 6xDNA loading buffer (30% glycerol (v/v), 300 mM boric acid, 300 mM Tris, 0.5 mg/ml bromphenol blue) and run in native polyacrylamide gradient gels (4-12%, Anamed) and 50 mM boric acid and 50 mM Tris (running buffer) at constant voltage (constant 200 V, 2 hours, Power source, VWR). Afterwards, the gel was placed in a beaker containing running buffer and DNA-stain (dilution 1:60000, GelRed nucleic acid gel stain, Biotium) and rotated for 20 minutes at room temperature prior to DNA-visualization by ultraviolet light (UV Transilluminator, UVP). The values for the apparent binding constant  $K_{app}$ , referred to as the protein concentration at which half of the total amount of linear DNA in the reaction is bound (room temperature, pH 7.6), were estimated from the respective gel-shift experiments.

## 2.11. Surface plasmon resonance experiments

Surface plasmon resonance (SPR) technique was applied to investigate protein-DNA interactions in real-time. The BIAcore 3000 apparatus (GE Healthcare) used for these measurements detects a real-time deviation of the angle of a laser beam that is focused on and reflected from the surface of the sensor chip [92]. This deviation is a result of a change in the mass concentration due to binding events to the surface-bound DNA (ligand) by the applied (His)<sub>6</sub>-wild type/mutant DnaA (analyte) and measured as resonance/response units (RU) [92]. Thus, linear *oriC*-DNA (0.25 pmol, 624 nt, amplified with primers *oriC\_up\_Biotin/oriC\_dw\_Biotin* [see chapter 2.7.1.]) was biotinylated both at its 5' and 3' ends (standard PCR with biotinylated primers, see chapter 2.7.1.) and noncovalently bound to a streptavidin coated sensor chip (~1700 RU, Sensor chip SA, GE Healthcare). The system was preequilibrated and permanently flushed (flow rate 20 µl/min) at room temperature with SPR-binding buffer (50 mM HEPES, 300 mM NaCl, 2.5 mM MgCl<sub>2</sub>, pH 7.6) containing or lacking ATP (2.5 mM). (His)<sub>6</sub>-wild type/mutant DnaA (2.5 µM) preincubated for one minute with or without 2.5 mM ATP in SPR-binding buffer was subsequently applied to the sensor chip (volume 75 µl) at a flow rate of 20 µl/min, i.e. for 225 seconds, followed by protein dissociation from the DNA. Protein-DNA interactions were measured in real-time over a period of 700 seconds. The response of the interaction of the protein to the *oriC*-DNA containing chamber was subtracted from unspecific binding to the chip surface monitored in a second DNA-free chamber. SPR-wash buffer (100 mM NaOH, 500 mM NaCl) was injected to remove bound proteins from the chip.

## 2.12. DSS-crosslink assays

The multimerization capacity of (His)<sub>6</sub>-wild type/mutant DnaA was examined using disuccinimidyl suberate (DSS) crosslinking assays. The reaction mixture with a final volume of 20 µl (2.5 mM HEPES, 31.25 mM NaH<sub>2</sub>PO<sub>4</sub>, 31.25 mM Na<sub>2</sub>HPO<sub>4</sub>, pH 7.6) was incubated with the respective protein (500 nM) with different salt concentrations (200/400 mM), in the absence or presence of linear *oriC*-DNA (36.4 nM) and under ATP containing (2.5 mM) or ATP-free conditions for 5 minutes at room temperature. Subsequently, DSS (125 µM, dissolved in DMSO) was added and the reaction continued for another five minutes. The reaction was stopped by application of 4xSDS loading buffer (100 mM Tris-HCl (pH 6.3), 10% glycerol (v/v), 2 mg/ml SDS, 3% β-mercaptoethanol (v/v), 1 mg/ml bromphenol blue) and the samples were run in an 8% SDS-PAGE (see chapter 2.8.2.) prior to immunoblotting with anti-DnaA antibodies (see chapter 2.8.3.).

### 2.13. Fluorescence microscopy

*B. subtilis* strains PY79 containing constructs that allow *oriC* visualization and wild type/mutant DnaA localization [*spo0J::(mIs lacO<sub>256</sub>, spo0J)*, *thrC::(cm p<sub>pen</sub>-lacI-cfp)*, *amyE::(spec p<sub>xyI</sub>-yfp-wt/mutdnaA)*] were grown until exponential growth (OD<sub>600</sub> ~0.6) in S750 minimal medium at 30°C under continuous shaking (200 rpm, Infors HT). CFP, cyan fluorescent protein (excitation: 433 nm/emission: 475 nm), and YFP, yellow fluorescent protein (excitation: 513 nm/emission: 527 nm), both are variants of GFP, green fluorescent protein (excitation: 488 nm/emission: 507 nm), originated from *Aequoria victoria* [93]. Cells were treated with red fluorescent membrane stain FM 4-64 (excitation: 515 nm/emission: 640 nm, final concentration 1 nM) and DNA intercalating blue fluorescent dye DAPI (excitation: 358 nm/emission: 461 nm, final concentration 0.72 nM) and incubated for 2 minutes at room temperature prior to microscopy. For this purpose, 2 µl of cells were pipetted on top of a glass slide (Microscope slides standard, Roth) precoated with a thin S750-agarose (S750 medium, 10 mg/ml agarose) layer and covered with a cover slip (Cover slips, Roth). The setup used for fluorescence microscopy included an Axio Observer Z1 (Carl Zeiss) with an oil immersion objective (100x magnification, 1.45 numerical aperture, alpha-Plan-FLUAR, Carl Zeiss), a mercury light source (LQ-HXP 120, LEJ), a Cool Snap EZ CCD-camera (Photometrics) and Metamorph 7.5.5.0. operational software (Universal Imaging Corporation).

### 2.14. Software

Computational processing of DNA and amino acid sequences, purification profiles, raw experimental data from scintillation counter analysis, surface plasmon resonance experiments and images from fluorescence microscopy required the application of several genomic databases and bioinformatic and data evaluation programs. DNA and amino acid sequences from *Bacillus subtilis* and *Escherichia coli* were obtained from the SubtiList server (<http://genolist.pasteur.fr/SubtiList/>) and the EcoCyc database (<http://ecocyc.org/>), respectively. The Basic Local Alignment Search Tool (BLAST, <http://blast.ncbi.nlm.nih.gov/Blast.cgi>), A plasmid Editor (ApE, <http://biologylabs.utah.edu/jorgensen/wayned/ape/>) and ClustalW (<http://www.genome.jp/tools/clustalw/>) were used for the comparison of DNA or amino acid sequences. Vector NTI software (<http://www.invitrogen.com/site/us/en/home/Products-and-Services/Applications/Cloning/vector-nti-software.html>) was used for cloning purposes in order to identify restriction sites within defined DNA sequences. ProtParam (<http://web.expasy.org/protparam/>) was applied to calculate the extinction coefficient of (His)<sub>6</sub>-DnaA for the determination of the concentration of purified proteins. Data of protein purification obtained during affinity and size-exclusion chromatography were analyzed with PrimeView software (GE Healthcare). QuantaSmart

(PerkinElmer) and BIAcore 3000 Control Software/BIAevaluation (GE Healthcare) were used as instrumental and evaluation software for the liquid scintillation analyzer and the BIAcore 3000 apparatus (GE Healthcare), respectively. Images of fluorescence microscopy were analyzed with Metamorph 7.5.5.0. (Universal Imaging Corporation) and ImageJ 1.43 (<http://rsbweb.nih.gov/ij/>). Microsoft Excel 2007 was used for statistical calculations and data visualization.

## RESULTS

---

### 3. Results

*E. coli* DnaA functions and their specific implication in the initiation of replication have been well characterized [1, 6, 41, 75]. Despite the highly conserved sequence of *E. coli* DnaA and *B. subtilis* DnaA, the process of initiation seems rather different and suggests a distinct role for the singular functional capacities [1, 4]. The principle objective of this work was the analysis of the involvement of these capacities in the mechanism of initiation. Therefore several *B. subtilis* DnaA mutants were obtained using site-directed mutagenesis for the substitution of single amino acids that were reported for *E. coli* DnaA to disrupt the ATP-binding capacity (*E. coli*: A184V/*B. subtilis*: A163V and *E. coli*: D235N/*B. subtilis*: D214N), ATP-hydrolysis (*E. coli*: E204Q/*B. subtilis*: E183Q), self-association (*E. coli*: W6A/*B. subtilis*: W8A), stable oligomerization (*E. coli*: R281A/*B. subtilis*: R260A) and double-stranded DNA-binding (*E. coli*: R407C/*B. subtilis*: R387C) [64, 70, 74, 79, 82, 94-98].

#### 3.1. Sequence Alignment of *E. coli* DnaA and *B. subtilis* DnaA

The alignment of the amino acid sequences of *E. coli* DnaA and *B. subtilis* DnaA revealed a sequence identity of 42% and sequence similarity of 63% (Fig. 3.1.). In particular, the N-terminus of the protein is not highly conserved between both species. However, AAA+ determining motifs (*E. coli* DnaA: 132-296 aa/*B. subtilis* DnaA: 111-275 aa) and DNA-binding motifs (*E. coli* DnaA: 399-444 aa/*B. subtilis* DnaA: 379-424 aa) are strongly conserved.

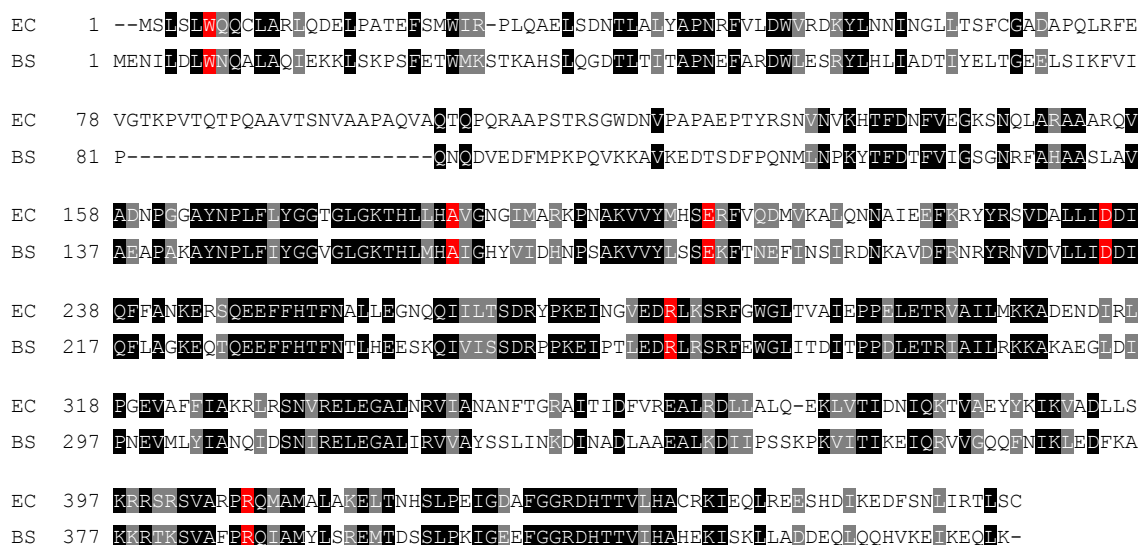


**Fig. 3.1.:** Sequence alignment of *E. coli* DnaA [EC] and *B. subtilis* DnaA [BS]. Numbers indicate amino acid positions in the respective sequences. Black shaded boxes: identical residues. Red shaded boxes: identical residues (targets of single point mutations in this work). Grey shaded boxes: similar residues. No box shades: residues with neither identity nor similarity to each other. Black bars: no corresponding residue. (Sequences: SubtiList/EcoCyc. Sequence alignment: ClustalW, BOXshade.)

### 3.2. Purification of recombinant (His)<sub>6</sub>-wtDnaA/(His)<sub>6</sub>-mutDnaA

Purification of (His)<sub>6</sub>-wtDnaA/(His)<sub>6</sub>-mutDnaA was carried out using *E. coli* strain Rosetta (DE3) pLysS appropriate for overexpression of recombinant proteins. The supernatant of lysed cells was loaded onto a nickel-column and the first protein purification level was achieved by affinity chromatography. Subsequently, the eluted (His)<sub>6</sub>-tagged proteins were applied to a size-exclusion column for further purification. The degree of purification of each fraction was checked by SDS-PAGE. As an example, figure 3.2.A shows a typical coomassie stained SDS gel loaded with fractions of purified (His)<sub>6</sub>-wtDnaA after gelfiltration. Immunoblotting of purified proteins with anti-DnaA antibodies revealed that weak additional bands observed by coomassie stained gels derived from degraded (His)<sub>6</sub>-tagged DnaA proteins (Fig. 3.2.B). The overexpression and purification efficiency was similar for all (His)<sub>6</sub>-tagged DnaA proteins, except for (His)<sub>6</sub>-DnaAA163V that needed slightly different purification conditions and only limited amounts of protein could be obtained. Interestingly, the experimentally determined molecular weight of monomeric (His)<sub>6</sub>-DnaA (~56 kDa) was slightly higher than the expected value of 51.6 kDa [(His)<sub>6</sub> 0.9 kDa, DnaA 50.7 kDa].

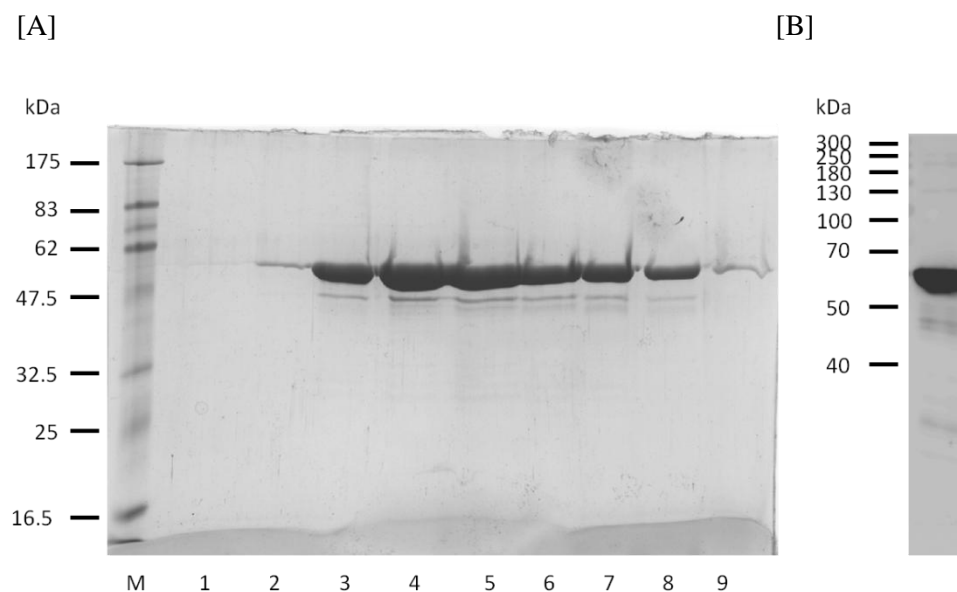


**Fig. 3.2.:** A, coomassie stain of a 12%-SDS gel, loaded with fractions of purified (His)<sub>6</sub>-wtDnaA after gelfiltration (M, marker. 1-9, fractions.). B, immunoblot with anti-DnaA antibodies, loaded with 50 pmol purified (His)<sub>6</sub>-wtDnaA.

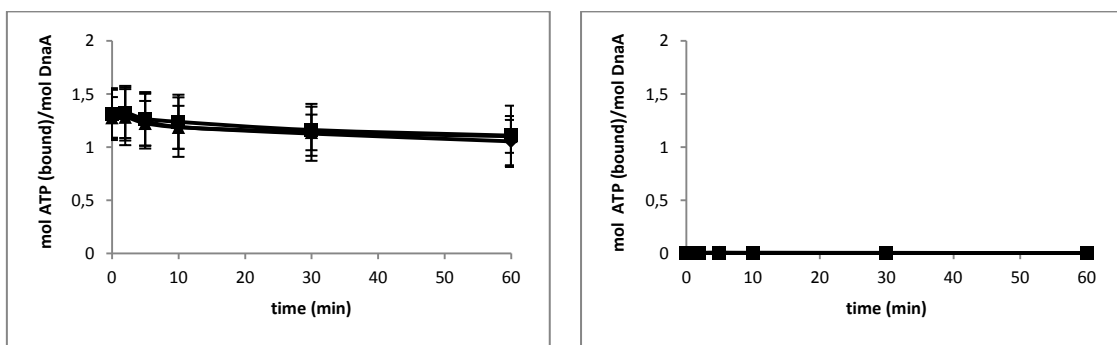
### 3.3. ATP-binding activity of recombinant (His)<sub>6</sub>-wtDnaA/(His)<sub>6</sub>-mutDnaA determined by filter binding assays using [ $\alpha$ -<sup>32</sup>P]-ATP

#### 3.3.1. (His)<sub>6</sub>-wtDnaA exhibits a very strong temperature independent ATP-binding activity

As previously reported, *E. coli* DnaA and *B. subtilis* DnaA show an extremely high affinity to ATP [11, 99]. The ATP-binding activity of recombinant *B. subtilis* (His)<sub>6</sub>-wtDnaA was examined using filter binding assays with radioactive [ $\alpha$ -<sup>32</sup>P]-ATP at different temperatures over an incubation time period of one hour. BSA was used as a negative control, and, as expected, did not show any binding to ATP. (His)<sub>6</sub>-wtDnaA affinity to ATP was temperature independent and full binding capacity to ATP was observed immediately after addition of [ $\alpha$ -<sup>32</sup>P]-ATP to the protein containing reaction buffer, which was determined as an approximate 1.2:1 stoichiometry of bound ATP per DnaA monomer (Fig. 3.3.1). This effect displays the strikingly high affinity of (His)<sub>6</sub>-DnaA to ATP, but the circumstance of the instantaneously reached saturation of ATP-binding made it impossible to determine the exact  $K_d$  value under the tested conditions. Attempts using lower amounts of (His)<sub>6</sub>-DnaA in the reaction to prevent immediate saturation with ATP resulted in decreased protein stability (data not shown). Moreover, the determined stoichiometry slightly deviates from the expected 1:1 stoichiometry of bound ATP per DnaA monomer, a discrepancy that is probably caused by the indirect determination of these values.

[A] (His)<sub>6</sub>-wtDnaA

[B] BSA (negative control)

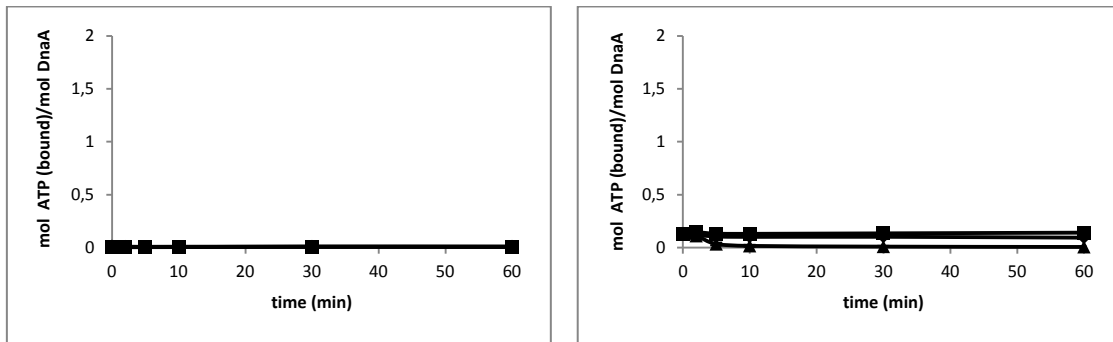


**Fig. 3.3.1.:** ATP-binding activity determined by filter binding assays using [ $\alpha$ -<sup>32</sup>P]-ATP. Values for molarities of bound ATP/DnaA were calculated from detected counts per minute on the respective filters. A, (His)<sub>6</sub>-wtDnaA. B, BSA (negative control). Diamonds: incubation at 0°C. Squares: incubation at 25°C. Triangles: incubation at 37°C.

#### 3.3.2. (His)<sub>6</sub>-DnaAA163V and (His)<sub>6</sub>-DnaAD214N do not or poorly bind ATP, respectively

Both (His)<sub>6</sub>-DnaAA163V and (His)<sub>6</sub>-DnaAD214N do not or poorly bind ATP, respectively. The ATP-binding deficiency was not restricted to high or low temperatures, but could be measured in a range between 0°C and 37°C. While only background signal of [ $\alpha$ -<sup>32</sup>P]-ATP could be detected on the filter when incubated with (His)<sub>6</sub>-DnaAA163V, (His)<sub>6</sub>-DnaAD214N showed a slight but still 10-fold reduced ATP-binding activity compared to (His)<sub>6</sub>-wtDnaA. This strongly

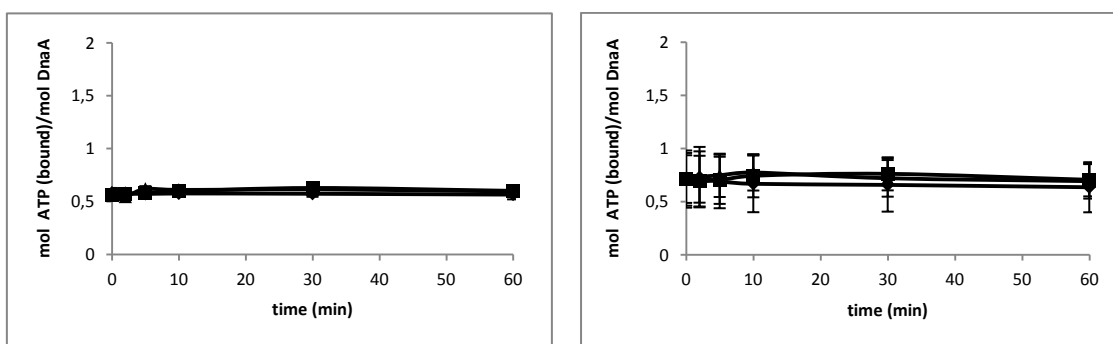
reduced level of ATP-binding was again persistent throughout the reaction period of one hour when incubated at 0°C or 25°C, but was fully abrogated shortly after the beginning of incubation at 37°C, probably due to protein instability of this specific mutant at high temperatures.

[A] (His)<sub>6</sub>-DnaAA163V[B] (His)<sub>6</sub>-DnaAD214N

**Fig. 3.3.2.:** ATP-binding activity determined by filter binding assays using [ $\alpha$ -<sup>32</sup>P]-ATP. Values for molarities of bound ATP/DnaA were calculated from detected counts per minute on the respective filters. A, (His)<sub>6</sub>-DnaAA163V. B, (His)<sub>6</sub>-DnaAD214N. Diamonds: incubation at 0°C. Squares: incubation at 25°C. Triangles: incubation at 37°C.

### 3.3.3. (His)<sub>6</sub>-DnaAE183Q and (His)<sub>6</sub>-DnaAR260A show an approximately 2-fold reduced ATP-binding capacity

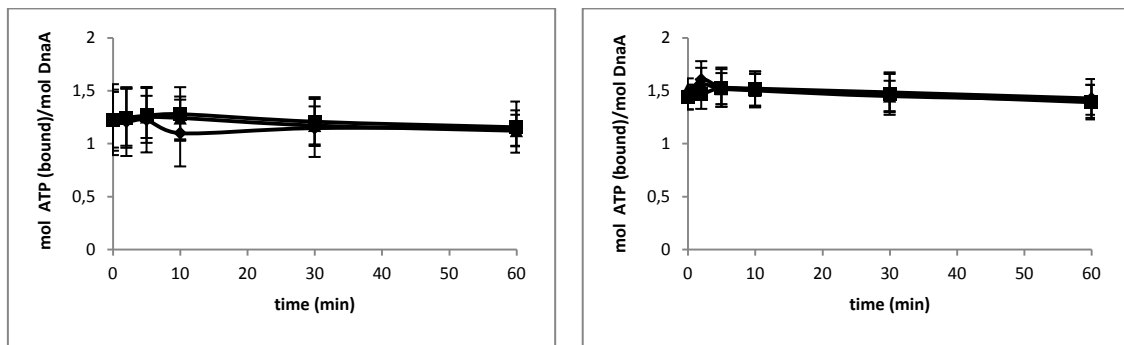
Proteins (His)<sub>6</sub>-DnaAE183Q and (His)<sub>6</sub>-DnaAR260A both show a nearly 2-fold reduced level (2-fold and 1.7-fold, respectively) in their ATP-binding capacities compared to (His)<sub>6</sub>-wtDnaA (Fig. 3.3.3.). Like (His)<sub>6</sub>-wtDnaA, (His)<sub>6</sub>-DnaAE183Q and (His)<sub>6</sub>-DnaAR260A both show immediate saturation with [ $\alpha$ -<sup>32</sup>P]-ATP that is bound with constant concentration in a temperature independent manner over a time period of one hour, but the determined stoichiometries of bound ATP per DnaA monomer were approximately 0.6:1 and 0.7:1 for (His)<sub>6</sub>-DnaAE183Q and (His)<sub>6</sub>-DnaAR260A, respectively.

[A] (His)<sub>6</sub>-DnaAE183Q[B] (His)<sub>6</sub>-DnaAR260A

**Fig. 3.3.3.:** ATP-binding activity determined by filter binding assays using [ $\alpha$ -<sup>32</sup>P]-ATP. Values for molarities of bound ATP/DnaA were calculated from detected counts per minute on the respective filters. A, (His)<sub>6</sub>-DnaAE183Q. B, (His)<sub>6</sub>-DnaAR260A. Diamonds: incubation at 0°C. Squares: incubation at 25°C. Triangles: incubation at 37°C.

### 3.3.4. (His)<sub>6</sub>-DnaAW8A and (His)<sub>6</sub>-DnaAR387C are not significantly affected in their ATP-binding activity

Proteins (His)<sub>6</sub>-DnaAW8A and (His)<sub>6</sub>-DnaAR387C both are not significantly affected either in their affinity nor their capacity in ATP-binding (Fig. 3.3.4.). Similar to (His)<sub>6</sub>-wtDnaA, (His)<sub>6</sub>-DnaAW8A and (His)<sub>6</sub>-DnaAR387C both show an extremely high temperature independent affinity to [ $\alpha$ -<sup>32</sup>P]-ATP and binding reaches saturation directly after incubation with the substrate. The stoichiometries of bound ATP per DnaA monomer were determined as approximately 1.2:1 and 1.5:1 for DnaAW8A and (His)<sub>6</sub>-DnaAR387C, respectively and are nearly similar to (His)<sub>6</sub>-wtDnaA values. However, the deviation to the expected 1:1 stoichiometry presumably results from indirect determination of the molarities of bound ATP per DnaA monomer.

[A] (His)<sub>6</sub>-DnaAW8A[B] (His)<sub>6</sub>-DnaAR387C

**Fig. 3.3.4.:** ATP-binding activity determined by filter binding assays using [ $\alpha$ -<sup>32</sup>P]-ATP. Values for molarities of bound ATP/DnaA were calculated from detected counts per minute on the respective filters. A, (His)<sub>6</sub>-DnaAW8A. B, (His)<sub>6</sub>-DnaAR387C. Diamonds: incubation at 0°C. Squares: incubation at 25°C. Triangles: incubation at 37°C.

## 3.4. ATPase activity of recombinant (His)<sub>6</sub>-wtDnaA/(His)<sub>6</sub>-mutDnaA determined by filter binding assays using [ $\gamma$ -<sup>32</sup>P]-ATP

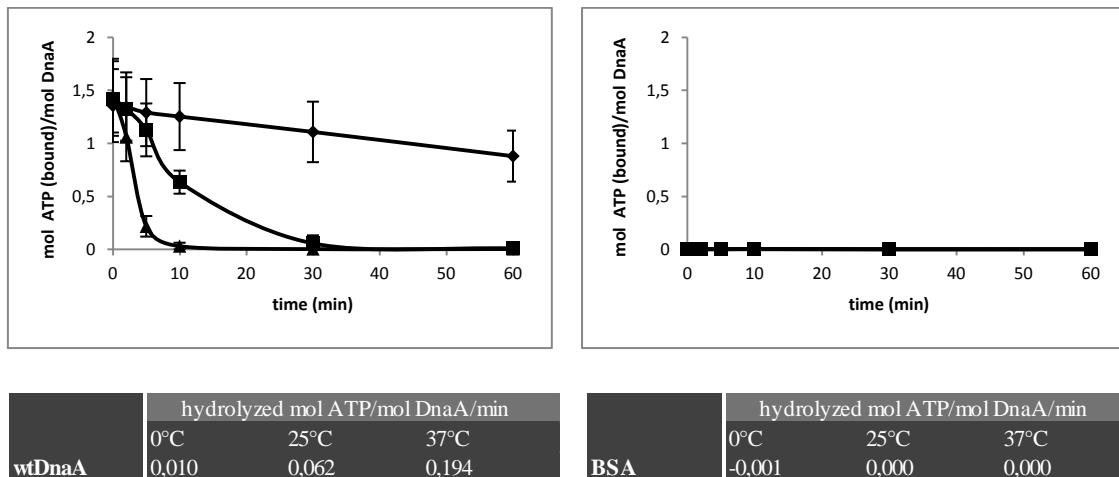
### 3.4.1. (His)<sub>6</sub>-wtDnaA exhibits a weak temperature dependent ATPase activity

DnaA, both from *E. coli* and *B. subtilis*, has been shown to hydrolyze ATP *in vitro*, but the intrinsic ATPase activity is rather weak [11, 99]. These results are consistent with the data determined by filter binding assays using [ $\gamma$ -<sup>32</sup>P]-ATP in this work. The ATPase rate of *B. subtilis* (His)<sub>6</sub>-wtDnaA was dependent on the reaction temperature and displayed its maximum at 37°C with an ATPase rate of 0.19 hydrolyzed mol ATP per mol (His)<sub>6</sub>-wtDnaA per minute (Fig. 3.4.1.). Only single cycles of ATP-hydrolysis were measured, i.e. the protein was first incubated with [ $\gamma$ -<sup>32</sup>P]-ATP and right afterwards treated with a 500-fold molar excess of non-

radiolabeled ATP prior to sample filtration. This prevents rebinding to  $[\gamma\text{-}^{32}\text{P}]\text{-ATP}$  during the measurement and allows to track only one hydrolysis cycle. Again, BSA was used as a negative control and did not show any ATPase activity.

[A]  $(\text{His})_6\text{-wtDnaA}$

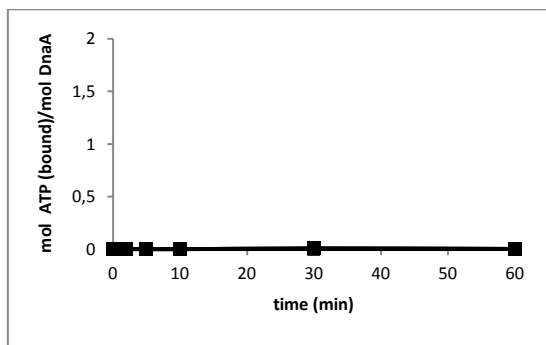
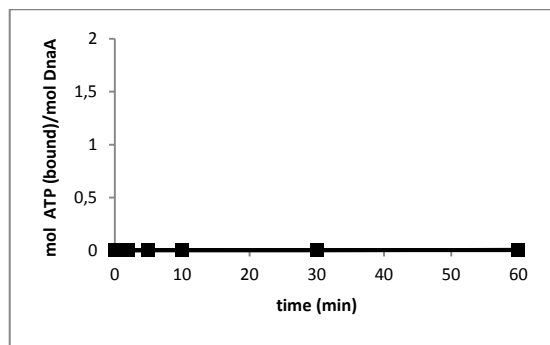
[B] BSA (negative control)



**Fig. 3.4.1.:** ATP-hydrolysis activity determined by filter binding assays using  $[\gamma\text{-}^{32}\text{P}]\text{-ATP}$ . Values for molarities of bound ATP/DnaA and average ATPase rates were calculated from detected counts per minute on the respective filters. A,  $(\text{His})_6\text{-wtDnaA}$ . B, BSA (negative control). Diamonds: incubation at 0°C. Squares: incubation at 25°C. Triangles: incubation at 37°C.

### 3.4.2. $(\text{His})_6\text{-DnaAA163V}$ and $(\text{His})_6\text{-DnaAD214N}$ do not hydrolyze ATP

Neither of both  $(\text{His})_6\text{-DnaAA163V}$  and  $(\text{His})_6\text{-DnaAD214N}$  display any measurable residual ATPase activity (Fig. 3.4.2.). As a consequence of the fact that these mutants do not show any significant ATP-binding capacity (see chapter 3.3.2.), no conclusion can be made about their potentially still functional capacity of hydrolyzing ATP. However, the deficiency of ATP-hydrolysis of both mutants was unaffected of the incubation temperature that varied between 0°C and 37°C. In contrast to the strongly reduced capacity of  $(\text{His})_6\text{-DnaAD214N}$  in ATP-binding when permanently incubated with  $[\alpha\text{-}^{32}\text{P}]\text{-ATP}$ , there is no ATP-binding activity detectable after the consecutive incubation of radiolabeled  $[\gamma\text{-}^{32}\text{P}]\text{-ATP}$  and 500-fold molar excess of non-radiolabeled ATP. This suggests, that ATP-binding of  $(\text{His})_6\text{-DnaAD214N}$  is highly unstable and cannot be maintained for effectively measuring a single cycle of ATP-hydrolysis.

[A] (His)<sub>6</sub>-DnaAA163V[B] (His)<sub>6</sub>-DnaAD214N

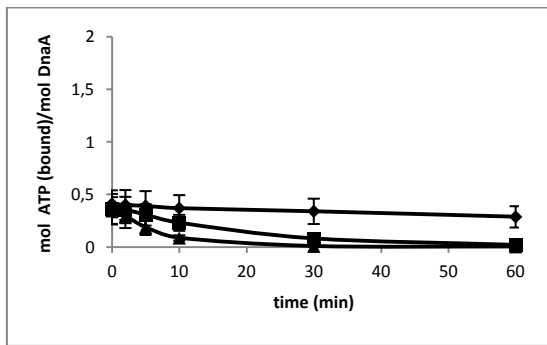
| DnaAA163V | hydrolyzed mol ATP/mol DnaA/min |       |       |
|-----------|---------------------------------|-------|-------|
|           | 0°C                             | 25°C  | 37°C  |
|           | 0,000                           | 0,000 | 0,000 |

| DnaAD214N | hydrolyzed mol ATP/mol DnaA/min |       |       |
|-----------|---------------------------------|-------|-------|
|           | 0°C                             | 25°C  | 37°C  |
|           | 0,001                           | 0,001 | 0,001 |

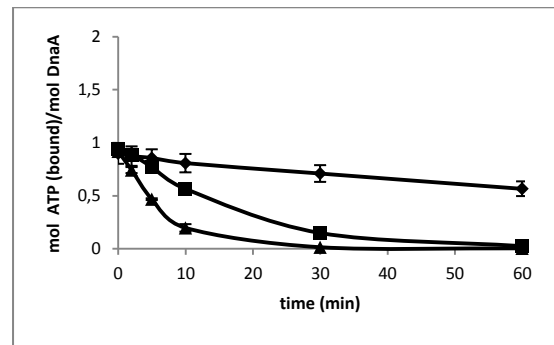
**Fig. 3.4.2.:** ATP-hydrolysis activity determined by filter binding assays using [ $\gamma$ -<sup>32</sup>P]-ATP. Values for molarities of bound ATP/DnaA and average ATPase rates were calculated from detected counts per minute on the respective filters. A, (His)<sub>6</sub>-DnaAA163V. B, (His)<sub>6</sub>-DnaAD214N. Diamonds: incubation at 0°C. Squares: incubation at 25°C. Triangles: incubation at 37°C.

### 3.4.3. (His)<sub>6</sub>-DnaAE183Q ATPase activity is strongly reduced, whereas (His)<sub>6</sub>-DnaAR260A shows a 2-fold reduced ATPase activity

Both proteins, (His)<sub>6</sub>-DnaAE183Q and (His)<sub>6</sub>-DnaAR260A, display an approximately 2-fold (2-fold and 1.7-fold, respectively) reduced ATP-binding activity compared to (His)<sub>6</sub>-wtDnaA (see chapter 3.3.3.), but their particular capacities of ATP-hydrolysis differ dramatically. While the ATPase rate of (His)<sub>6</sub>-DnaAR260A ranges around a 2-fold reduction with its maximum of 0.083 hydrolyzed mol ATP per mol (His)<sub>6</sub>-DnaAR260A per minute at 37°C, (His)<sub>6</sub>-DnaAE183Q shows a strongly decreased ATPase rate, with a reduction between 6-7-fold compared to (His)<sub>6</sub>-wtDnaA levels, according to their respective reaction temperature, i.e. the ATPase rate of (His)<sub>6</sub>-DnaAE183Q reaches its maximum at 0.028 hydrolyzed mol ATP per mol (His)<sub>6</sub>-DnaAE183Q per minute at 37°C (Fig. 3.4.3.). The ATPase activities of both proteins were temperature dependent showing minimal rates at 0°C and maximal activity at 37°C. Nonetheless, it was surprising that the ATP-binding activity of (His)<sub>6</sub>-DnaAR260A at timepoint zero differed reproducibly from the determined one with [ $\alpha$ -<sup>32</sup>P]-ATP (1.3-fold and 1.7-fold reduced, respectively).

[A] (His)<sub>6</sub>-DnaAE183Q

| DnaAE183Q | hydrolyzed mol ATP/mol DnaA/min |       |       |
|-----------|---------------------------------|-------|-------|
|           | 0°C                             | 25°C  | 37°C  |
|           | 0,004                           | 0,010 | 0,028 |

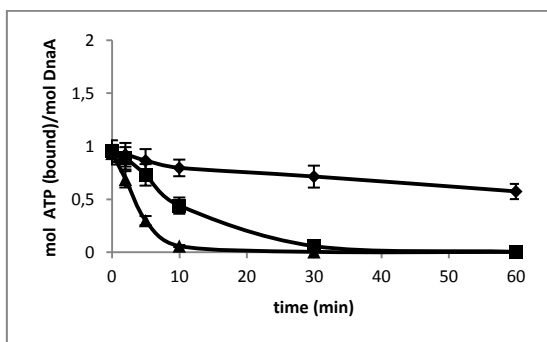
[B] (His)<sub>6</sub>-DnaAR260A

| DnaAR260A | hydrolyzed mol ATP/mol DnaA/min |       |       |
|-----------|---------------------------------|-------|-------|
|           | 0°C                             | 25°C  | 37°C  |
|           | 0,010                           | 0,031 | 0,083 |

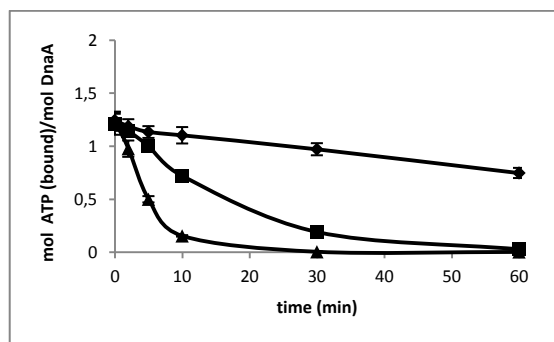
**Fig. 3.4.3.:** ATP-hydrolysis activity determined by filter binding assays using [ $\gamma$ -<sup>32</sup>P]-ATP. Values for molarities of bound ATP/DnaA and average ATPase rates were calculated from detected counts per minute on the respective filters. A, (His)<sub>6</sub>-DnaAE183Q. B, (His)<sub>6</sub>-DnaAR260A. Diamonds: incubation at 0°C. Squares: incubation at 25°C. Triangles: incubation at 37°C.

#### 3.4.4. (His)<sub>6</sub>-DnaAW8A and (His)<sub>6</sub>-DnaAR387C are not significantly affected in their respective ATPase activities

Proteins (His)<sub>6</sub>-DnaAW8A and (His)<sub>6</sub>-DnaAR387C both are not significantly affected in their ATPase activities (Fig. 3.4.4.). The ATPase rates slightly differ from (His)<sub>6</sub>-wtDnaA, with an approximate reduction of 1.5-fold. The ATPase activities were temperature dependent in a manner of increasing ATPase rates at increasing temperatures. However, the slight differences of the ATPase activity between (His)<sub>6</sub>-wtDnaA and (His)<sub>6</sub>-DnaAW8A and (His)<sub>6</sub>-DnaAR387C might result from indirectly determining the molarities of bound ATP per DnaA monomer.

[A] (His)<sub>6</sub>-DnaAW8A

| DnaAW8A | hydrolyzed mol ATP/mol DnaA/min |       |       |
|---------|---------------------------------|-------|-------|
|         | 0°C                             | 25°C  | 37°C  |
|         | 0,008                           | 0,043 | 0,112 |

[B] (His)<sub>6</sub>-DnaAR387C

| DnaAR387C | hydrolyzed mol ATP/mol DnaA/min |       |       |
|-----------|---------------------------------|-------|-------|
|           | 0°C                             | 25°C  | 37°C  |
|           | 0,021                           | 0,041 | 0,128 |

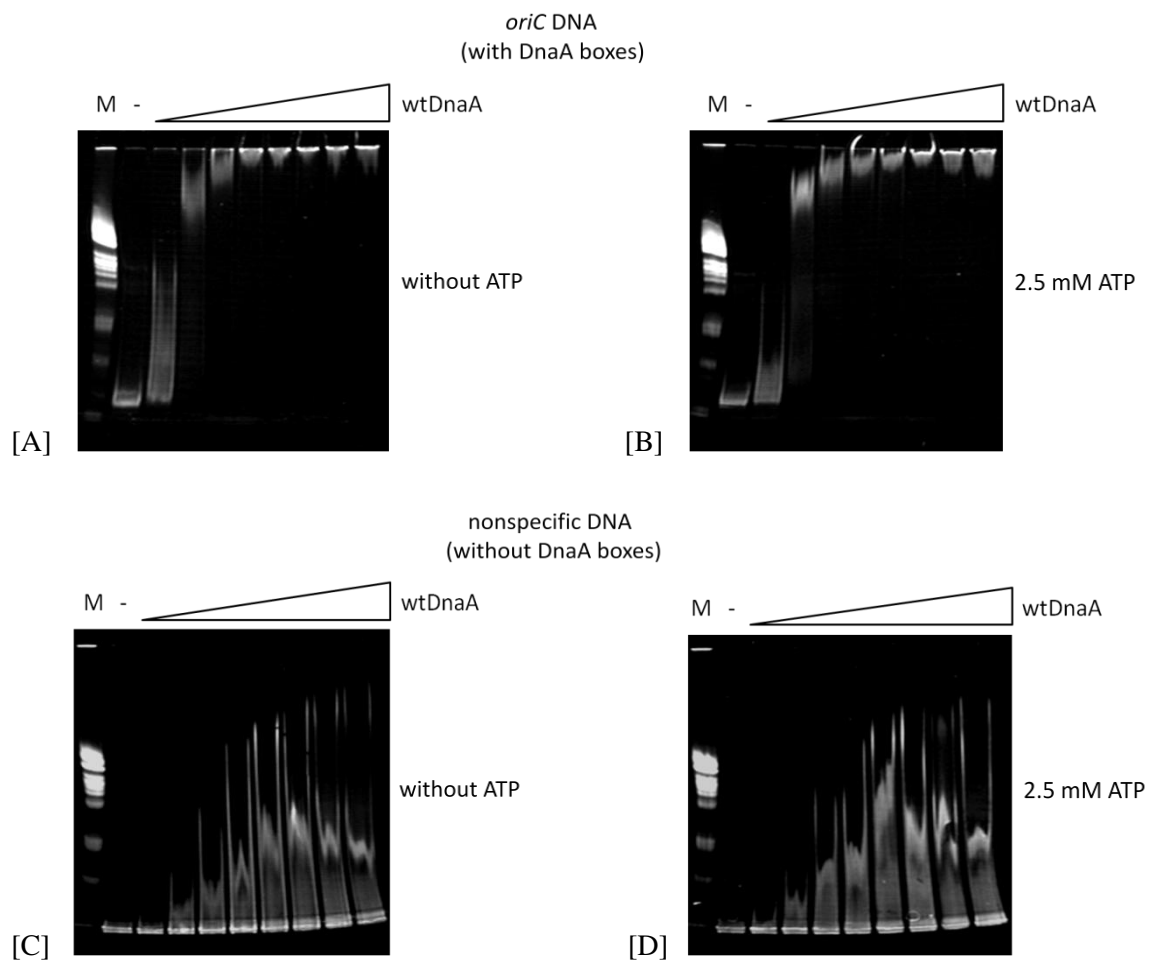
**Fig. 3.4.4.:** ATP-hydrolysis activity determined by filter binding assays using [ $\gamma$ -<sup>32</sup>P]-ATP. Values for molarities of bound ATP/DnaA and average ATPase rates were calculated from detected counts per minute on the respective filters. A, (His)<sub>6</sub>-DnaAW8A. B, (His)<sub>6</sub>-DnaAR387C. Diamonds: incubation at 0°C. Squares: incubation at 25°C. Triangles: incubation at 37°C.

### 3.5. DNA-binding activity of recombinant (His)<sub>6</sub>-wtDnaA/(His)<sub>6</sub>-mutDnaA determined by electrophoretic mobility shift assays (EMSA) and surface plasmon resonance (SPR)

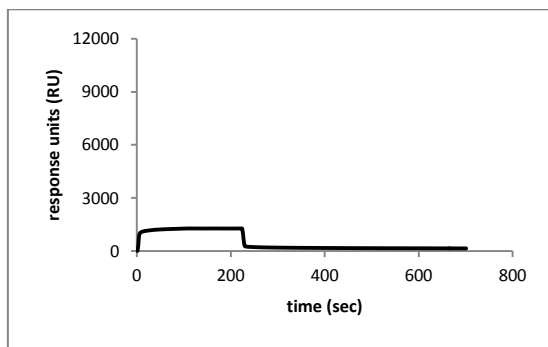
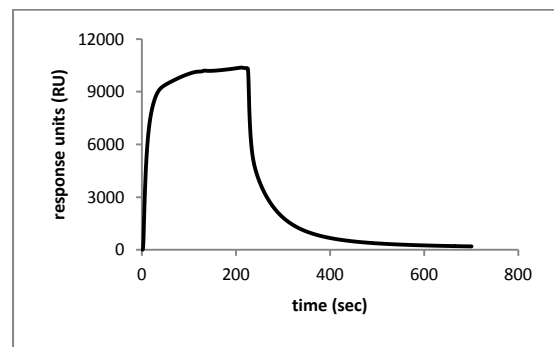
#### 3.5.1. (His)<sub>6</sub>-wtDnaA exhibits a cofactor-dependent sequence specific DNA-binding activity

*E. coli* DnaA and *B. subtilis* DnaA display a very specific DNA-binding activity [11, 99]. Previous studies showed that DnaA protein from both organisms binds sequence specifically to DnaA-box containing double-stranded DNA [11, 99]. The affinity of DnaA to these DnaA-boxes is dependent on the type of DnaA-boxes, i.e. high- or low affinity boxes, and of the bound cofactor, i.e. ATP or ADP [6, 11, 99]. To make sure, that the conditions of protein purification and storage allow full activity of (His)<sub>6</sub>-wtDnaA, DNA-binding control experiments have been carried out. Binding of (His)<sub>6</sub>-wtDnaA can be measured by electromobility shift assays (EMSA). Therefore, increasing amounts of (His)<sub>6</sub>-wtDnaA were incubated for 30 minutes at room temperature with specific DNA, i.e. linear DnaA-box containing *oriC*-DNA or nonspecific DNA, i.e. linear DNA without DnaA-boxes both in the presence or absence of 2.5 mM ATP. As expected, (His)<sub>6</sub>-wtDnaA binds sequence specifically to DNA (Fig. 3.5.1.1.). Interestingly, a small amount of transient unstable binding events of nonspecific DNA occurred (weak DNA-shifting), though the main fraction of DNA remained unbound. However, the DNA-binding capacity was not affected when either incubated with or without ATP. The determined values for the apparent binding constant  $K_{app}$ , referred to as the protein concentration at which half of the total amount of (*oriC*-) DNA in the reaction is bound (room temperature, pH 7.6), both in the presence or absence of ATP were similar and approximately 0.8  $\mu$ M (50% saturation with 43.5 nM *oriC*-DNA). Thus, no conclusion can be made about the cofactor-dependent DNA-binding affinity of (His)<sub>6</sub>-wtDnaA to specific DNA by EMSA. To approach this question surface plasmon resonance (SPR) technique was used. For this purpose, the same linear *oriC*-containing DNA-molecules used for EMSA were biotinylated both at its 5' and 3' ends and noncovalently bound to a streptavidin coated sensor chip. (His)<sub>6</sub>-wtDnaA preincubated for one minute with or without 2.5 mM ATP was subsequently applied to the sensor chip at room temperature. The Biacore 3000 apparatus used for these measurements detects a real-time deviation of the angle of a laser beam that is focused on and reflected from the surface of the sensor chip [92]. This deviation is a result of a change in the mass concentration due to binding events to the surface-bound DNA (ligand) by the applied (His)<sub>6</sub>-wtDnaA (analyte) and measured as resonance/response units (RU) [92]. As expected, there is a significant difference of the affinity of (His)<sub>6</sub>-wtDnaA to specific DNA when incubated with or without ATP (1300 RU and 10000 RU, respectively), i.e. the capacity of (His)<sub>6</sub>-wtDnaA to bind DnaA-box containing DNA is 7.7-fold increased in the presence of ATP (Fig. 3.5.1.2.). The DNA-binding reaction can be separated into three different phases, both in the presence and absence of ATP.

During ongoing loading of  $(\text{His})_6\text{-wtDnaA}$  to the sensor chip, binding to the DNA occurs first as a sharp increase of the resonance units (I) until it reaches saturation (II) that can be described as the equilibrium of consecutive binding and dissociation events of  $(\text{His})_6\text{-wtDnaA}$  to the limited amount of DNA-molecules on the sensor chip surface. Once loading of  $(\text{His})_6\text{-wtDnaA}$  stops, only dissociation of the protein can be measured and occurs as a rather fast decrease of the resonance units (III). It is noteworthy that the stability of the DNA-binding events appears to be stronger in the presence of ATP, as dissociation reaches its minimum considerably later than in the absence of ATP.



**Fig. 3.5.1.1.:** Electromobility shift assays [EMSA] with increasing amounts [0-80 pmol] of  $(\text{His})_6\text{-wtDnaA}$  and different DNA substrates [0.9 pmol] under ATP-containing and ATP-free conditions. Samples were run in native polyacrylamide gradient gels [4-12%]. A, EMSA without ATP; linear *oriC*-DNA substrate. B, EMSA with 2.5 mM ATP; linear *oriC*-DNA substrate. C, EMSA without ATP; nonspecific DNA substrate. B, EMSA with 2.5 mM ATP; nonspecific DNA substrate. M, marker. Black bar: no protein content.

[A] SPR (His)<sub>6</sub>-wtDnaA (without ATP)[B] SPR (His)<sub>6</sub>-wtDnaA (with 2.5 mM ATP)

**Fig. 3.5.1.2.:** Surface plasmon resonance [SPR] experiments with (His)<sub>6</sub>-wtDnaA [2.5 μM] binding to double-biotinylated [5′ and 3′ ends] *oriC*-DNA [0.25 pmol] that is bound to a streptavidin coated sensor chip surface. The protein sample [75 μl] was loaded to the chip at a flow rate of 20 μl/min, i.e. for 225 seconds, followed by protein dissociation from the DNA. Protein-DNA interactions were measured as response units [RU] in real time over a period of 700 seconds. All values represent the difference of absolute measured response units that have been subtracted from unspecific binding events in a control flow chamber. A, SPR without ATP. B, SPR with 2.5 mM ATP.

### 3.5.2. (His)<sub>6</sub>-DnaAR387C displays a strongly reduced DNA-binding activity

The first mutant DnaA tested for its DNA-binding features was (His)<sub>6</sub>-DnaAR387C that was predicted to be DNA-binding deficient and should serve as an appropriate negative control, both for the EMSA and the experimental SPR setup. The apparent binding constants of (His)<sub>6</sub>-DnaAR387C both in the presence or absence of ATP could not be determined, since retention of only a small DNA-fraction was observed (Fig. 3.5.2.1.). This binding activity to specific *oriC*-DNA resembled strongly to that one of (His)<sub>6</sub>-wtDnaA incubated with nonspecific DNA (Fig. 3.5.1.1.). Similar to this protein-DNA interaction of (His)<sub>6</sub>-wtDnaA a weak shifting of *oriC*-DNA by (His)<sub>6</sub>-DnaAR387C could be observed, suggesting that a small amount of unstable transient binding events occurred.

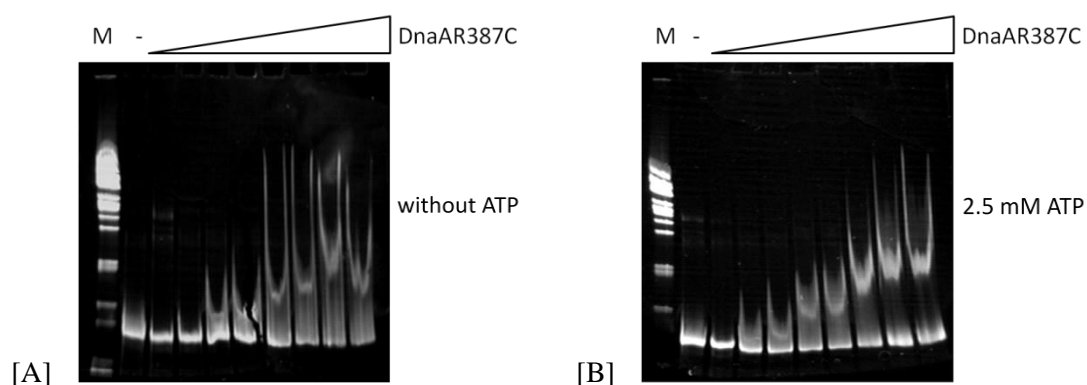


**Fig. 3.5.2.1.:** Electromobility shift assays [EMSA] with increasing amounts [0-80 pmol] of (His)<sub>6</sub>-DnaAR387C and DnaA-box containing *oriC*-DNA [0.9 pmol] under ATP-containing and ATP-free conditions. Samples were run in native polyacrylamide gradient gels [4-12%]. A, EMSA without ATP; linear *oriC*-DNA. B, EMSA with 2.5 mM ATP; linear *oriC*-DNA. M. marker. Black bar: no protein content.

SPR experiments, performed in order to study the low affinity and the real-time binding events of (His)<sub>6</sub>-DnaAR387C did not show any interaction of the protein to the sensor chip bound DNA beyond background levels (Fig. 3.5.2.2.). This was independent of the presence or absence of ATP.

[A] (His)<sub>6</sub>-DnaAR387C (without ATP)

[B] (His)<sub>6</sub>-DnaAR387C (with 2.5 mM ATP)

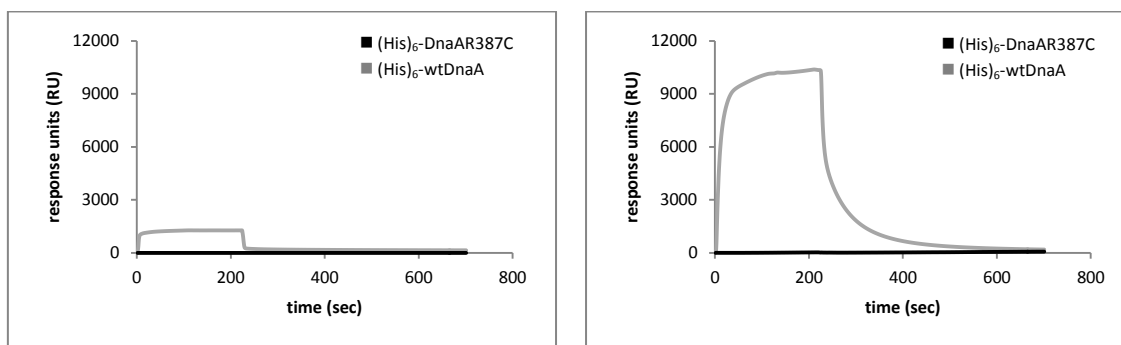


**Fig. 3.5.2.2.:** Surface plasmon resonance [SPR] experiments with (His)<sub>6</sub>-DnaAR387C [2.5 μM] binding to double-biotinylated [5′ and 3′ ends] *oriC*-DNA [0.25 pmol] that is bound to a streptavidin coated sensor chip surface. The protein sample [75 μl] was loaded to the chip at a flow rate of 20 μl/min, i.e. for 225 seconds, followed by protein dissociation from the DNA. Protein-DNA interactions were measured as response units [RU] in real time over a period of 700 seconds. All values represent the difference of absolute measured response units that have been subtracted from unspecific binding events in a control flow chamber. Black line: (His)<sub>6</sub>-DnaAR387C. Grey line: (His)<sub>6</sub>-wtDnaA. A, SPR without ATP. B, SPR with 2.5 mM ATP.

### 3.5.3. (His)<sub>6</sub>-DnaAA163V exhibits a stable cofactor-independent DNA-binding activity

Electromobility shift assays with increasing amounts of (His)<sub>6</sub>-DnaAA163V show a very strong cofactor independent DNA retention when incubated with linear DnaA-box containing DNA, i.e. binding of (His)<sub>6</sub>-DnaAA163V to *oriC*-DNA occurs in a non-stepwise manner suggesting that only one type of DNA-binding complexes is formed (Fig. 3.5.3.1.). The determined apparent constant of binding of (His)<sub>6</sub>-DnaAA163V ( $K_{app}$  0.8 μM) is similar to (His)<sub>6</sub>-wtDnaA ( $K_{app}$  0.8 μM), suggesting that (His)<sub>6</sub>-DnaAA163V shows full DNA-binding activity. Moreover, SPR experiments of (His)<sub>6</sub>-DnaAA163V revealed that binding to *oriC*-DNA is not affected in the presence or absence of ATP in the medium. Under the conditions tested, (His)<sub>6</sub>-DnaAA163V showed a reproducible strong response with a maximum of around 7000 RU both in the presence and absence of ATP (Fig. 3.5.3.2.). Beside the differences in the measured values in comparison to (His)<sub>6</sub>-wtDnaA, (His)<sub>6</sub>-DnaAA163V does not reach saturation during ongoing application, but a continuous decelerated accumulation on the DNA after a short but intense initial increase of the RU upon addition of the protein, indicating a reduced affinity to *oriC*-DNA. Furthermore, no significant dissociation from the DNA could be observed, suggesting that the established protein-DNA interaction is highly stable.

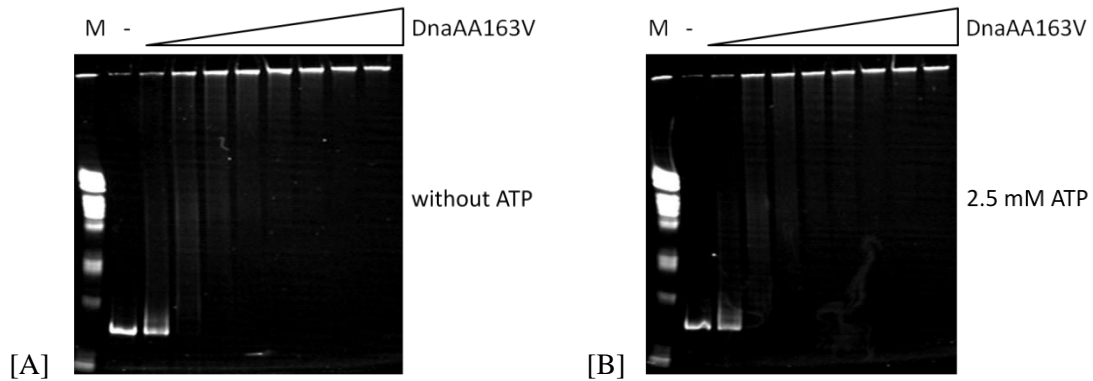


**Fig. 3.5.3.1.:** Electromobility shift assays [EMSA] with increasing amounts [0-80 pmol] of  $(\text{His})_6$ -DnaAA163V and DnaA-box containing *oriC*-DNA [0.9 pmol] under ATP-containing and ATP-free conditions. Samples were run in native polyacrylamide gradient gels [4-12%]. A, EMSA without ATP; linear *oriC*-DNA. B, EMSA with 2.5 mM ATP; linear *oriC*-DNA. M, marker. Black bar: no protein content.

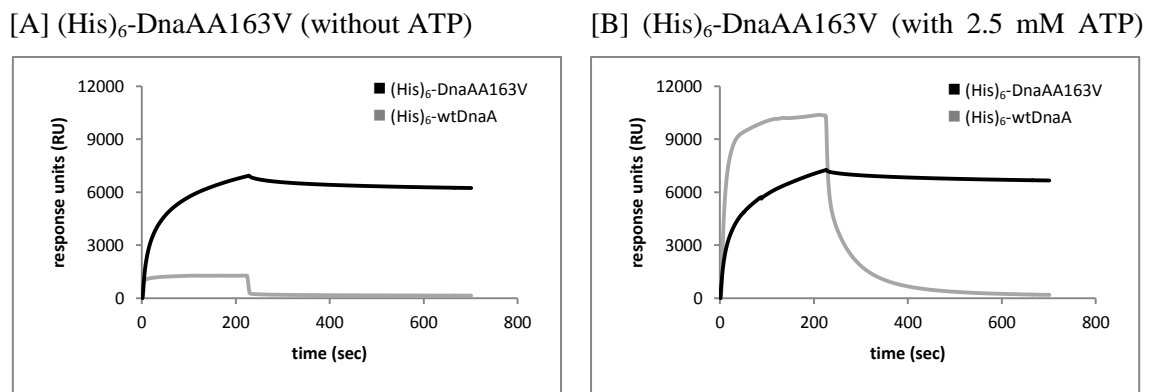


**Fig. 3.5.3.2.:** Surface plasmon resonance [SPR] experiments with  $(\text{His})_6$ -DnaAA163V [2.5  $\mu\text{M}$ ] binding to double-biotinylated [5' and 3' ends] *oriC*-DNA [0.25 pmol] that is bound to a streptavidin coated sensor chip surface. The protein sample [75  $\mu\text{l}$ ] was loaded to the chip at a flow rate of 20  $\mu\text{l}/\text{min}$ , i.e. for 225 seconds, followed by protein dissociation from the DNA. Protein-DNA interactions were measured as response units [RU] in real time over a period of 700 seconds. All values represent the difference of absolute measured response units that have been subtracted from unspecific binding events in a control flow chamber. Black line:  $(\text{His})_6$ -DnaAA163V. Grey line:  $(\text{His})_6$ -wtDnaA. A, SPR without ATP. B, SPR with 2.5 mM ATP.

#### 3.5.4. $(\text{His})_6$ -DnaAE183Q has an abrogated cofactor-dependent differential DNA-binding activity

EMSA experiments with  $(\text{His})_6$ -DnaAE183Q showed an ATP independent DNA retention when incubated with linear *oriC*-DNA. Like  $(\text{His})_6$ -wtDnaA  $(\text{His})_6$ -DnaAE183Q ( $K_{app}$  1  $\mu\text{M}$ ) formed high-molecular weight complexes (HMWCs) that led to DNA retention on the top of the gel (Fig. 3.5.4.1.). Intriguingly, in sharp contrast to  $(\text{His})_6$ -wtDnaA the DNA-shifting of  $(\text{His})_6$ -DnaAE183Q occurred in two phases whereby a considerable amount of the DNA was retained by an intermediate complex in the middle of the gel within a broad range of protein concentrations, while the remaining DNA was further shifted. This suggests that  $(\text{His})_6$ -

DnaAE183Q constitutes two different major DNA-binding competent complexes. Another difference when compared to  $(\text{His})_6\text{-wtDnaA}$  was the capacity of  $(\text{His})_6\text{-DnaAE183Q}$  to shift DNA as a high-molecular weight complex only at very high protein concentrations (4  $\mu\text{M}$ ) after long incubation times (30 minutes), which indicates that not DNA-affinity but the DNA-binding stability of  $(\text{His})_6\text{-DnaAE183Q}$  is rather low.

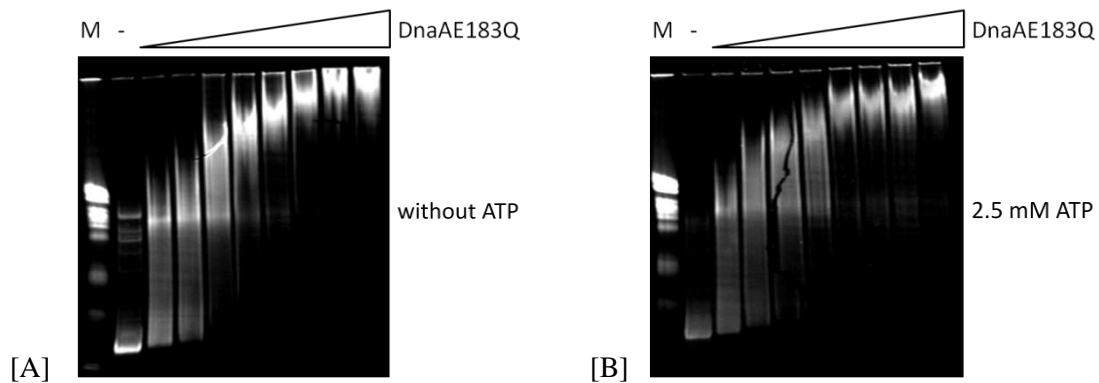
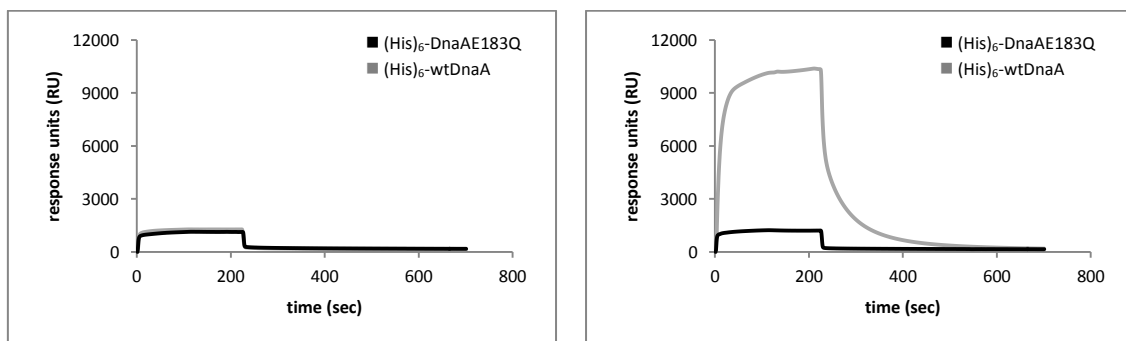


**Fig. 3.5.4.1.:** Electromobility shift assays [EMSA] with increasing amounts [0-80 pmol] of  $(\text{His})_6\text{-DnaAE183Q}$  and DnaA-box containing *oriC*-DNA [0.9 pmol] under ATP-containing and ATP-free conditions. Samples were run in native polyacrylamide gradient gels [4-12%]. A, EMSA without ATP; linear *oriC*-DNA. B, EMSA with 2.5 mM ATP; linear *oriC*-DNA. M, marker. Black bar: no protein content.

SPR experiments of  $(\text{His})_6\text{-DnaAE183Q}$  clearly showed that the binding characteristics to *oriC*-DNA in the absence of ATP, including affinity, saturation levels (1300 RU) and dissociation rates were similar to those of  $(\text{His})_6\text{-wtDnaA}$ . But strikingly, in the presence of ATP the response was nearly identical (Fig. 3.5.4.2.). Intermediate and high-molecular weight complex formation as observed in EMSA probably occurred during the rather long incubation time of protein and DNA, but was not detectable in real-time SPR measurements.

[A]  $(\text{His})_6\text{-DnaAE183Q}$  (without ATP)

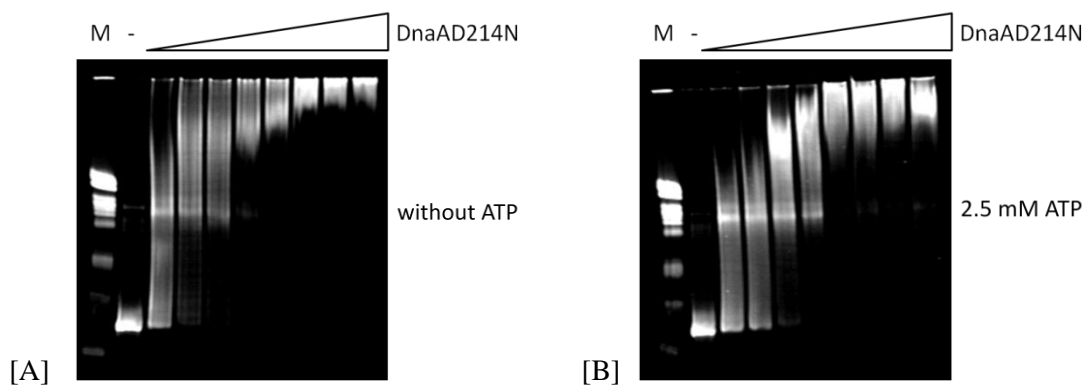
[B]  $(\text{His})_6\text{-DnaAE183Q}$  (with 2.5 mM ATP)



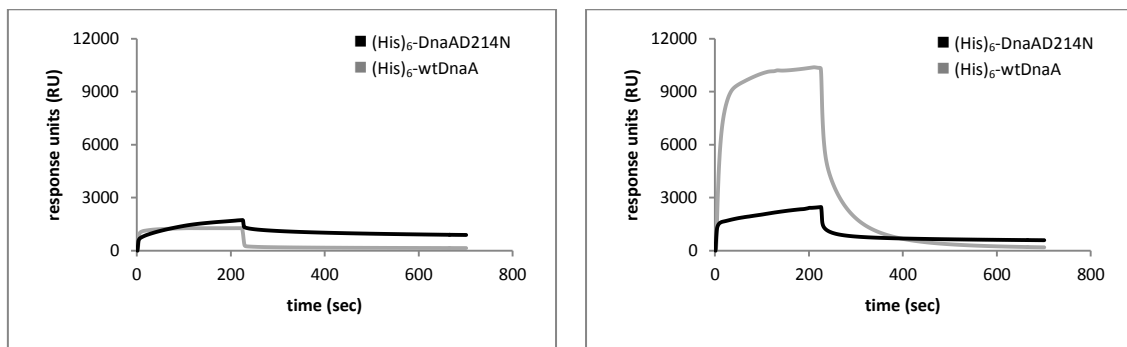
**Fig. 3.5.4.2.:** Surface plasmon resonance [SPR] experiments with  $(\text{His})_6\text{-DnaAE183Q}$  [2.5  $\mu\text{M}$ ] binding to double-biotinylated [5' and 3' ends] *oriC*-DNA [0.25 pmol] that is bound to a streptavidin coated sensor chip surface. The protein sample [75  $\mu\text{l}$ ] was loaded to the chip at a flow rate of 20  $\mu\text{l}/\text{min}$ , i.e. for 225 seconds, followed by protein dissociation from the DNA. Protein-DNA interactions were measured as response units [RU] in real time over a period of 700 seconds. All values represent the difference of absolute measured response units that have been subtracted from unspecific binding events in a control flow chamber. Black line:  $(\text{His})_6\text{-DnaAE183Q}$ . Grey line:  $(\text{His})_6\text{-wtDnaA}$ . A, SPR without ATP. B, SPR with 2.5 mM ATP.

### 3.5.5. (His)<sub>6</sub>-DnaAD214N displays a strongly reduced cofactor-dependent differential DNA-binding activity

EMSA experiments with (His)<sub>6</sub>-DnaAD214N incubated with linear *oriC*-DNA display strong similarities with those of (His)<sub>6</sub>-DnaAE183Q, hence an ATP independent DNA retention, an apparent binding constant  $K_{app}$  1  $\mu$ M, formation of an intermediate complex and the requirement of very high protein levels (4  $\mu$ M) to form DNA-binding competent high-molecular weight complexes (Fig. 3.5.5.1.). However, the DNA-binding characteristics of (His)<sub>6</sub>-DnaAD214N and (His)<sub>6</sub>-DnaAE183Q showed several differences when analyzed by SPR. Both in the presence and absence of ATP, binding of (His)<sub>6</sub>-DnaAD214N to the sensor chip bound DNA occurred as a short but very sharp increase of the resonance units, which was followed by a continuous decelerated but not saturated accumulation of the protein until loading stopped and dissociation from the DNA took place (Fig. 3.5.5.2.). Dissociation was very weak in the absence of ATP and thus protein-DNA interactions seemed to be rather stable under these conditions. Moreover, the maximal response reached was 1700 RU without and 2500 RU with ATP, thus respectively 1.3- and 2-fold higher than for (His)<sub>6</sub>-wtDnaA in the absence of ATP. Besides, dissociation from the DNA was promoted by ATP, since two times more protein dissociated when incubated with 2.5 mM ATP. Though, dissociation reached its minimum at a much higher level than (His)<sub>6</sub>-wtDnaA.



**Fig. 3.5.5.1.:** Electromobility shift assays [EMSA] with increasing amounts [0-80 pmol] of (His)<sub>6</sub>-DnaAD214N and DnaA-box containing *oriC*-DNA [0.9 pmol] under ATP-containing and ATP-free conditions. Samples were run in native polyacrylamide gradient gels [4-12%]. A, EMSA without ATP; linear *oriC*-DNA. B, EMSA with 2.5 mM ATP; linear *oriC*-DNA. M, marker. Black bar: no protein content.

[A] (His)<sub>6</sub>-DnaAD214N (without ATP)[B] (His)<sub>6</sub>-DnaAD214N (with 2.5 mM ATP)

**Fig. 3.5.5.2.:** Surface plasmon resonance [SPR] experiments with (His)<sub>6</sub>-DnaAD214N [2.5 μM] binding to double-biotinylated [5′ and 3′ ends] *oriC*-DNA [0.25 pmol] that is bound to a streptavidin coated sensor chip surface. The protein sample [75 μl] was loaded to the chip at a flow rate of 20 μl/min, i.e. for 225 seconds, followed by protein dissociation from the DNA. Protein-DNA interactions were measured as response units [RU] in real time over a period of 700 seconds. All values represent the difference of absolute measured response units that have been subtracted from unspecific binding events in a control flow chamber. Black line: (His)<sub>6</sub>-DnaAD214N. Grey line: (His)<sub>6</sub>-wtDnaA. A, SPR without ATP. B, SPR with 2.5 mM ATP.

### 3.5.6. (His)<sub>6</sub>-DnaAR260A exhibits a cofactor-dependent DNA-binding activity

Electromobility shift assays with (His)<sub>6</sub>-DnaAR260A showed an ATP independent DNA-retention when incubated with linear *oriC*-DNA ( $K_{app}$  0.8 μM) (Fig. 3.5.6.1.). Similar to (His)<sub>6</sub>-DnaAE183Q and (His)<sub>6</sub>-DnaAD214N, (His)<sub>6</sub>-DnaAR260A forms intermediate complexes and requires very high protein levels (4 μM) to form DNA-binding competent high-molecular weight complexes. Hence, EMSA revealed no differences in the DNA-binding capacities of these three proteins. Nonetheless, SPR analyses showed that (His)<sub>6</sub>-DnaAR260A binds in the absence of ATP to surface bound *oriC*-DNA in a (His)<sub>6</sub>-DnaAD214N like manner, thus as a short but very sharp increase of the resonance units followed by a continuous decelerated but not saturated accumulation up to (His)<sub>6</sub>-wtDnaA levels of around 1400 RU until loading stops and bound (His)<sub>6</sub>-DnaAR260A slowly dissociates from the DNA (Fig. 3.5.6.2.). Though, in the presence of ATP (His)<sub>6</sub>-DnaAR260A reached maximum binding values of around 7000 RU (1.5-fold reduced compared to (His)<sub>6</sub>-wtDnaA).

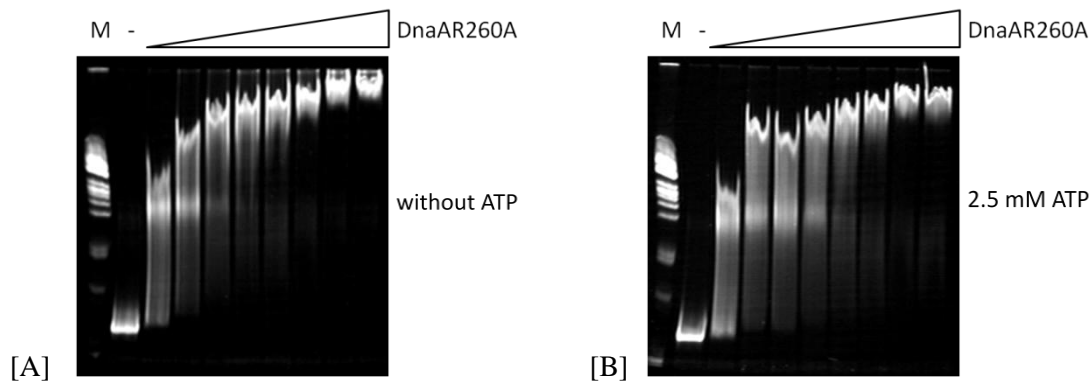


**Fig. 3.5.6.1.:** Electromobility shift assays [EMSA] with increasing amounts [0-80 pmol] of  $(\text{His})_6$ -DnaAR260A and DnaA-box containing *oriC*-DNA [0.9 pmol] under ATP-containing and ATP-free conditions. Samples were run in native polyacrylamide gradient gels [4-12%]. A, EMSA without ATP; linear *oriC*-DNA. B, EMSA with 2.5 mM ATP; linear *oriC*-DNA. M, marker. Black bar: no protein content.

[A]  $(\text{His})_6$ -DnaAR260A (without ATP)

[B]  $(\text{His})_6$ -DnaAR260A (with 2.5 mM ATP)

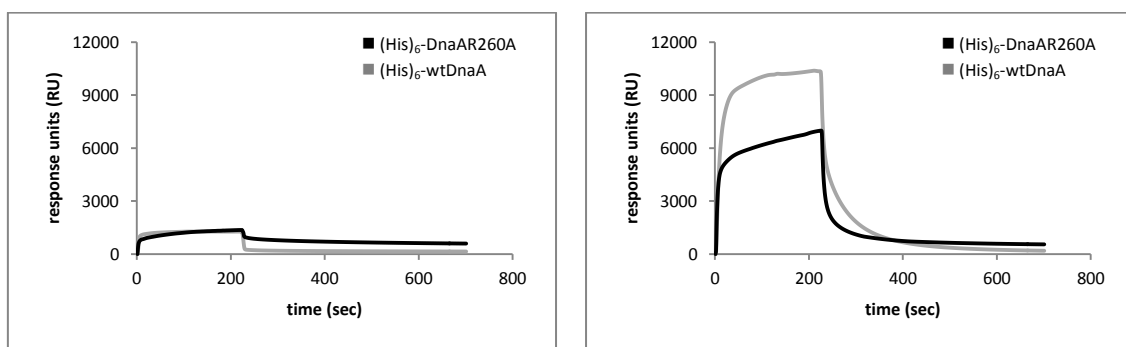


**Fig. 3.5.6.2.:** Surface plasmon resonance [SPR] experiments with  $(\text{His})_6$ -DnaAR260A [2.5  $\mu\text{M}$ ] binding to double-biotinylated [5' and 3' ends] *oriC*-DNA [0.25 pmol] that is bound to a streptavidin coated sensor chip surface. The protein sample [75  $\mu\text{l}$ ] was loaded to the chip at a flow rate of 20  $\mu\text{l}/\text{min}$ , i.e. for 225 seconds, followed by protein dissociation from the DNA. Protein-DNA interactions were measured as response units [RU] in real time over a period of 700 seconds. All values represent the difference of absolute measured response units that have been subtracted from unspecific binding events in a control flow chamber. Black line:  $(\text{His})_6$ -DnaAR260A. Grey line:  $(\text{His})_6$ -wtDnaA. A, SPR without ATP. B, SPR with 2.5 mM ATP.

3.5.7.  $(\text{His})_6$ -DnaAW8A exhibits a cofactor-independent strongly reduced capacity in the formation of DNA-binding competent high-molecular weight complexes

EMSA experiments with  $(\text{His})_6$ -DnaAW8A showed an unaffected DNA-binding activity ( $K_{app}$  0.8  $\mu\text{M}$ ). Strikingly, the detected protein-DNA complexes had a significantly lower molecular weight than those constituted with  $(\text{His})_6$ -wtDnaA (Fig. 3.5.7.1.).

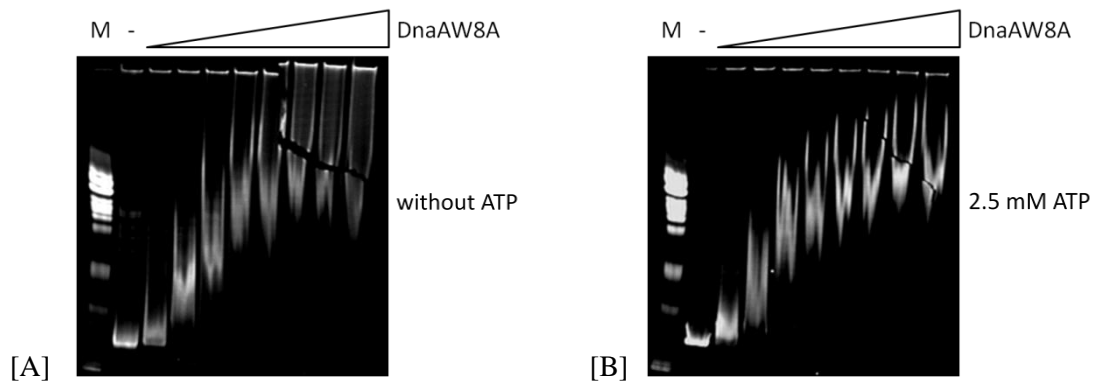
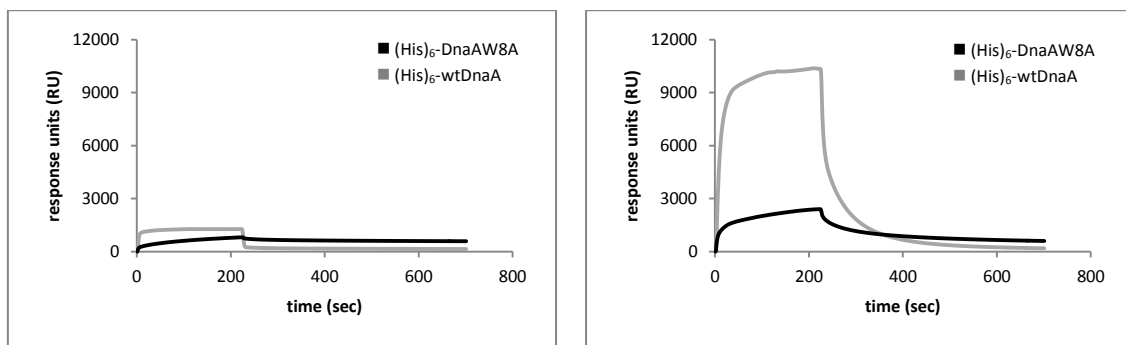


**Fig. 3.5.7.1.:** Electromobility shift assays [EMSA] with increasing amounts [0-80 pmol] of  $(\text{His})_6$ -DnaAW8A and DnaA-box containing *oriC*-DNA [0.9 pmol] under ATP-containing and ATP-free conditions. Samples were run in native polyacrylamide gradient gels [4-12%]. A, EMSA without ATP; linear *oriC*-DNA. B, EMSA with 2.5 mM ATP; linear *oriC*-DNA. M, marker. Black bar: no protein content.

SPR analyses examining the binding characteristics of  $(\text{His})_6$ -DnaAW8A to *oriC*-DNA clearly showed a strongly reduced maximal signal, both in the presence (2500 RU) and absence (800 RU) of ATP when compared to  $(\text{His})_6$ -wtDnaA (10000 RU and 1300 RU, respectively) (Figs. 3.5.7.2. and 3.5.1.2., respectively). In addition, the SPR interaction curves also showed a significantly decreased affinity to DNA. In the absence of ATP, binding of  $(\text{His})_6$ -DnaAW8A to the sensor chip bound DNA occurred as a rather weak but continuous increase of the resonance units without reaching saturation during loading. The established protein-DNA interactions were probably highly stable, since dissociation was very low.

[A]  $(\text{His})_6$ -DnaAW8A (without ATP)

[B]  $(\text{His})_6$ -DnaAW8A (with 2.5 mM ATP)

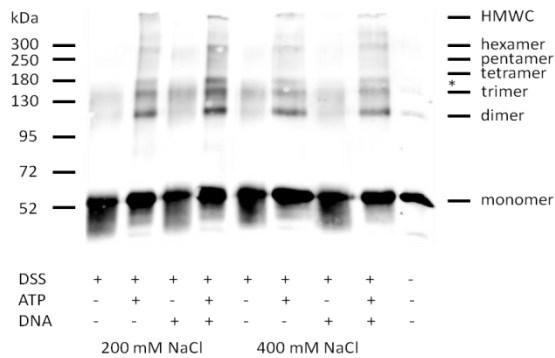
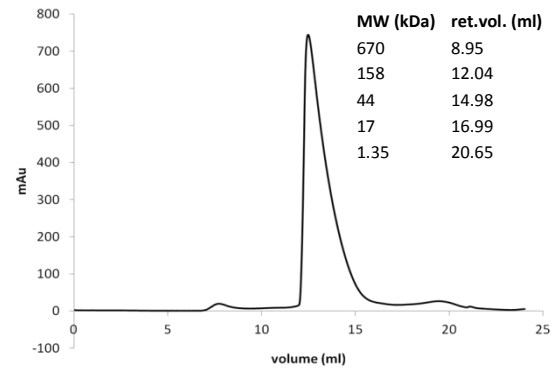


**Fig. 3.5.7.2.:** Surface plasmon resonance [SPR] experiments with  $(\text{His})_6$ -DnaAW8A [2.5  $\mu\text{M}$ ] binding to double-biotinylated [5' and 3' ends] *oriC*-DNA [0.25 pmol] that is bound to a streptavidin coated sensor chip surface. The protein sample [75  $\mu\text{l}$ ] was loaded to the chip at a flow rate of 20  $\mu\text{l}/\text{min}$ , i.e. for 225 seconds, followed by protein dissociation from the DNA. Protein-DNA interactions were measured as response units [RU] in real time over a period of 700 seconds. All values represent the difference of absolute measured response units that have been subtracted from unspecific binding events in a control flow chamber. Black line:  $(\text{His})_6$ -DnaAW8A. Grey line:  $(\text{His})_6$ -wtDnaA. A, SPR without ATP. B, SPR with 2.5 mM ATP.

### 3.6. Multimer formation capacity of recombinant (His)<sub>6</sub>-wtDnaA/ (His)<sub>6</sub>-mutDnaA determined by disuccinimidyl suberate crosslinking assays

#### 3.6.1. (His)<sub>6</sub>-wtDnaA exhibits a cofactor-dependent self-oligomerization capacity

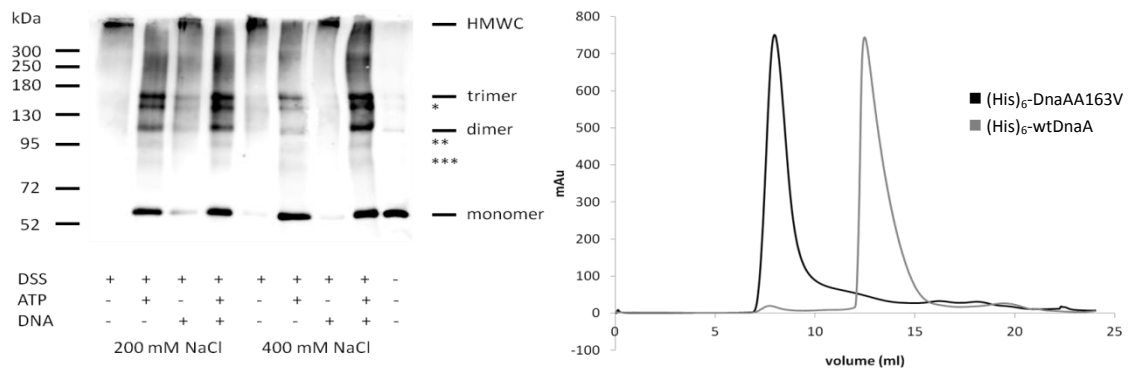
DnaA self-oligomerization at *oriC* is required to constitute a functional pre-RC [1, 4, 7, 25, 41, 75]. It has been shown that different factors such as DiaA and IHF are promoting multimerization in *E. coli* [18, 63, 73]. However, *E. coli* DnaA can also form multimeric structures in the absence of DNA or such accessory factors if only ATP is available. DnaA remains imperatively monomeric in the absence of ATP or an artificial non-hydrolyzable ATP-analogue, such as AMP-PCP [2, 7, 23, 75]. The multimerization capacity of (His)<sub>6</sub>-wtDnaA from *B. subtilis* was examined using disuccinimidyl suberate (DSS) crosslinking assays. Thus, (His)<sub>6</sub>-wtDnaA was incubated at different salt concentrations in the absence or presence of 2.5 mM ATP and/or linear *oriC*-DNA. Right after an incubation of five minutes at room temperature DSS (amine-to-amine crosslinker) was added and the reaction continued for another five minutes. Subsequently, SDS-loading buffer was applied and the samples were run in an 8% SDS-PAGE prior to immunoblotting with anti-DnaA antibodies. It was confirmed, that (His)<sub>6</sub>-wtDnaA constitutes high-molecular weight complexes (HMWCs) far bigger than 300 kDa only in the presence of ATP, whereas ATP-free conditions led to homo-dimer and homo-trimer formation (Fig. 3.6.1.A). This was consistent with the observation that (His)<sub>6</sub>-wtDnaA eluted as a trimer when purified by size-exclusion chromatography in the absence of ATP (Fig. 3.6.1.B). Nonetheless, self-multimerization of (His)<sub>6</sub>-wtDnaA seems to be slightly stimulated by *oriC*-DNA, since a certain amount of the protein-fraction was retained at approximately 270 kDa that corresponds to the size of a DnaA-pentamer. However, this feature could no longer be seen at 400 mM NaCl. Moreover, an additional band with a size of around 180 kDa (\*) that does not correspond to any possible multiple protomeric constitution of (His)<sub>6</sub>-wtDnaA was present in the blot, irrespective of the particular salt concentration. This unexpected structure might result from partly degraded protein particles that have been crosslinked. Besides, though it appears contradictory that despite identical protein concentrations in the samples the detected signal intensity varied strongly within one blot, particularly between samples containing and lacking ATP, this observation could not be assigned to inaccurate protein contents, but rather seems to be due to a molecular stabilization of (His)<sub>6</sub>-wtDnaA protomers through interaction with ATP, since this effect was perfectly reproducible.

[A] DSS-crosslink of (His)<sub>6</sub>-wtDnaA[B] Gelfiltration of (His)<sub>6</sub>-wtDnaA

**Fig. 3.6.1.:** Self-multimerization of (His)<sub>6</sub>-wtDnaA. A, disuccinimidyl suberate [DSS] crosslinking assays with DSS [125 μM], (His)<sub>6</sub>-wtDnaA [500 nM] under different NaCl concentrations [200 mM, 400 mM] and in the absence [-] or presence [+] of ATP [2.5 mM] and linear DnaA-box containing *oriC*-DNA [36.4 nM]. Samples were immunoblotted with anti-DnaA antibodies. B, Size-exclusion chromatography profile (Superdex 200 10/300 GL column) of a (His)<sub>6</sub>-wtDnaA containing fraction after purification. The major peak shows the native trimeric state of (His)<sub>6</sub>-wtDnaA.

3.6.2. (His)<sub>6</sub>-DnaAA163V forms stable HMWCs in the absence of ATP

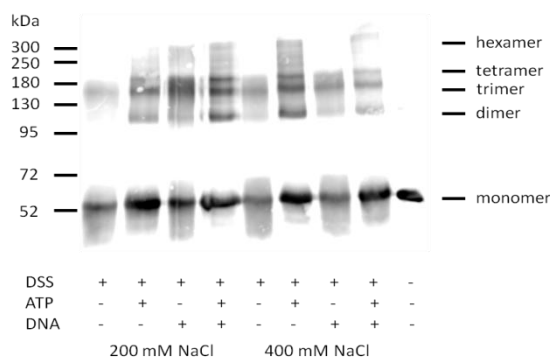
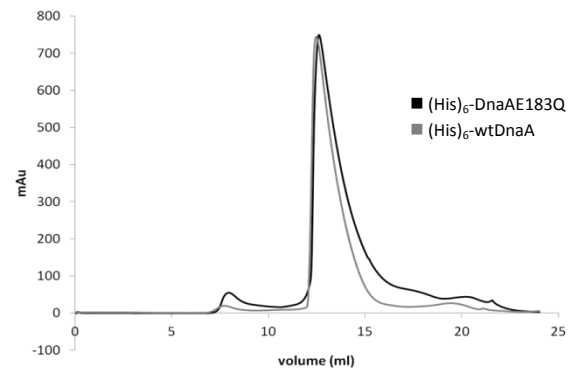
DSS crosslinking assays in ATP-free conditions, but independently of specific DNA, revealed that (His)<sub>6</sub>-DnaAA163V constitutively forms stable high-molecular weight complexes (Fig. 3.6.2.A). This again is consistent with its size-exclusion chromatography elution pattern (Fig. 3.6.2.B). Surprisingly, ATP seems to interfere with the intrinsic capacity to form these high-molecular structures, so that monomeric, dimeric and trimeric structures could be detected. Three additional bands with an unexpected size of around 140 kDa (\*), 95 kDa (\*\*), and 80 kDa were also present in the blot when ATP was available, but like for (His)<sub>6</sub>-wtDnaA they did not correspond to any possible multiple protomeric constitution of (His)<sub>6</sub>-DnaAA163V and probably resulted from partly degraded protein particles that have been crosslinked. Despite an obvious reduction in the capacity to establish high-molecular weight complexes, the detected smear suggests that even in the presence of ATP higher-order multimers are still formed, but with a highly decreased efficiency. Nevertheless, a constitutive multimeric constitution has previously been shown *in vitro* for DnaAA184V, the analogous *E. coli* mutant protein of (His)<sub>6</sub>-DnaAA163V [79-80].

[A] DSS-crosslink of (His)<sub>6</sub>-DnaAA163V[B] Gelfiltration of (His)<sub>6</sub>-DnaAA163V

**Fig. 3.6.2.:** Self-multimerization of (His)<sub>6</sub>-DnaAA163V. A, disuccinimidyl suberate [DSS] crosslinking assays with DSS [125 μM], (His)<sub>6</sub>-DnaAA163V [500 nM] under different NaCl concentrations [200 mM, 400 mM] and in the absence [-] or presence [+] of ATP [2.5 mM] and linear DnaA-box containing *oriC*-DNA [36.4 nM]. Samples were immunoblotted with anti-DnaA antibodies. B, normalized size-exclusion chromatography profiles (Superdex 200 10/300 GL column) of a (His)<sub>6</sub>-DnaAA163V (black line) and (His)<sub>6</sub>-wtDnaA (grey line) containing fraction after purification. The two major peaks show the native multimeric and trimeric states of (His)<sub>6</sub>-DnaAA163V and (His)<sub>6</sub>-wtDnaA, respectively.

### 3.6.3. (His)<sub>6</sub>-DnaAE183Q does not constitute stable higher-order multimers

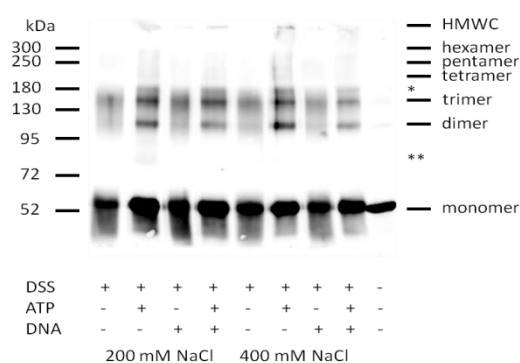
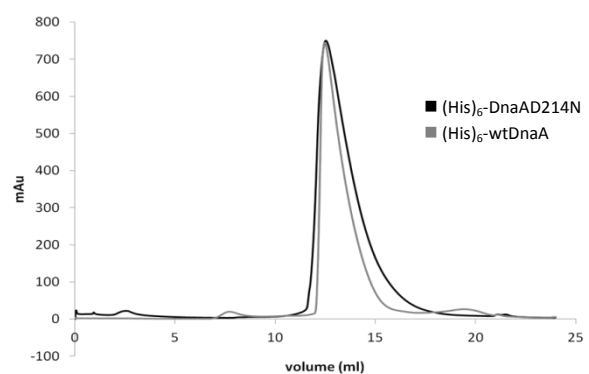
The multimeric structure of (His)<sub>6</sub>-DnaAE183Q is indistinguishable from (His)<sub>6</sub>-wtDnaA in ATP-free conditions. Hence, (His)<sub>6</sub>-DnaAE183Q adopts dimeric and trimeric constitutions and homo-pentamer formation can slightly be stimulated by linear *oriC*-DNA (Fig. 3.6.3.A/B). Remarkably, in the presence of ATP the self-multimerization capacity of (His)<sub>6</sub>-DnaAE183Q was drastically reduced, i.e. no high-molecular weight complexes bigger than 300 kDa were detectable. Moreover, mostly in all experiments, signals detected above 200 kDa (approximately corresponding to (His)<sub>6</sub>-DnaAE183Q tetramers) appeared as a pronounced smear, suggesting unstable multimeric structures, which is indicative for a decreased self-multimerization capacity of (His)<sub>6</sub>-DnaAE183Q.

[A] DSS-crosslink of (His)<sub>6</sub>-DnaAE183Q[B] Gelfiltration of (His)<sub>6</sub>-DnaAE183Q

**Fig. 3.6.3.:** Self-multimerization of (His)<sub>6</sub>-DnaAE183Q. A, disuccinimidyl suberate [DSS] crosslinking assays with DSS [125 μM], (His)<sub>6</sub>-DnaAE183Q [500 nM] under different NaCl concentrations [200 mM, 400 mM] and in the absence [-] or presence [+] of ATP [2.5 mM] and linear DnaA-box containing *oriC*-DNA [36.4 nM]. Samples were immunoblotted with anti-DnaA antibodies. B, normalized size-exclusion chromatography profiles (Superdex 200 10/300 GL column) of a (His)<sub>6</sub>-DnaAE183Q (black line) and (His)<sub>6</sub>-wtDnaA (grey line) containing fraction after purification. The two major peaks overlap and show the native trimeric state of (His)<sub>6</sub>-DnaAE183Q and (His)<sub>6</sub>-wtDnaA.

### 3.6.4. (His)<sub>6</sub>-DnaAD214N has a reduced capacity in constituting stable higher-order multimers

(His)<sub>6</sub>-DnaAD214N has been characterized as a DnaA mutant protein with a strongly reduced ATP-binding activity (see chapter 3.3.2.). Thus, it is not surprising that ATP-dependent self-multimerization is affected. Like (His)<sub>6</sub>-wtDnaA and (His)<sub>6</sub>-DnaAE183Q, (His)<sub>6</sub>-DnaAD214N forms dimeric and trimeric structures in the absence of ATP, which was confirmed by size-exclusion chromatography (Fig. 3.6.4.A/B). These multimeric constitutions are more pronounced in the presence of ATP, but higher-order structures were evident in only low amounts in most of the experiments.

[A] DSS-crosslink of (His)<sub>6</sub>-DnaAD214N[B] Gelfiltration of (His)<sub>6</sub>-DnaAD214N

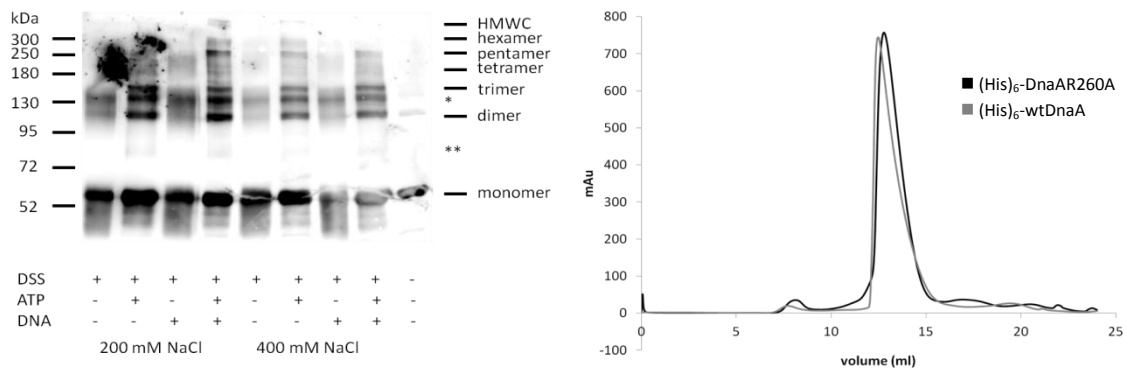
**Fig. 3.6.4.:** Self-multimerization of (His)<sub>6</sub>-DnaAD214N. A, disuccinimidyl suberate [DSS] crosslinking assays with DSS [125 μM], (His)<sub>6</sub>-DnaAD214N [500 nM] under different NaCl concentrations [200 mM, 400 mM] and in the absence [-] or presence [+] of ATP [2.5 mM] and linear DnaA-box containing *oriC*-DNA [36.4 nM]. Samples were immunoblotted with anti-DnaA antibodies. B, normalized size-exclusion chromatography profiles (Superdex 200 10/300 GL column) of a (His)<sub>6</sub>-DnaAD214N (black line) and (His)<sub>6</sub>-wtDnaA (grey line) containing fraction after purification. The two major peaks overlap and show the native trimeric state of (His)<sub>6</sub>-DnaAD214N and (His)<sub>6</sub>-wtDnaA.

### 3.6.5. Self-multimerization capacity of (His)<sub>6</sub>-DnaAR260A is not affected

(His)<sub>6</sub>-DnaAR260A is self-multimerization proficient. The ATP-dependent formation of multimers, both low- and high-molecular weight structures occurs in a (His)<sub>6</sub>-wtDnaA-like manner (Fig. 3.6.5.A/B). Moreover, linear *oriC*-DNA stimulates pentamerization of (His)<sub>6</sub>-DnaAR260A. Nevertheless, high molecular-weight complexes bigger than 300 kDa were not detectable at 400 mM salt, whereas *oriC*-DNA could still trigger homo-pentamer formation.

[A] DSS-crosslink of (His)<sub>6</sub>-DnaAR260A

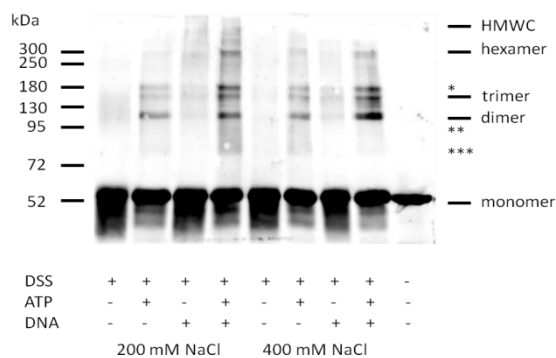
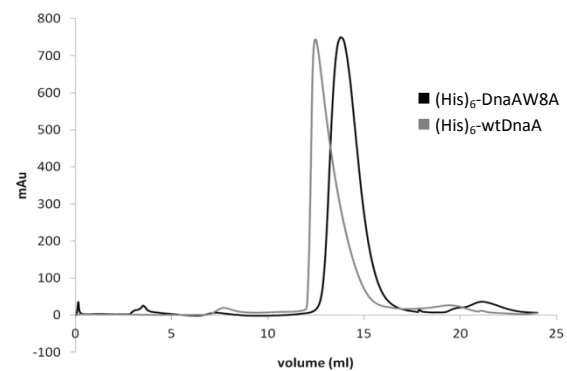
[B] Gelfiltration of (His)<sub>6</sub>-DnaAR260A



**Fig. 3.6.5.:** Self-multimerization of (His)<sub>6</sub>-DnaAR260A. A, disuccinimidyl suberate [DSS] crosslinking assays with DSS [125 μM], (His)<sub>6</sub>-DnaAR260A [500 nM] under different NaCl concentrations [200 mM, 400 mM] and in the absence [-] or presence [+] of ATP [2.5 mM] and linear DnaA-box containing *oriC*-DNA [36.4 nM]. Samples were immunoblotted with anti-DnaA antibodies. B, normalized size-exclusion chromatography profiles (Superdex 200 10/300 GL column) of a (His)<sub>6</sub>-DnaAR260A (black line) and (His)<sub>6</sub>-wtDnaA (grey line) containing fraction after purification. The two major peaks overlap and show the native trimeric state of (His)<sub>6</sub>-DnaAR260A and (His)<sub>6</sub>-wtDnaA.

### 3.6.6. (His)<sub>6</sub>-DnaAW8A displays a conditional dimerization deficiency in the absence of ATP

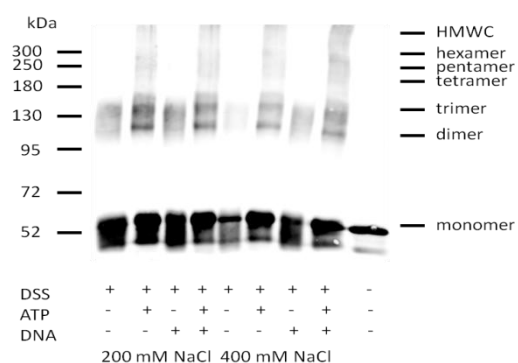
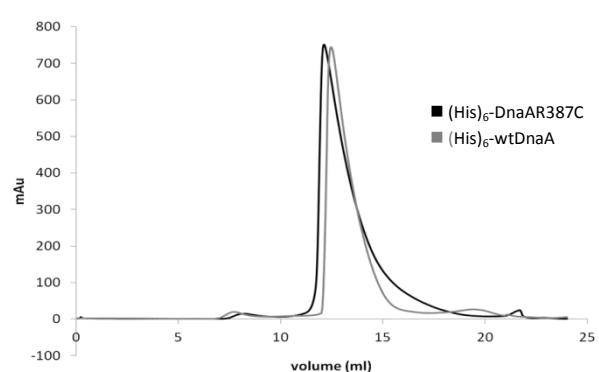
The self-multimerization capacity of (His)<sub>6</sub>-DnaAW8A is significantly affected only at the level of dimerization. Under ATP-free conditions, (His)<sub>6</sub>-DnaAW8A can be detected almost exclusively as monomers, whereas (His)<sub>6</sub>-wtDnaA adopts dimeric and trimeric forms (Figs. 3.6.6.A and 3.6.1.A, respectively). A very small protein fraction of (His)<sub>6</sub>-DnaAW8A was detectable as homo-dimers and homo-trimers. The fact, that most of the protein remains in its monomeric constitution was confirmed by size-exclusion chromatography (Fig. 3.6.6.B). However, dimerization and formation of high-molecular weight complexes could be maintained in the presence of ATP and was slightly reduced at 400 mM NaCl. It is interesting to notice that linear *oriC*-DNA might stimulate both dimerization and self-multimerization, even at high salt concentrations. Like for the previously described crosslinking assays, additional bands with corresponding sizes of around 180 kDa (\*), 95 kDa (\*\*), and 80 kDa (\*\*\*) could be detected and presumably result from crosslinked degraded protein particles.

[A] DSS-crosslink of (His)<sub>6</sub>-DnaAW8A[B] Gelfiltration of (His)<sub>6</sub>-DnaAW8A

**Fig. 3.6.6.:** Self-multimerization of (His)<sub>6</sub>-DnaAW8A. A, disuccinimidyl suberate [DSS] crosslinking assays with DSS [125 μM], (His)<sub>6</sub>-DnaAW8A [500 nM] under different NaCl concentrations [200 mM, 400 mM] and in the absence [-] or presence [+] of ATP [2.5 mM] and linear DnaA-box containing *oriC*-DNA [36.4 nM]. Samples were immunoblotted with anti-DnaA antibodies. B, normalized size-exclusion chromatography profiles (Superdex 200 10/300 GL column) of a (His)<sub>6</sub>-DnaAW8A (black line) and (His)<sub>6</sub>-wtDnaA (grey line) containing fraction after purification. The two major peaks show the native monomeric and trimeric states of (His)<sub>6</sub>-DnaAW8A and (His)<sub>6</sub>-wtDnaA, respectively.

### 3.6.7. Self-multimerization capacity of (His)<sub>6</sub>-DnaAR387C is irresponsive to linear *oriC*-DNA

(His)<sub>6</sub>-DnaAR387C self-multimerizes in an ATP-dependent manner similar to (His)<sub>6</sub>-wtDnaA (Fig. 3.6.7.A). In the absence of ATP (His)<sub>6</sub>-DnaAR387C dimerizes or adopts trimeric structures, which was also shown by size-exclusion chromatography (Fig. 3.6.7.B). ATP availability immediately leads to the formation of multimeric structures. Strikingly, in contrast to (His)<sub>6</sub>-wtDnaA, *oriC*-DNA did not stimulate self-multimerization of (His)<sub>6</sub>-DnaAR387C, irrespective to the tested salt concentrations.

[A] DSS-crosslink of (His)<sub>6</sub>-DnaAR387C[B] Gelfiltration of (His)<sub>6</sub>-DnaAR387C

**Fig. 3.6.7.:** Self-multimerization of (His)<sub>6</sub>-DnaAR387C. A, disuccinimidyl suberate [DSS] crosslinking assays with DSS [125 μM], (His)<sub>6</sub>-DnaAR387C [500 nM] under different NaCl concentrations [200 mM, 400 mM] and in the absence [-] or presence [+] of ATP [2.5 mM] and linear DnaA-box containing *oriC*-DNA [36.4 nM]. Samples were immunoblotted with anti-DnaA antibodies. B, normalized size-exclusion chromatography profiles (Superdex 200 10/300 GL column) of a (His)<sub>6</sub>-DnaAR387C (black line) and (His)<sub>6</sub>-wtDnaA (grey line) containing fraction after purification. The two major peaks overlap and show the native trimeric state of (His)<sub>6</sub>-DnaAR387C and (His)<sub>6</sub>-wtDnaA.

### 3.7. Growth of *B. subtilis* PY79 expressing N-terminal YFP-fusions of wtDnaA/mutDnaA from an ectopic site *in vivo*

To study the effect of mutant DnaA *in vivo*, *B. subtilis* wild type strain PY79 carrying a constitutively expressed origin-tag [*spo0J*::(*mls lacO*<sub>256</sub>, *spo0J*), *thrC*::(*cm p*<sub>pen</sub>-*lacI-cfp*)] was transformed with plasmid-DNA to construct strains that express N-terminal YFP-fusions of wild type and mutant DnaA from an ectopic locus [*amyE*::(*spec p*<sub>xyl</sub>-*yfp-wt/mutdnaA*)]. Mutagenesis of the original wild type copy of *dnaA* would probably lead to immediate suppressor mutations, and thus, obvious effects would not necessarily reflect the direct influence on the cell cycle. Ectopic protein expression can bypass this genetical inconvenience, but imperatively increases the intracellular DnaA concentration. Although repressed by glucose containing LB medium, the xylose inducible promoter upstream of the construct does not perfectly prevent constitutive expression of low amounts of the protein (Fig. 3.7.1.).

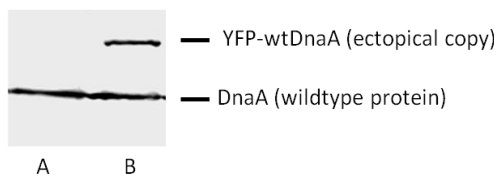


**Fig. 3.7.1.:** Immunoblot of *B. subtilis* cell lysates with anti-DnaA antibodies. Cells were grown in LB-medium supplemented with glucose until exponential growth (OD<sub>600</sub> 0.6) and subsequently treated with lysozyme prior to immunoblotting. A, PY79. B, PY79 [*amyE*::(*spec p*<sub>xyl</sub>-*yfp-dnaA*)].

Since DnaA is one of the key regulators of the cell cycle, the initial attempt to understand the effects of mutant DnaA *in vivo*, was to examine growth under induced and non-induced conditions [1, 4, 6-7, 25]. To make sure that the additionally integrated construct of the *B. subtilis* control strain, i.e. genotype [*spo0J*::(*mls lacO*<sub>256</sub>, *spo0J*), *thrC*::(*cm p*<sub>pen</sub>-*lacI-cfp*), *amyE*::(*spec p*<sub>xyl</sub>-*yfp-wtdnaA*)], in the following referred to as PY79-YFP-wtDnaA, is fully functional, several control experiments were carried out. First, *B. subtilis* wild type strain PY79 and PY79 [*spo0J*::(*mls lacO*<sub>256</sub>, *spo0J*), *thrC*::(*cm p*<sub>pen</sub>-*lacI-cfp*)] with origin tag, in the following termed PY79-oriC-CFP, were grown in rich (LB-) medium (30°C, 200 rpm, 20 ml culture, inoculated OD<sub>600</sub> 0.05) and growth was monitored. Surprisingly, PY79-oriC-CFP entered exponential phase with a slight delay compared to PY79 (Fig. 3.7.2.), but the doubling times (exponential growth, ~45 minutes) and the optical densities of stationary phase cultures (OD<sub>600</sub> ~4) were nearly identical for both strains, suggesting that the origin-tag does not interfere with cell cycle regulating parameters. As mentioned above, PY79-YFP-wtDnaA permanently synthesizes low amounts of YFP-wtDnaA (Fig. 3.7.1.), even in the presence of glucose (5 mg/ml). Despite this considerable aspect, exponential growth of a non-induced culture is indistinguishable from PY79 (Fig. 3.7.3.). Induction (xylose, 5 mg/ml) of YFP-

wtDnaA leads to a strong growth delay, probably due to stopped replication as a consequence of a lack of DnaN. Since *dnaA-dnaN* transcription is regulated by DnaA protein, overexpressed YFP-DnaA would lead to blocked transcription, suggesting that this construct is fully functional and can be used as an appropriate control strain for PY79 carrying YFP-mutant DnaA fusions [8-9]. Remarkably, PY79-YFP-wtDnaA enters stationary phase at a lower optical density ( $OD_{600} \sim 3$ ) than PY79 ( $OD_{600} \sim 4$ ).

PY79/PY79-*oriC*-CFP

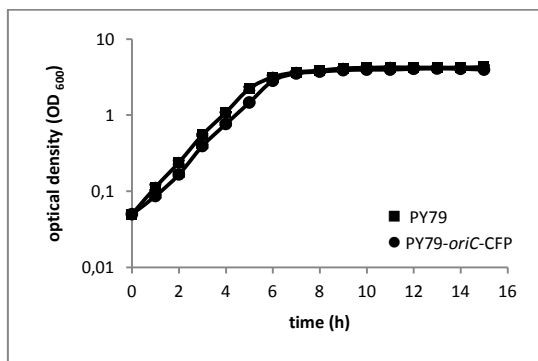


**Fig. 3.7.2.:** Growth curves of *B. subtilis* cultures. 20 ml of rich medium (LB, supplemented with glucose or xylose, if indicated) were inoculated to an initial  $OD_{600}$  0.05 from an overnight culture. Cells were continuously shaken with 200 rpm at 30°C and samples for  $OD_{600}$  determination were taken every hour. Black squares: PY79. Black circles: PY79-*oriC*-CFP.

PY79/PY79-YFP-wtDnaA

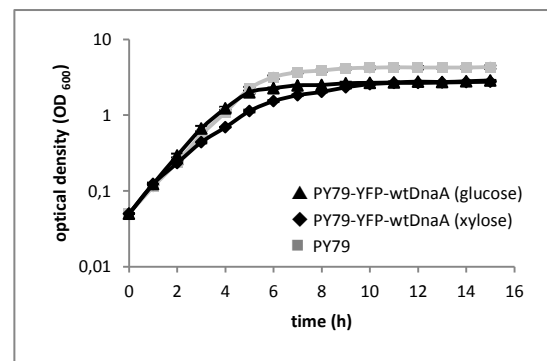


**Fig. 3.7.3.:** Growth curves of *B. subtilis* cultures. 20 ml of rich medium (LB, supplemented with glucose or xylose, if indicated) were inoculated to an initial  $OD_{600}$  0.05 from an overnight culture. Cells were continuously shaken with 200 rpm at 30°C and samples for  $OD_{600}$  determination were taken every hour. Grey squares: PY79. Black triangles: PY79-YFP-wtDnaA (glucose). Black diamonds: PY79-YFP-wtDnaA (xylose).

Expression of YFP-DnaA mutants in *B. subtilis* has different impacts on growth. PY79-YFP-DnaAA163V displayed a significant but slight decrease in growth with doubling times in exponential growth of approximately 60 minutes, both for induced and non-induced cells (Fig. 3.7.4.). On the contrary, PY79-YFP-DnaAE183Q had a strong growth defect and did not enter exponential growth. The maximal doubling time of approximately 90 minutes was achieved independently of the presence of glucose or xylose in the medium (Fig. 3.7.5.).

PY79/PY79-YFP-DnaAA163V

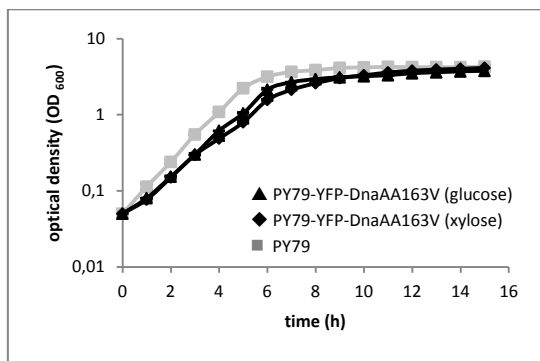


**Fig. 3.7.4.:** Growth curves of *B. subtilis* cultures. 20 ml of rich medium (LB, supplemented with glucose or xylose, if indicated) were inoculated to an initial OD<sub>600</sub> 0.05 from an overnight culture. Cells were continuously shaken with 200 rpm at 30°C and samples for OD<sub>600</sub> determination were taken every hour. Grey squares: PY79. Black triangles: PY79-YFP-DnaAA163V (glucose). Black diamonds: PY79-YFP-DnaAA163V (xylose).

PY79/PY79-YFP-DnaAE183Q

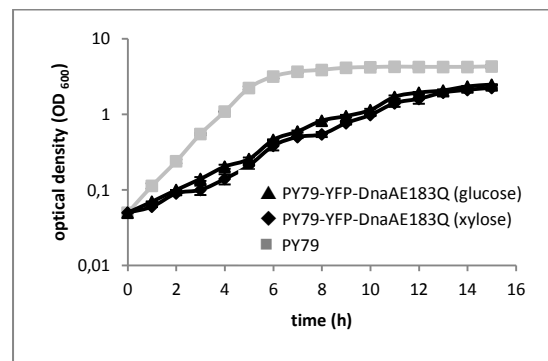


**Fig. 3.7.5.:** Growth curves of *B. subtilis* cultures. 20 ml of rich medium (LB, supplemented with glucose or xylose, if indicated) were inoculated to an initial OD<sub>600</sub> 0.05 from an overnight culture. Cells were continuously shaken with 200 rpm at 30°C and samples for OD<sub>600</sub> determination were taken every hour. Grey squares: PY79. Black triangles: PY79-YFP-DnaAE183Q (glucose). Black diamonds: PY79-YFP-DnaAE183Q (xylose).

PY79-YFP-DnaAD214N entered exponential growth phase with a significant delay, whereas PY79-YFP-DnaAR260A reached log phase rather fast when compared to PY79 (Figs. 3.7.6. and 3.7.7., respectively). Under non-induced conditions, PY79-YFP-DnaAD214N displayed a significant reduction of growth with doubling times of approximately 70 minutes. In contrast, exponential growth of PY79-YFP-DnaAR260A appeared to be unaffected (doubling time ~50 minutes). However, the optical density decayed shortly after reaching stationary phase when grown in glucose supplemented LB-medium, suggesting that the constitutively expressed low amount of YFP-DnaAR260A interferes with the regulation of replication with severe consequences for stationary phase conditions. Both mutant strains showed a strong growth defect when permanently expressing their respective YFP-mutant DnaA, which was more pronounced than the effect of overexpressed YFP-wtDnaA. Moreover, entering into stationary phase occurred at relatively low optical densities for both strains (OD<sub>600</sub> ~2).

PY79/PY79-YFP-DnaAD214N

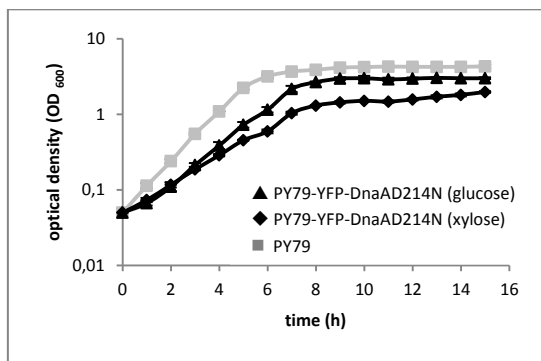


**Fig. 3.7.6.:** Growth curves of *B. subtilis* cultures. 20 ml of rich medium (LB, supplemented with glucose or xylose, if indicated) were inoculated to an initial OD<sub>600</sub> 0.05 from an overnight culture. Cells were continuously shaken with 200 rpm at 30°C and samples for OD<sub>600</sub> determination were taken every hour. Grey squares: PY79. Black triangles: PY79-YFP-DnaAD214N (glucose). Black diamonds: PY79-YFP-DnaAD214N (xylose).

PY79/PY79-YFP-DnaAR260A

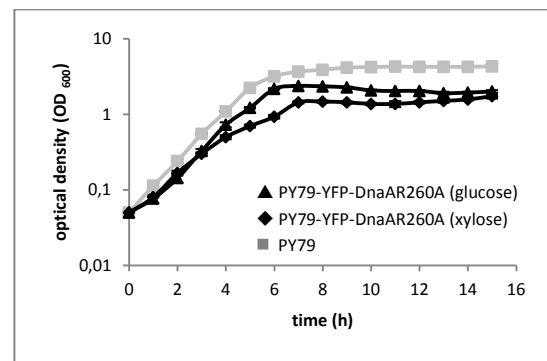


**Fig. 3.7.7.:** Growth curves of *B. subtilis* cultures. 20 ml of rich medium (LB, supplemented with glucose or xylose, if indicated) were inoculated to an initial OD<sub>600</sub> 0.05 from an overnight culture. Cells were continuously shaken with 200 rpm at 30°C and samples for OD<sub>600</sub> determination were taken every hour. Grey squares: PY79. Black triangles: PY79-YFP-DnaAR260A (glucose). Black diamonds: PY79-YFP-DnaAR260A (xylose).

Both PY79-YFP-DnaAW8A and PY79-DnaAR387C entered exponential growth phase with a short delay compared to PY79 (Figs. 3.7.8. and 3.7.9., respectively). Under non-induced conditions, maximal doubling times of PY79-YFP-DnaAW8A and PY79-YFP-DnaAR387C were approximately 55 and 45 minutes, respectively. Continuous induction resulted in reduced growth of both strains, whereby the effect of overexpressed YFP-DnaAR387C was much less prominent than of YFP-DnaAW8A and YFP-wtDnaA, suggesting that growth of PY79-YFP-DnaAR387C is not severely affected by the presence of high quantities of this mutant protein.

PY79/PY79-YFP-DnaAW8A

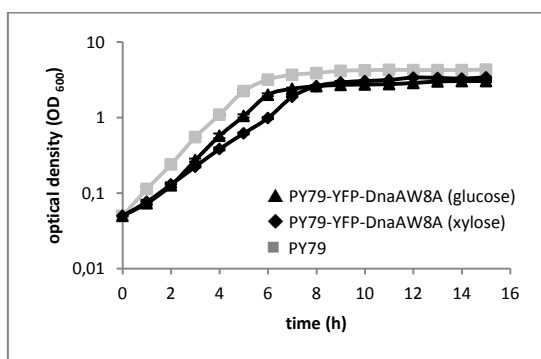


**Fig. 3.7.8.:** Growth curves of *B. subtilis* cultures. 20 ml of rich medium (LB, supplemented with glucose or xylose, if indicated) were inoculated to an initial OD<sub>600</sub> 0.05 from an overnight culture. Cells were continuously shaken with 200 rpm at 30°C and samples for OD<sub>600</sub> determination were taken every hour. Grey squares: PY79. Black triangles: PY79-YFP-DnaAW8A (glucose). Black diamonds: PY79-YFP-DnaAW8A (xylose).

PY79/PY79-YFP-DnaAR387C

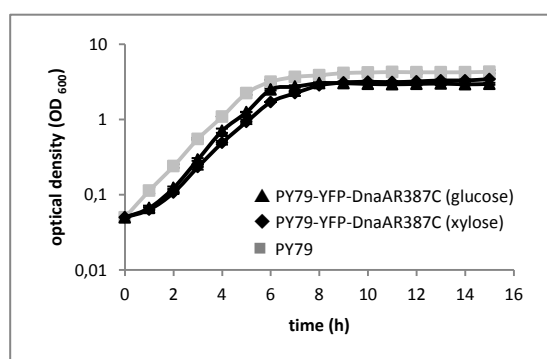


**Fig. 3.7.9.:** Growth curves of *B. subtilis* cultures. 20 ml of rich medium (LB, supplemented with glucose or xylose, if indicated) were inoculated to an initial OD<sub>600</sub> 0.05 from an overnight culture. Cells were continuously shaken with 200 rpm at 30°C and samples for OD<sub>600</sub> determination were taken every hour. Grey squares: PY79. Black triangles: PY79-YFP-DnaAR387C (glucose). Black diamonds: PY79-YFP-DnaAR387C (xylose).

### 3.8. Transcriptional regulation of the *dnaA-dnaN* operon by ectopically expressed N-terminal YFP-fusions of wtDnaA/mutDnaA *in vivo*

Genes *dnaA* and *dnaN* form an operon and are located at 0° on the *B. subtilis* chromosome, partially overlapping with the bipartite *oriC* [8-9]. The expression level of DnaA and DnaN is regulated by a negative feedback loop [8-9]. High DnaA amounts repress the transcription of the operon, whereas low amounts of DnaA lead to increased transcription [8-9]. It has been postulated that the amount of DnaA molecules represents a factor that controls the rate of replication initiation and thus the rate of the cell cycle [8-9]. Hence, it was important to understand, if ectopically expressed mutant DnaA proteins were functionally active to outcompete or to interfere with wildtype DnaA to regulate *dnaA-dnaN* transcription. Despite repressed transcription of the ectopic copy of *yfp-wtdnaA* by addition of glucose (5 mg/ml) to the medium, the xylose inducible promoter upstream of the construct allows constitutive expression of low amounts of the protein (see chapter 3.7.). Thus, *B. subtilis* strains PY79 (control) and PY79-YFP-wt/mutDnaA were grown until exponential growth in S750 minimal medium either supplemented with glucose or xylose. A third growth condition allows moderate expression of the ectopic copy by growth in glucose containing medium until entering into log phase and subsequent induction of ectopic expression for 60 minutes by exchange of the medium (S750-glucose exchanged for S750-xylose).

#### 3.8.1. Moderate ectopic expression of YFP-wtDnaA *in vivo* does not affect the transcriptional regulation of *dnaA-dnaN*

The expression level of DnaA in *B. subtilis* wild type strain PY79 is not affected by either glucose or xylose (Fig. 3.8.1.1.). Ectopic expression of YFP-wtDnaA (*amyE*-locus) in strain PY79-YFP-wtDnaA can be distinguished from DnaA expression (original locus) by immunoblotting with anti-DnaA antibodies, due to the different molecular weight of YFP-wtDnaA (~78 kDa) and DnaA (~56 kDa). Though, during reduced synthesis of YFP-wtDnaA by glucose the total cellular level of YFP-wtDnaA appeared to be rather similar with the amount of DnaA (Fig. 3.8.1.2.). Moderate induced expression of YFP-wtDnaA (~3-fold) did not seem to interfere with the transcriptional regulation of the *dnaA-dnaN* operon, since almost equal amounts of DnaA were still measurable. On the contrary, permanently induced expression of YFP-wtDnaA (~6-fold) consequently repressed *dnaA-dnaN* transcription, since no signal of DnaA was detectable any longer. This demonstrates that YFP-wtDnaA is functional and that moderate synthesis of this protein does not impede with the tight regulation of DnaA transcription.

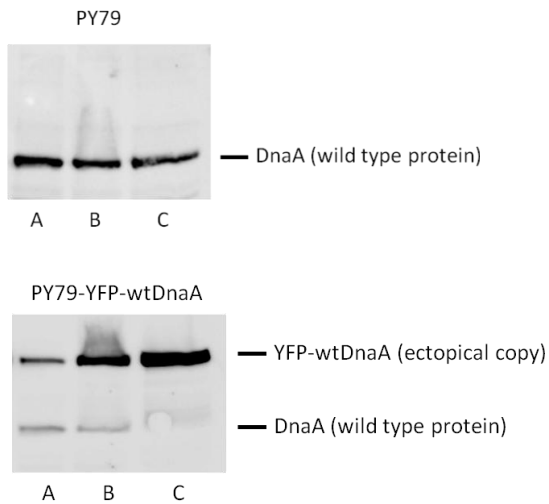


**Fig. 3.8.1.1.:** Immunoblot of PY79 cell lysates with anti-DnaA antibodies. Cells were grown in S750 minimal medium (supplemented as indicated below) until exponential growth ( $OD_{600}$  0.6) and subsequently treated with lysozyme prior to immunoblotting. A, glucose (5 mg/ml). B, xylose (5 mg/ml, 60 min). C, xylose (5 mg/ml).

**Fig. 3.8.1.2.:** Immunoblot of PY79-YFP-wtDnaA cell lysates with anti-DnaA antibodies. Cells were grown in S750 minimal medium (supplemented as indicated below) until exponential growth ( $OD_{600}$  0.6) and subsequently treated with lysozyme prior to immunoblotting. A, glucose (5 mg/ml). B, xylose (5 mg/ml, 60 min). C, xylose (5 mg/ml).

### 3.8.2. Overexpression of YFP-DnaAA163V, YFP-DnaAD214N, YFP-DnaAR260A and YFP-DnaAW8A outcompetes DnaA in regulating *dnaA-dnaN* transcription *in vivo*

Ectopic overexpression of YFP-DnaAA163V, YFP-DnaAD214N, YFP-DnaAR260A and YFP-DnaAW8A led to repression of *dnaA-dnaN* transcription similar to YFP-wtDnaA (Figs. 3.8.2.1., 3.8.2.2., 3.8.2.3., 3.8.2.4. and 3.8.1.2., respectively). Furthermore, moderate expression of all of these proteins still allowed DnaA synthesis in quantities equal to non-induced conditions. Surprisingly, in contrast to all other ectopically encoded constructs, expression of YFP-DnaAW8A could completely be inhibited by addition of glucose to the medium (Fig. 3.8.2.4.).

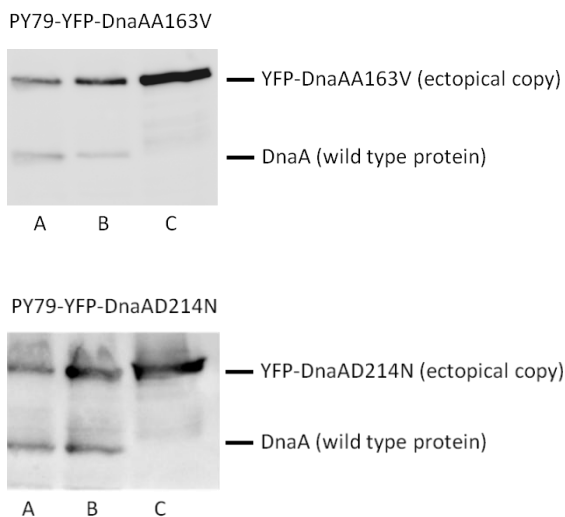


**Fig. 3.8.2.1.:** Immunoblot of PY79-YFP-DnaAA163V cell lysates with anti-DnaA antibodies. Cells were grown in S750 minimal medium (supplemented as indicated below) until exponential growth ( $OD_{600}$  0.6) and subsequently treated with lysozyme prior to immunoblotting. A, glucose (5 mg/ml). B, xylose (5 mg/ml, 60 min). C, xylose (5 mg/ml).

**Fig. 3.8.2.2.:** Immunoblot of PY79-YFP-DnaAD214N cell lysates with anti-DnaA antibodies. Cells were grown in S750 minimal medium (supplemented as indicated below) until exponential growth ( $OD_{600}$  0.6) and subsequently treated with lysozyme prior to immunoblotting. A, glucose (5 mg/ml). B, xylose (5 mg/ml, 60 min). C, xylose (5 mg/ml).

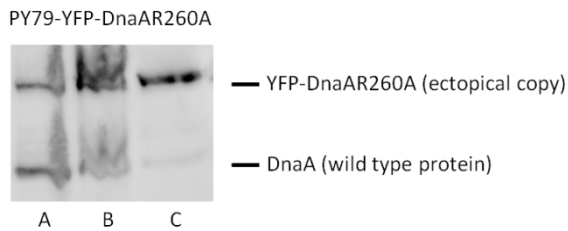


**Fig. 3.8.2.3.:** Immunoblot of PY79-YFP-DnaAR260A cell lysates with anti-DnaA antibodies. Cells were grown in S750 minimal medium (supplemented as indicated below) until exponential growth ( $OD_{600}$  0.6) and subsequently treated with lysozyme prior to immunoblotting. A, glucose (5 mg/ml). B, xylose (5 mg/ml, 60 min). C, xylose (5 mg/ml).

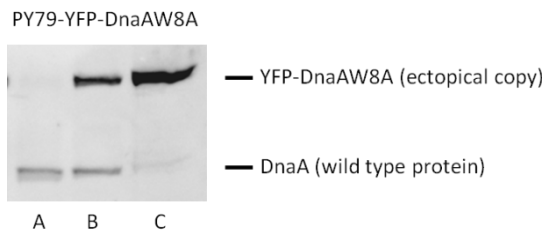


**Fig. 3.8.2.4.:** Immunoblot of PY79-YFP-DnaAW8A cell lysates with anti-DnaA antibodies. Cells were grown in S750 minimal medium (supplemented as indicated below) until exponential growth ( $OD_{600}$  0.6) and subsequently treated with lysozyme prior to immunoblotting. A, glucose (5 mg/ml). B, xylose (5 mg/ml, 60 min). C, xylose (5 mg/ml).

### 3.8.3. Ectopic expression of YFP-DnaAE183Q does not reach sufficient protein levels to repress *dnaA-dnaN* transcription *in vivo*

The expression level of YFP-DnaAE183Q (ATPase deficient mutant protein) *in vivo* suggests that only certain amounts of this protein are tolerated. The quantities of YFP-DnaAE183Q of cells grown in xylose and those induced with xylose for only 60 minutes were rather similar, indicating that higher protein levels would be lethal (Fig. 3.8.3.1.). In addition to this, either the amount of YFP-DnaAE183Q was not sufficient or the protein itself was mechanistically inactive to repress transcription of the *dnaA-dnaN* operon, since DnaA was still detectable.

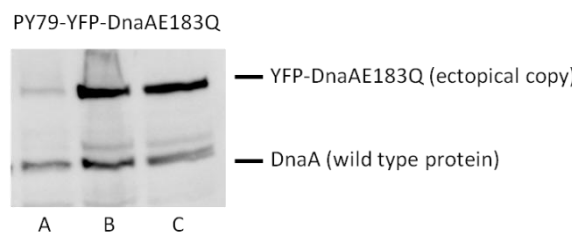


**Fig. 3.8.3.1.:** Immunoblot of PY79-YFP-DnaAE183Q cell lysates with anti-DnaA antibodies. Cells were grown in S750 minimal medium (supplemented as indicated below) until exponential growth ( $OD_{600}$  0.6) and subsequently treated with lysozyme prior to immunoblotting. A, glucose (5 mg/ml). B, xylose (5 mg/ml, 60 min). C, xylose (5 mg/ml).

### 3.8.4. Overexpression of YFP-DnaAR387C does not interfere with the transcriptional regulation of *dnaA-dnaN* by DnaA *in vivo*

Ectopic overexpression of YFP-DnaAR387C exceeded cellular protein levels of all other mutant DnaA proteins without leading to repression of *dnaA-dnaN* transcription (Fig. 3.8.4.1.). This effect could be attributed to the DNA-binding defect of YFP-DnaAR387C (see chapter 3.5.2. for (His)<sub>6</sub>-DnaAR387C). Moreover, moderate expression of YFP-DnaAR387C still allowed DnaA synthesis up to levels similar to non-induced cells.

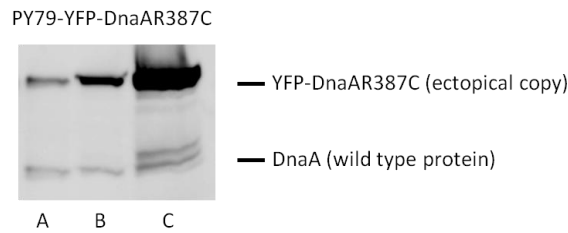


**Fig. 3.8.4.1.:** Immunoblot of PY79-YFP-DnaAR387C cell lysates with anti-DnaA antibodies. Cells were grown in S750 minimal medium (supplemented as indicated below) until exponential growth ( $OD_{600}$  0.6) and subsequently treated with lysozyme prior to immunoblotting. A, glucose (5 mg/ml). B, xylose (5 mg/ml, 60 min). C, xylose (5 mg/ml).

### 3.9. Fluorescence microscopy of *B. subtilis* PY79 expressing N-terminal YFP-fusions of wtDnaA/mutDnaA from an ectopic site *in vivo*

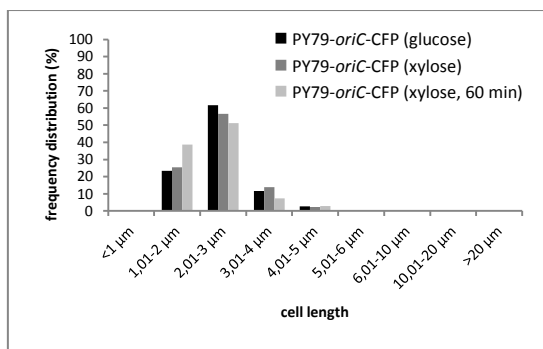
The final aspect of the characterization of wild type and mutant DnaA was the analysis of the effect of ectopically expressed YFP-wtDnaA and mutant forms in live *B. subtilis* cells using fluorescence microscopy. The particular interest was focused on the consequences on cell cycle specific parameters, like the frequency of initiation of replication, chromosomal segregation, septum formation, cell length and subcellular positioning of YFP-wt/mutDnaA relative to the origins of replication as an indirect means of *oriC*-wt/mutDnaA interaction. *B. subtilis* strains PY79-*oriC*-CFP (control) and PY79-YFP-wt/mutDnaA were grown until exponential growth in S750 minimal medium at 30°C and 200 rpm under conditions allowing maximal repression (5 mg/ml glucose), moderate expression (5 mg/ml xylose for 60 minutes after entering into exponential growth) or maximal induction (5 mg/ml xylose) of the ectopically encoded construct. Cells were treated with membrane stain FM 4-64 and DNA stain DAPI prior to microscopy. All charts below display the distribution of an indicated number of cells differing in length, number of nucleoids, number of origins of replication, number of YFP-wt/mutDnaA-foci and occurrence of *oriC*-CFP - YFP-wt/mutDnaA colocalization events.

#### 3.9.1. *B. subtilis* PY79-*oriC*-CFP

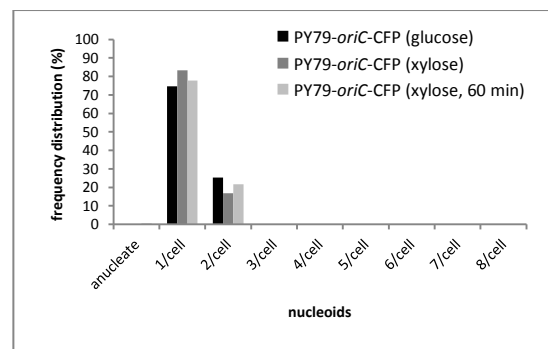
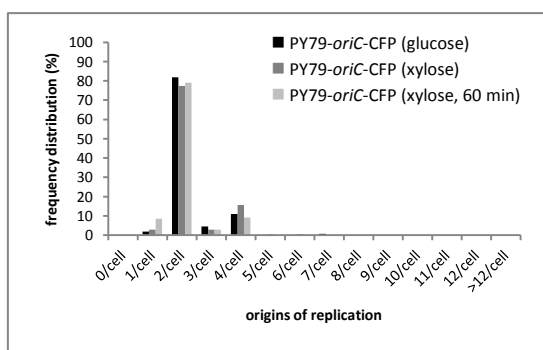
*B. subtilis* wild type strain PY79 with CFP-labeled origins of replication [*spo0J*::(*mIs lacO*<sub>256</sub>, *spo0J*), *thrC*::(*cm p<sub>pen</sub>-lacI-cfp*)] was first analyzed to compare wild type like parameters with those of strains carrying ectopically encoded versions of YFP-DnaA. It was important to figure out if moderate ectopic expression of YFP-wtDnaA interferes with the regulation of the initiation of replication and in turn can be used as an appropriate control for YFP-mutant DnaA expression in live *B. subtilis* cells. As expected, PY79-*oriC*-CFP did not show any significant change in cell length, number of chromosomes per cell or number of origins of replication per cell when grown under all three conditions, since this specific strain did not contain any xylose inducible construct. Thus, most of the analyzed cells were 2-3  $\mu$ m long (~50-60%) or smaller (~25-35%) and only a small fraction of cells (~10-15%) was slightly longer (3-5  $\mu$ m) (Figs.

3.9.1.1.A, 3.9.1.2.A, 3.9.1.3.A, 3.9.1.4.A). A predominant majority of these cells contained only one chromosome per cell (~70-80%) and the remaining cells had two nucleoids (Figs. 3.9.1.1.B, 3.9.1.2.B, 3.9.1.3.B, 3.9.1.4.B). Furthermore, approximately 80% of all cells contained two origins of replication, whereas a little number of cells displayed four *oriC*-CFP foci (~15%) (Figs. 3.9.1.1.C, 3.9.1.2.D, 3.9.1.3.D, 3.9.1.4.D).

[A] Cell length distribution

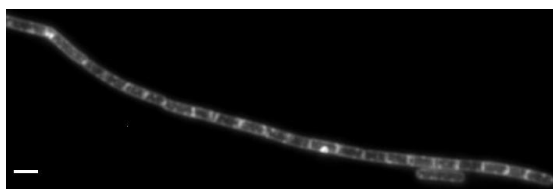


[B] Nucleoid distribution

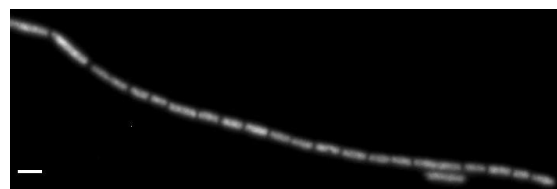
[C] *oriC*-CFP distribution

**Fig. 3.9.1.1:** Charts displaying the distribution of several live cell parameters of *B. subtilis* strain PY79-*oriC*-CFP grown in S750 minimal medium (supplemented as indicated below) until exponential growth at 30°C. Black columns: glucose (5 mg/ml) [cells analyzed: 154]. Dark grey columns: xylose (5 mg/ml) [cells analyzed: 173]. Light grey columns: xylose (5 mg/ml, 60 min) [cells analyzed: 176]. A, frequency distribution of cell length. B, frequency distribution of number of chromosomes per cell. C, frequency distribution of number of origins of replication (*oriC*-CFP) per cell.

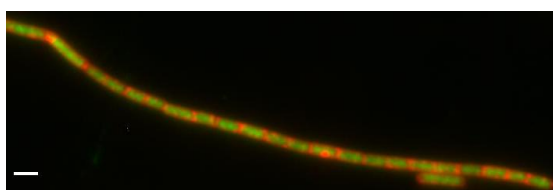
[A] membrane



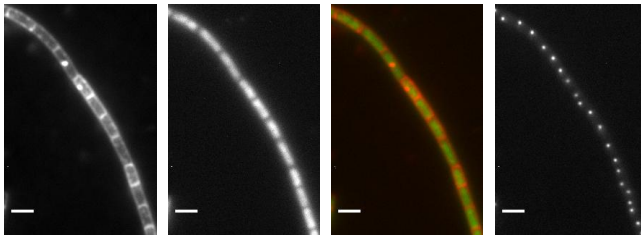
[B] DNA



[C] merge

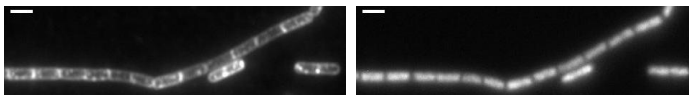
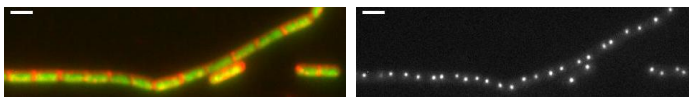
[D] *oriC*

**Fig. 3.9.1.2:** Fluorescence microscopy of *B. subtilis* strain PY79-*oriC*-CFP grown in S750 minimal medium (supplemented with glucose) until exponential growth at 30°C. A, membrane. B, DNA (nucleoids). C, overlay of membrane (red) and DNA (green). D, origins of replication (*oriC*-CFP). White bar: 2 μm.

[A] mem. [B] DNA [C] merge [D] *oriC*

**Fig. 3.9.1.3.:** Fluorescence microscopy of *B. subtilis* strain PY79-*oriC*-CFP grown in S750 minimal medium (supplemented with xylose) until exponential growth at 30°C. A, membrane. B, DNA (nucleoids). C, overlay of membrane (red) and DNA (green). D, origins of replication (*oriC*-CFP). White bar: 2  $\mu$ m.

[A] membrane [B] DNA

[C] merge [D] *oriC*

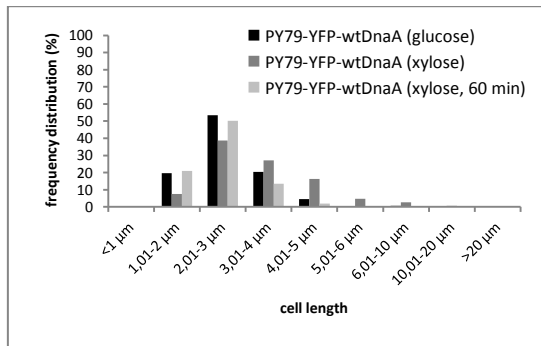
**Fig. 3.9.1.4.:** Fluorescence microscopy of *B. subtilis* strain PY79-*oriC*-CFP grown in S750 minimal medium (supplemented with xylose for 60 min after entering exponential growth phase) at 30°C. A, membrane. B, DNA (nucleoids). C, overlay of membrane (red) and DNA (green). D, origins of replication (*oriC*-CFP). White bar: 2  $\mu$ m.

### 3.9.2. *B. subtilis* PY79-YFP-wtDnaA

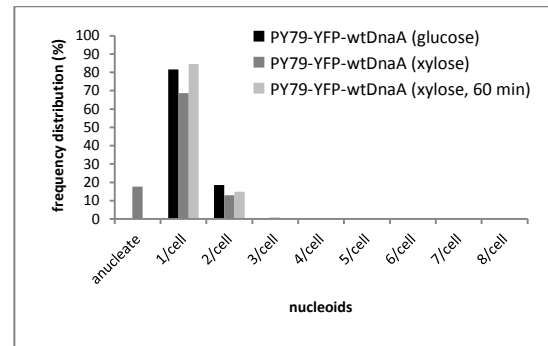
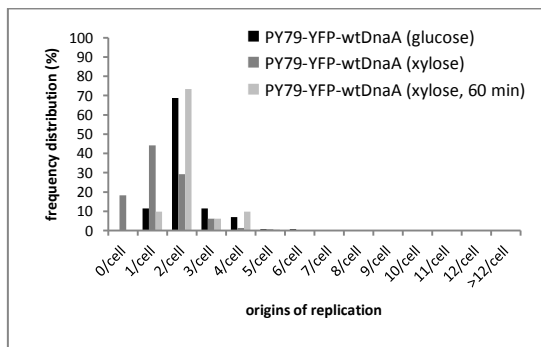
*B. subtilis* strain PY79-YFP-wtDnaA [*spo0J::(mIs lacO<sub>256</sub>, spo0J), thrC::(cm p<sub>pen</sub>-lacI-cfp), amyE::(spec p<sub>xyI</sub>-yfp-wtdnaA)*] was compared to PY79-*oriC*-CFP. Under conditions of maximal repression or moderate ectopic expression of YFP-wtDnaA, observed parameters, such as cell length, number of nucleoids and origins per cell were similar to PY79-*oriC*-CFP (Figs. 3.9.2.1.A/B/C, 3.9.2.2.A/B/D, 3.9.2.4.A/B/D). When cells were grown in glucose containing medium, as expected, no YFP-wtDnaA foci were detectable (Figs. 3.9.2.1.D, 3.9.2.2.E). However, moderate expression of YFP-wtDnaA led to the formation of clearly detectable foci that perfectly colocalized with *oriC*-CFP foci in ~30% of all cells, whereas ~30% of the cells did not show any colocalization event and another ~20% displayed partial colocalization (Figs. 3.9.2.1.D/E, 3.9.2.4.E/F). Around 35% of the cells contained one YFP-wtDnaA focus, ~25% two foci, ~20% three or four foci and ~15% no focus (Figs. 3.9.2.1.D, 3.9.2.4.E). Maximal induction of the ectopically encoded construct severely interfered with the regulation of the cell cycle, probably due to blocked replication as a consequence of repressed *dnaA-dnaN* transcription leading to a lack of DnaN essential for replication elongation (see chapter 3.8.1.) [8-9]. Cells showed a strongly filamentous phenotype (~50% of all cells were longer than 3  $\mu$ m) without replicating their chromosomes, since most of the cells contained only one nucleoid (~70%) and an important number of cells were anucleate (~20%) (Figs. 3.9.2.1.A/B, 3.9.2.3.A/B). The reduction of the frequency of initiation of replication was confirmed by a significant decrease of the number of *oriC*-CFP foci per cell (~40% one focus, ~30% two foci) (Figs. 3.9.2.1.C, 3.9.2.3.D). The distribution of YFP-wtDnaA foci was similar to moderate

expression levels, though beyond, high protein accumulation could be detected as diffuse fluorescence distributed in the cytoplasm (Figs. 3.9.2.1.D, 3.9.2.3.E).

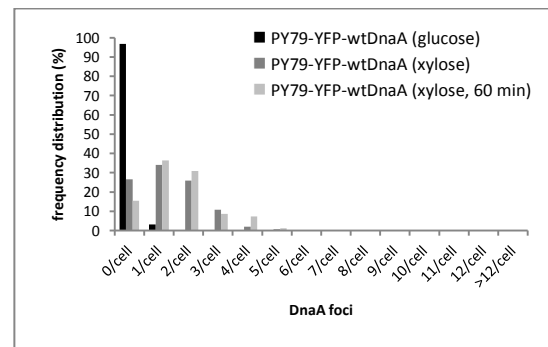
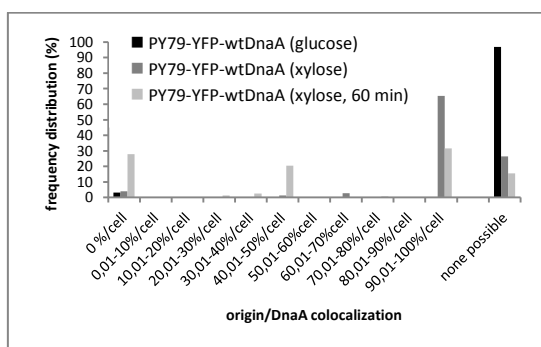
[A] Cell length distribution



[B] Nucleoid distribution

[C] *oriC*-CFP distribution

[D] YFP-wtDnaA distribution

[E] *oriC*-CFP/YFP-wtDnaA colocalization

**Fig. 3.9.2.1.:** Charts displaying the distribution of several live cell parameters of *B. subtilis* strain PY79-YFP-wtDnaA grown in S750 minimal medium (supplemented as indicated below) at 30°C until exponential growth. Black columns: glucose (5 mg/ml) [cells analyzed: 157]. Dark grey columns: xylose (5 mg/ml) [cells analyzed: 147]. Light grey columns: xylose (5 mg/ml, 60 min) [cells analyzed: 162]. A, frequency distribution of cell length. B, frequency distribution of number of chromosomes per cell. C, frequency distribution of number of origins of replication (*oriC*-CFP) per cell. D, frequency distribution of number of YFP-wtDnaA foci per cell. E, frequency distribution of *oriC*-CFP/YFP-wtDnaA colocalization events.

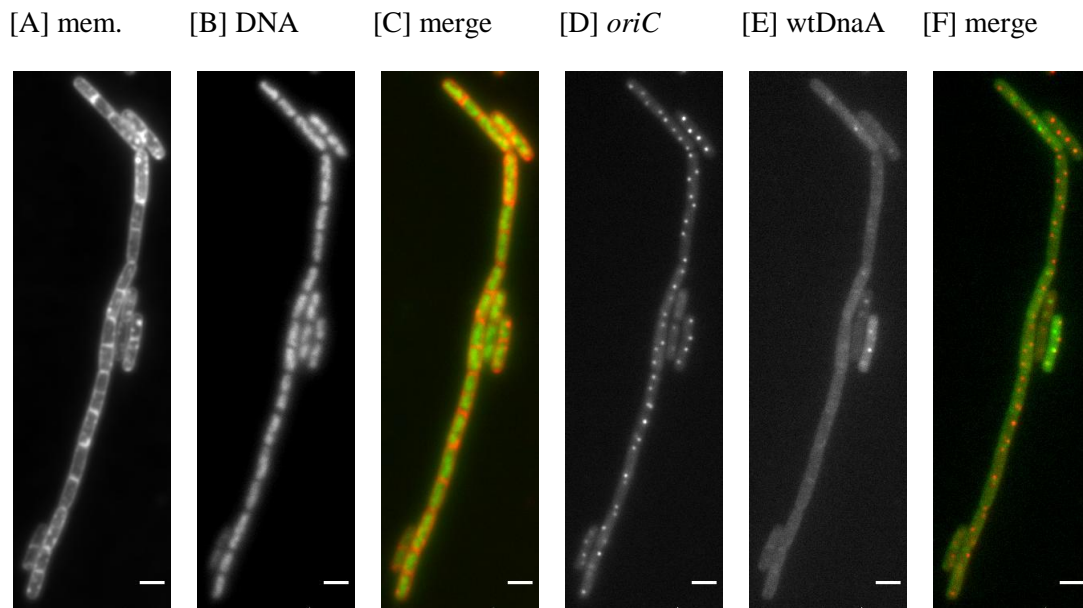


**Fig. 3.9.2.2.:** Fluorescence microscopy of *B. subtilis* strain PY79-YFP-wtDnaA grown in S750 minimal medium (supplemented with glucose) until exponential growth at 30°C. A, membrane. B, DNA (nucleoids). C, overlay of membrane (red) and DNA (green). D, origins of replication (*oriC*-CFP). E, YFP-wtDnaA. F, overlay of *oriC*-CFP (red) and YFP-wtDnaA (green). White bar: 2  $\mu$ m.

[A] mem. [B] DNA [C] merge [D] *oriC* [E] wtDnaA [F] merge

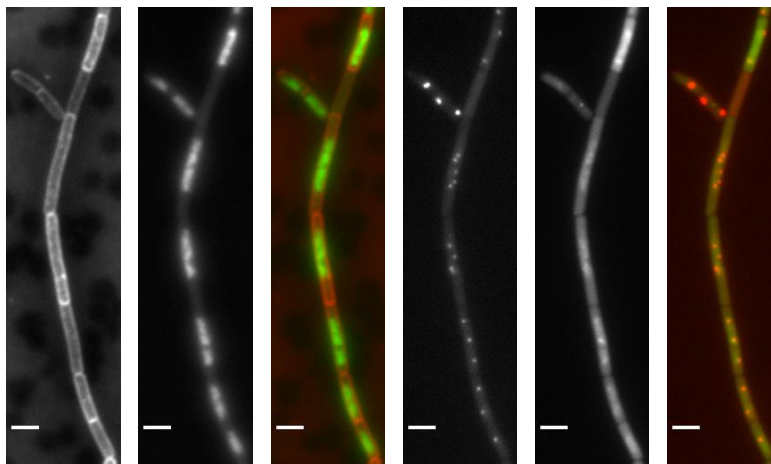


**Fig. 3.9.2.3.:** Fluorescence microscopy of *B. subtilis* strain PY79-YFP-wtDnaA grown in S750 minimal medium (supplemented with xylose) until exponential growth at 30°C. A, membrane. B, DNA (nucleoids). C, overlay of membrane (red) and DNA (green). D, origins of replication (*oriC*-CFP). E, YFP-wtDnaA. F, overlay of *oriC*-CFP (red) and YFP-wtDnaA (green). White bar: 2  $\mu$ m.

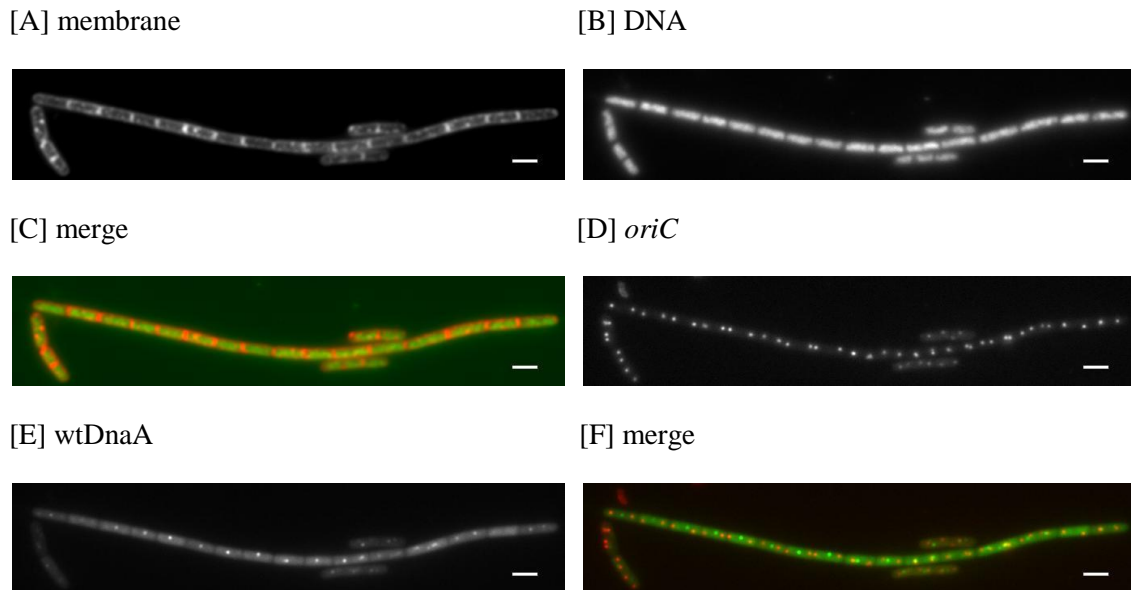
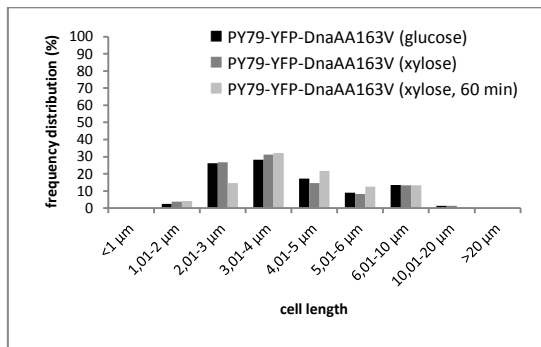


**Fig. 3.9.2.4.:** Fluorescence microscopy of *B. subtilis* strain PY79-YFP-wtDnaA grown in S750 minimal medium (supplemented with xylose for 60 min after entering exponential growth phase) at 30°C. A, membrane. B, DNA (nucleoids). C, overlay of membrane (red) and DNA (green). D, origins of replication (*oriC*-CFP). E, YFP-wtDnaA. F, overlay of *oriC*-CFP (red) and YFP-wtDnaA (green). White bar: 2  $\mu$ m.

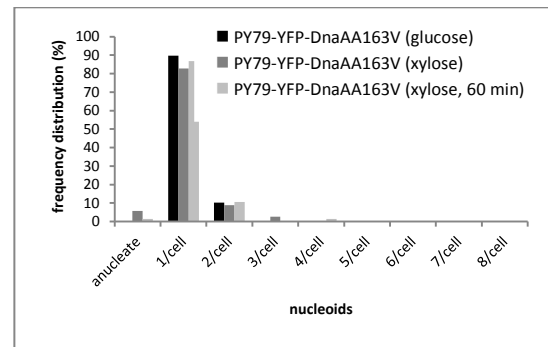
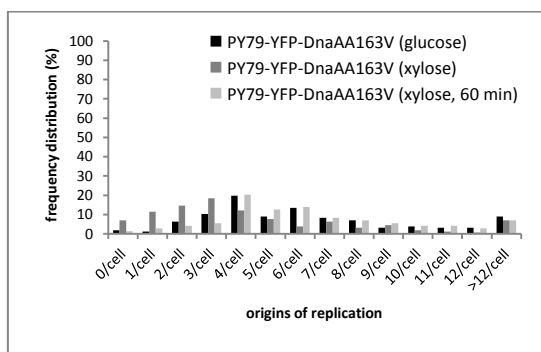
### 3.9.3. *B. subtilis* PY79-YFP-DnaAA163V displays a strong overinitiation phenotype *in vivo*

*B. subtilis* strain PY79-YFP-DnaAA163V [*spo0J::(mIs lacO<sub>256</sub>, spo0J)*, *thrC::(cm p<sub>pen</sub>-lacI-cfp)*, *amyE::(spec p<sub>xyt</sub>-yfp-dnaAA163V)*] displayed a strong phenotypic effect in the frequency of initiation of replication. The observation that under conditions of maximal repression, hence growth in glucose containing medium, cells were already abnormally elongated (~70% of all cells were longer than 3  $\mu$ m), mostly contained one highly decondensed nucleoid (~85%) and exhibited a strongly increased number of origins (~85% of all cells contained four or more *oriC*-CFP foci), suggest that YFP-DnaAA163V is dominant negative over chromosomally encoded DnaA (Figs. 3.9.3.1.A/B/C, 3.9.3.2.A/B/D). The observed effects of moderate ectopic expression or maximal expression of YFP-DnaAA163V did not significantly differ from non-induced conditions, except for a strongly increased number of YFP-DnaAA163V foci that mostly colocalized with *oriC*-CFP foci (Figs. 3.9.3.1.A/B/C/D/E, 3.9.3.2.A/B/D/E, 3.9.3.3.A/B/D/E/F, 3.9.3.4.A/B/D/E/F). The highly increased amount of YFP-DnaAA163V (under maximally induced conditions), which leads to repression of the *dnaA-dnaN* operon (see chapter 3.8.2.), did not result in blocked replication, as would have been expected as a consequence of reduced DnaN levels. On the contrary, PY79-YFP-DnaAA163V displayed a strong overinitiation phenotype.

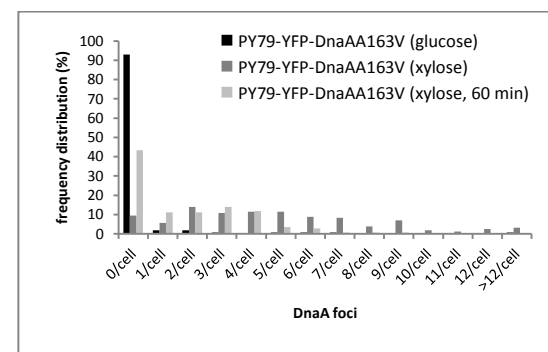
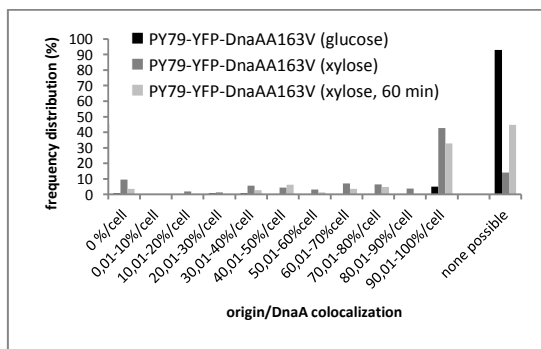
[A] Cell length distribution



[B] Nucleoid distribution

[C] *oriC*-CFP distribution

[D] YFP-DnaAA163V distribution

[E] *oriC*-CFP/YFP-DnaAA163V colocalization

**Fig. 3.9.3.1.:** Charts displaying the distribution of several live cell parameters of *B. subtilis* strain PY79-YFP-DnaAA163V grown in S750 minimal medium (supplemented as indicated below) at 30°C until exponential growth. Black columns: glucose (5 mg/ml) [cells analyzed: 156]. Dark grey columns: xylose (5 mg/ml) [cells analyzed: 157]. Light grey columns: xylose (5 mg/ml, 60 min) [cells analyzed: 143]. A, frequency distribution of cell length. B, frequency distribution of number of chromosomes per cell. C, frequency distribution of number of origins of replication (*oriC*-CFP) per cell. D, frequency distribution of number of YFP-DnaAA163V foci per cell. E, frequency distribution of *oriC*-CFP/YFP-DnaAA163V colocalization events.

[A] mem. [B] DNA [C] merge [D] *oriC* [E] A163V [F] merge

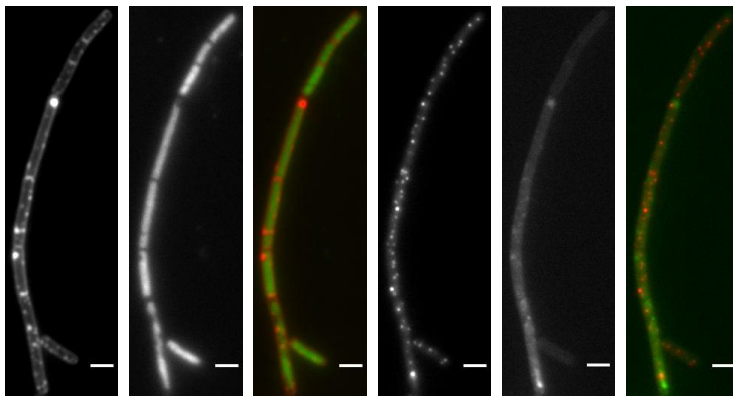
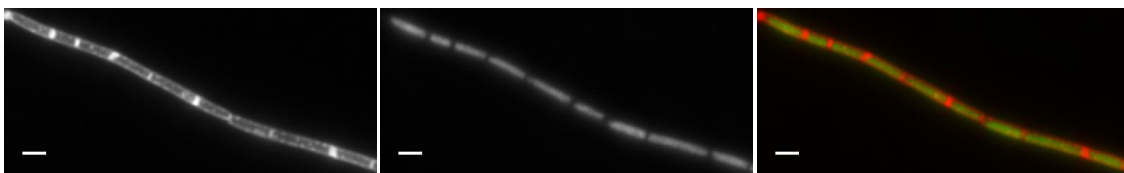


**Fig. 3.9.3.2.:** Fluorescence microscopy of *B. subtilis* strain PY79-YFP-DnaAA163V grown in S750 minimal medium (supplemented with glucose) until exponential growth at 30°C. A, membrane. B, DNA (nucleoids). C, overlay of membrane (red) and DNA (green). D, origins of replication (*oriC*-CFP). E, YFP-DnaAA163V. F, overlay of *oriC*-CFP (red) and YFP-DnaAA163V (green). White bar: 2 µm.

[A] membrane

[B] DNA

[C] merge



[D] *oriC*

[E] DnaAA163V

[F] merge

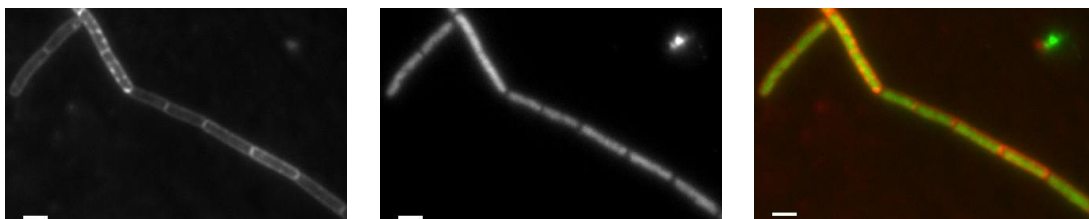


**Fig. 3.9.3.3.:** Fluorescence microscopy of *B. subtilis* strain PY79-YFP-DnaAA163V grown in S750 minimal medium (supplemented with xylose) until exponential growth at 30°C. A, membrane. B, DNA (nucleoids). C, overlay of membrane (red) and DNA (green). D, origins of replication (*oriC*-CFP). E, YFP-DnaAA163V. F, overlay of *oriC*-CFP (red) and YFP-DnaAA163V (green). White bar: 2 µm.

[A] membrane

[B] DNA

[C] merge



[D] *oriC*

[E] DnaAA163V

[F] merge

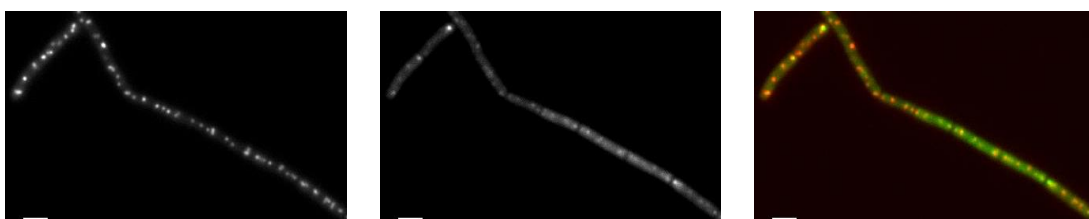
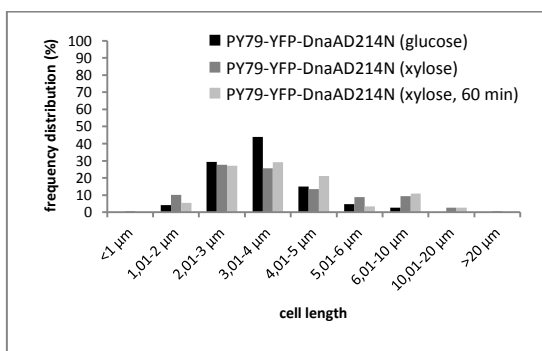


**Fig. 3.9.3.4.:** Fluorescence microscopy of *B. subtilis* strain PY79-YFP-DnaAA163V grown in S750 minimal medium (supplemented with xylose for 60 min after entering exponential growth phase) at 30°C. A, membrane. B, DNA (nucleoids). C, overlay of membrane (red) and DNA (green). D, origins of replication (*oriC*-CFP). E, YFP-DnaAA163V. F, overlay of *oriC*-CFP (red) and YFP-DnaAA163V (green). White bar: 2 µm.

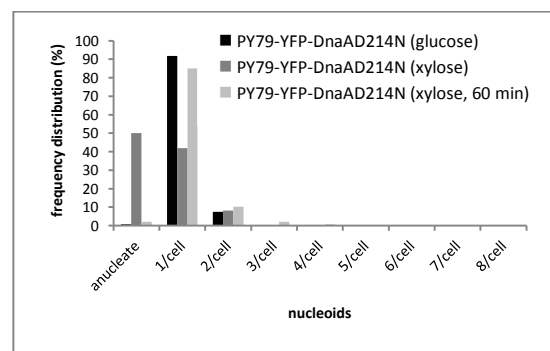
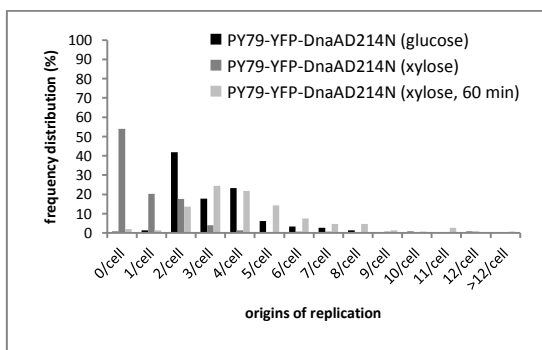
### 3.9.4. *B. subtilis* PY79-YFP-DnaAD214N displays an increased replication initiation frequency *in vivo*

*B. subtilis* strain PY79-YFP-DnaAD214N [*spo0J::(mIs lacO<sub>256</sub>, spo0J), thrC::(cm p<sub>pen</sub>-lacI-cfp), amyE::(spec p<sub>xyI</sub>-yfp-dnaAD214N)*] showed slightly elongated cells compared to PY79-YFP-wtDnaA (~65% of all cells were longer than 3  $\mu\text{m}$ ) with generally one nucleoid (~85%) both under conditions of maximal repression or moderate ectopic expression of YFP-DnaAD214N (Figs. 3.9.4.1.A/B, 3.9.4.2.A/B, 3.9.4.4.A/B). No YFP-DnaAD214N focus was detectable when the cells were grown in glucose containing medium (Figs. 3.9.4.1.D, 3.9.4.2.E).

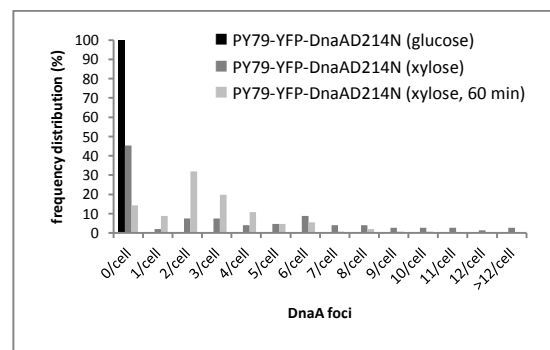
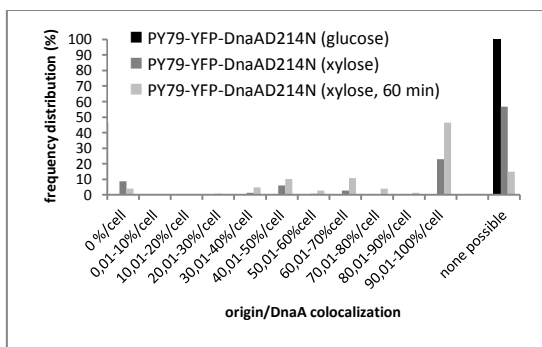
[A] Cell length distribution



[B] Nucleoid distribution

[C] *oriC*-CFP distribution

[D] YFP-DnaAD214N distribution

[E] *oriC*-CFP/YFP-DnaAD214N colocalization

**Fig. 3.9.4.1:** Charts displaying the distribution of several live cell parameters of *B. subtilis* strain PY79-YFP-DnaAD214N grown in S750 minimal medium (supplemented as indicated below) at 30°C until exponential growth. Black columns: glucose (5 mg/ml) [cells analyzed: 146]. Dark grey columns: xylose (5 mg/ml) [cells analyzed: 148]. Light grey columns: xylose (5 mg/ml, 60 min) [cells analyzed: 147]. A, frequency distribution of cell length. B, frequency distribution of number of chromosomes per cell. C, frequency distribution of number of origins of replication (*oriC*-CFP) per cell. D, frequency distribution of number of YFP-DnaAD214N foci per cell. E, frequency distribution of *oriC*-CFP/YFP-DnaAD214N colocalization events.

Moderate induction resulted in an increased number of DnaA foci (~70% of all cells contained two or more foci) that colocalized in ~50% with the origins of replication (Figs. 3.9.4.1.E, 3.9.4.4.F). Approximately 40% of the non-induced cells contained two, ~15% three and ~20% four *oriC*-CFP foci per cell, whereas moderately expressing cells displayed a significant increase in the frequency of initiation, since ~60% contained four or more origins per cell (Figs. 3.9.4.1.C, 3.9.4.2.D, 3.9.4.4.D). Maximal induction of the construct led to repression of the *dnaA-dnaN* operon (see chapter 3.8.2.), but strikingly had more severe consequences than overexpression of YFP-wtDnaA. Blocked replication in PY79-YFP-DnaAD214N resulted in ~50% anucleate cells. The remaining fraction of cells mostly contained one condensed nucleoid (~40%), one or two *oriC*-CFP foci per cell (~20% and 18%, respectively) and a highly variable number of YFP-DnaAD214N foci (Figs. 3.9.4.1.B/C/D, 3.9.4.3.A/B/D/E).

[A] mem. [B] DNA [C] merge [D] *oriC* [E] D214N [F] merge

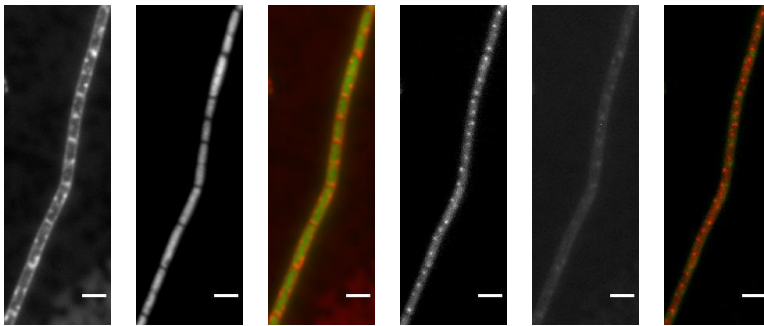


**Fig. 3.9.4.2.:** Fluorescence microscopy of *B. subtilis* strain PY79-YFP-DnaAD214N grown in S750 minimal medium (supplemented with glucose) until exponential growth at 30°C. A, membrane. B, DNA (nucleoids). C, overlay of membrane (red) and DNA (green). D, origins of replication (*oriC*-CFP). E, YFP-DnaAD214N. F, overlay of *oriC*-CFP (red) and YFP-DnaAD214N (green). White bar: 2  $\mu$ m.

[A] mem. [B] DNA [C] merge [D] *oriC* [E] D214N [F] merge

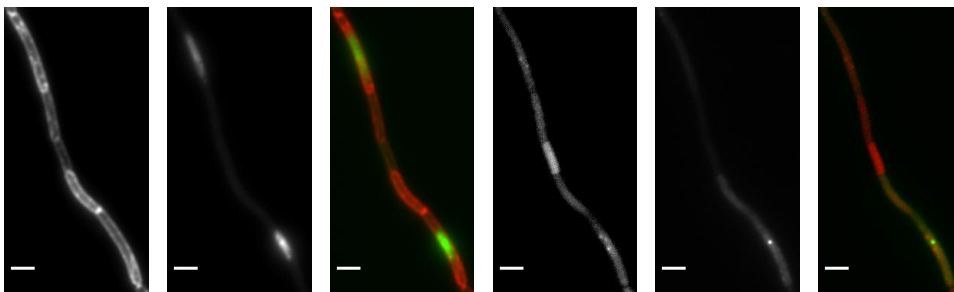


**Fig. 3.9.4.3.:** Fluorescence microscopy of *B. subtilis* strain PY79-YFP-DnaAD214N grown in S750 minimal medium (supplemented with xylose) until exponential growth at 30°C. A, membrane. B, DNA (nucleoids). C, overlay of membrane (red) and DNA (green). D, origins of replication (*oriC*-CFP). E, YFP-DnaAD214N. F, overlay of *oriC*-CFP (red) and YFP-DnaAD214N (green). White bar: 2  $\mu$ m.

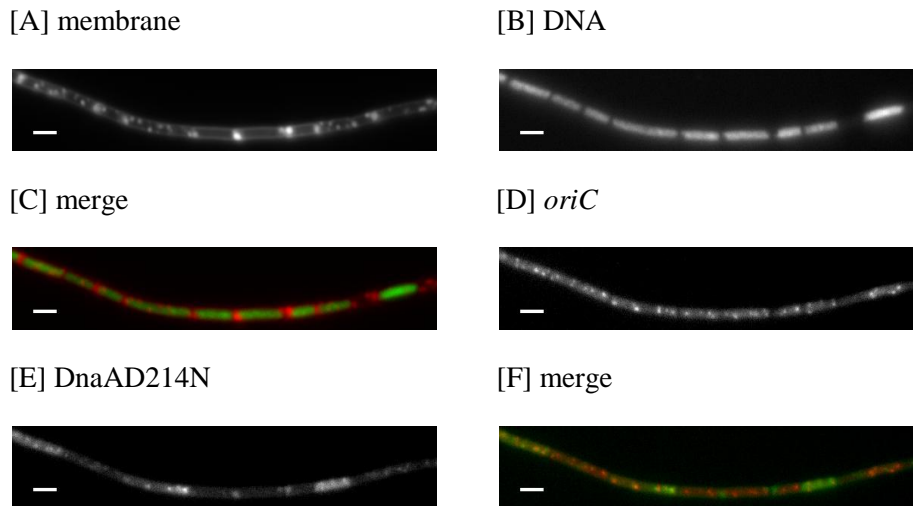
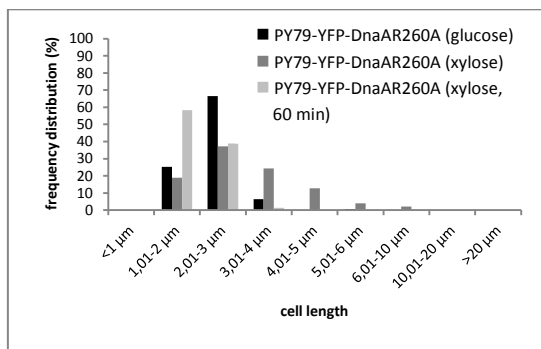


**Fig. 3.9.4.4.:** Fluorescence microscopy of *B. subtilis* strain PY79-YFP-DnaAD214N grown in S750 minimal medium (supplemented with xylose for 60 min after entering exponential growth phase) at 30°C. A, membrane. B, DNA (nucleoids). C, overlay of membrane (red) and DNA (green). D, origins of replication (*oriC*-CFP). E, YFP-DnaAD214N. F, overlay of *oriC*-CFP (red) and YFP-DnaAD214N (green). White bar: 2  $\mu$ m.

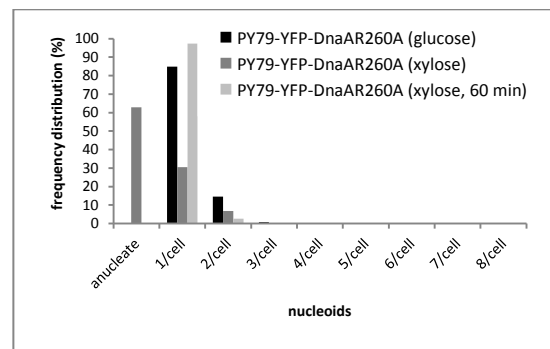
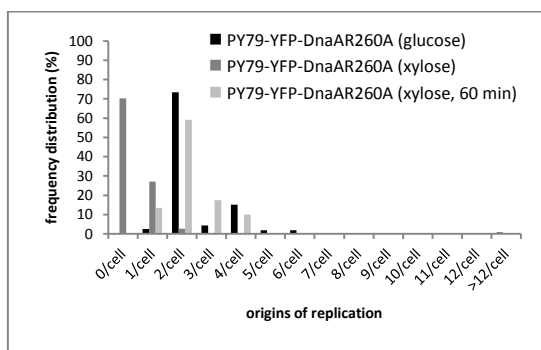
### 3.9.5. *B. subtilis* PY79-YFP-DnaAR260A prematurely initiates replication *in vivo*

*B. subtilis* strain PY79-YFP-DnaAR260A [*spo0J::(mIs lacO<sub>256</sub>, spo0J), thrC::(cm p<sub>pen</sub>-lacI-cfp), amyE::(spec p<sub>xyI</sub>-yfp-dnaAR260A)*] did not show any significant differences compared to PY79-YFP-wtDnaA when grown in glucose containing minimal medium, i.e. ~70% of all cells were 2-3  $\mu$ m long, ~85% contained one nucleoid, ~75% had two and ~15% four *oriC*-CFP foci and no YFP-DnaAR260A focus could be detected (Figs. 3.9.5.1.A/B/C/D, 3.9.5.2.A/B/D/E). Under conditions of moderate ectopic expression of YFP-DnaAR260A the observed cells were considerably smaller (~60% of all cells were 1-2  $\mu$ m long), suggesting premature initiation of replication and/or cell division (Figs. 3.9.5.1.A, 3.9.5.4.A). However, the frequency distribution of the number of nucleoids and origins was nearly identical to non-induced conditions (Figs. 3.9.1.B/C, 3.9.5.4.B/D). Moreover, ~50% of all cells did not show any YFP-DnaAR260A focus, but, unlike PY79-YFP-wtDnaA, most of the remaining cells contained one focus per cell that generally did not colocalize with the origins of replication (Figs. 3.9.1.D/E, 3.9.5.4.E/F). Maximal induction of the construct led to repression of the *dnaA-dnaN* operon (see chapter 3.8.2.), which had severe consequences on the cell cycle similar to PY79-YFP-DnaAD214N (see chapter 3.9.4.). Blocked replication resulted in elongated cells (~40% of all cells were longer than 3  $\mu$ m), out of which ~60% were anucleate, while the other fraction of cells mostly contained one condensed nucleoid (~30%), one *oriC*-CFP focus per cell (~25%) and a highly variable number of YFP-DnaAR260A foci, which in some cases localized as an arranged helical pattern in the cell membrane (Figs. 3.9.5.1.A/B/C/D, 3.9.5.3.A/B/D/E).

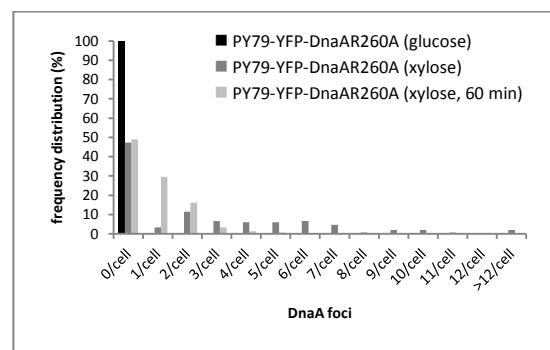
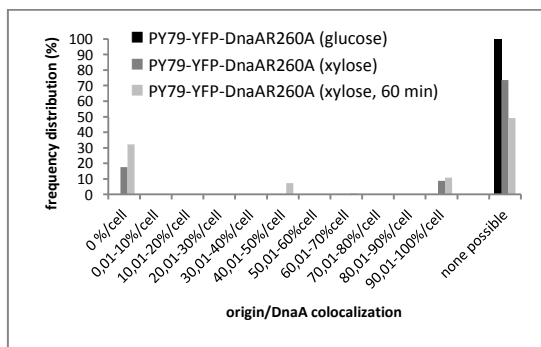
[A] Cell length distribution



[B] Nucleoid distribution

[C] *oriC*-CFP distribution

[D] YFP-DnaAR260A distribution

[E] *oriC*-CFP/YFP-DnaAR260A colocalization

**Fig. 3.9.5.1:** Charts displaying the distribution of several live cell parameters of *B. subtilis* strain PY79-YFP-DnaAR260A grown in S750 minimal medium (supplemented as indicated below) at 30°C until exponential growth. Black columns: glucose (5 mg/ml) [cells analyzed: 158]. Dark grey columns: xylose (5 mg/ml) [cells analyzed: 148]. Light grey columns: xylose (5 mg/ml, 60 min) [cells analyzed: 149]. A, frequency distribution of cell length. B, frequency distribution of number of chromosomes per cell. C, frequency distribution of number of origins of replication (*oriC*-CFP) per cell. D, frequency distribution of number of YFP-DnaAR260A foci per cell. E, frequency distribution of *oriC*-CFP/YFP-DnaAR260A colocalization events.

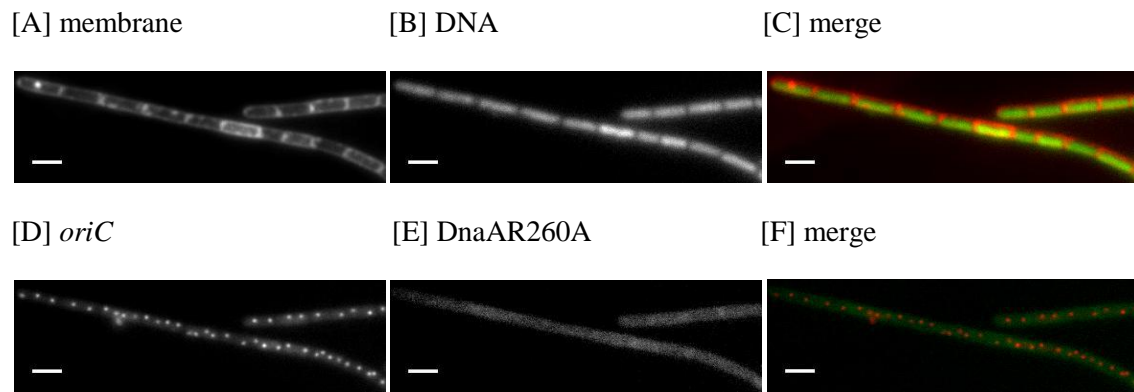


**Fig. 3.9.5.2.:** Fluorescence microscopy of *B. subtilis* strain PY79-YFP-DnaAR260A grown in S750 minimal medium (supplemented with glucose) until exponential growth at 30°C. A, membrane. B, DNA (nucleoids). C, overlay of membrane (red) and DNA (green). D, origins of replication (*oriC*-CFP). E, YFP-DnaAR260A. F, overlay of *oriC*-CFP (red) and YFP-DnaAR260A (green). White bar: 2  $\mu$ m.

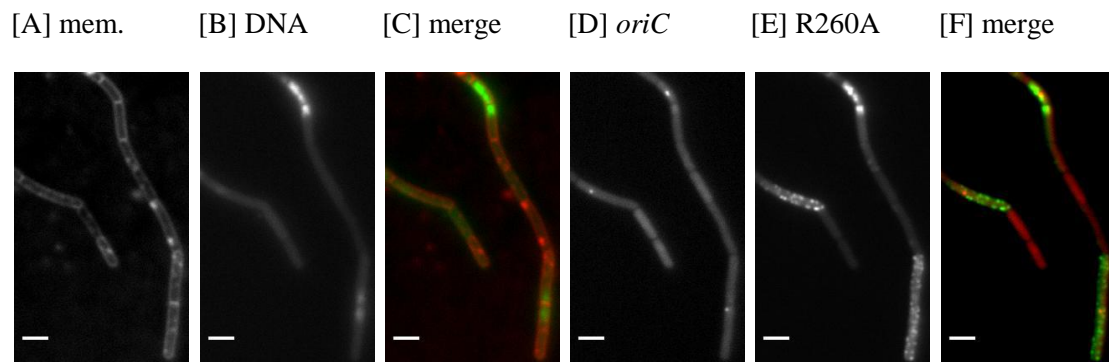


**Fig. 3.9.5.3.:** Fluorescence microscopy of *B. subtilis* strain PY79-YFP-DnaAR260A grown in S750 minimal medium (supplemented with xylose) until exponential growth at 30°C. A, membrane. B, DNA (nucleoids). C, overlay of membrane (red) and DNA (green). D, origins of replication (*oriC*-CFP). E, YFP-DnaAR260A. F, overlay of *oriC*-CFP (red) and YFP-DnaAR260A (green). White bar: 2  $\mu$ m.

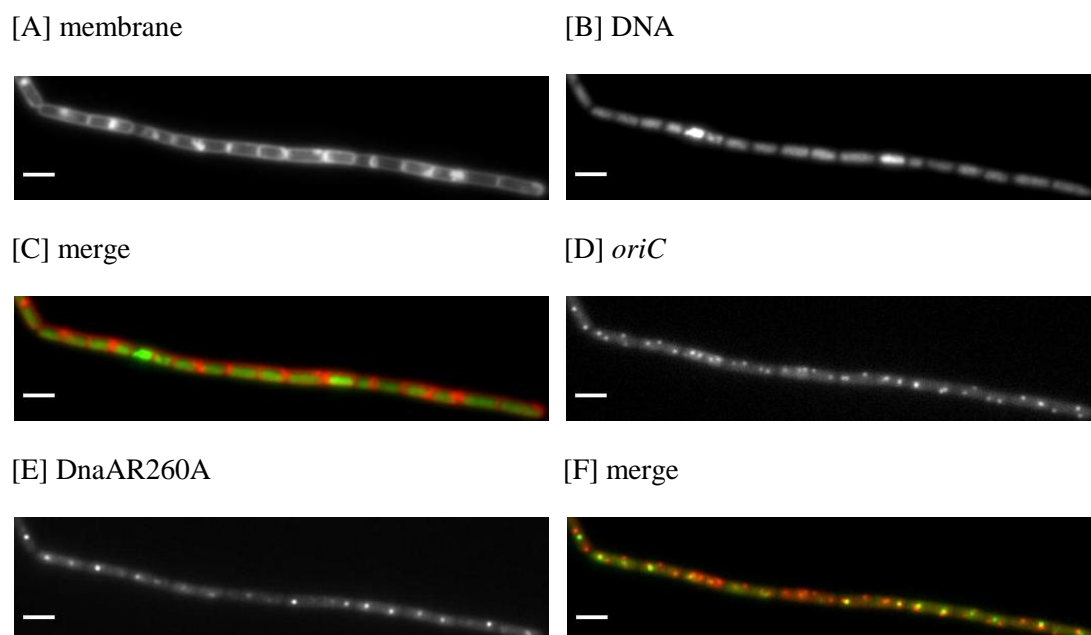
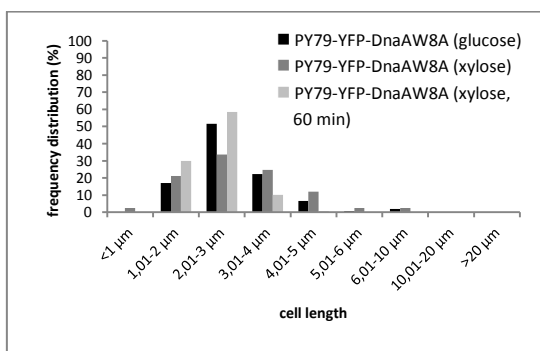


**Fig. 3.9.5.4.:** Fluorescence microscopy of *B. subtilis* strain PY79-YFP-DnaAR260A grown in S750 minimal medium (supplemented with xylose for 60 min after entering exponential growth phase) at 30°C. A, membrane. B, DNA (nucleoids). C, overlay of membrane (red) and DNA (green). D, origins of replication (*oriC*-CFP). E, YFP-DnaAR260A. F, overlay of *oriC*-CFP (red) and YFP-DnaAR260A (green). White bar: 2  $\mu$ m.

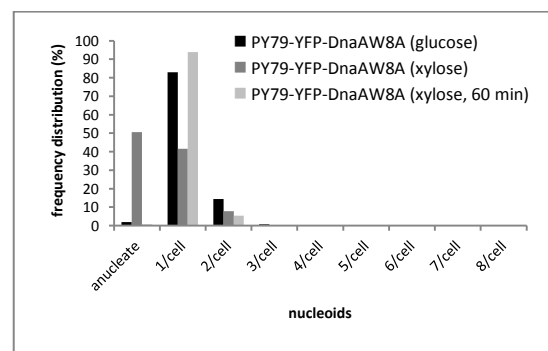
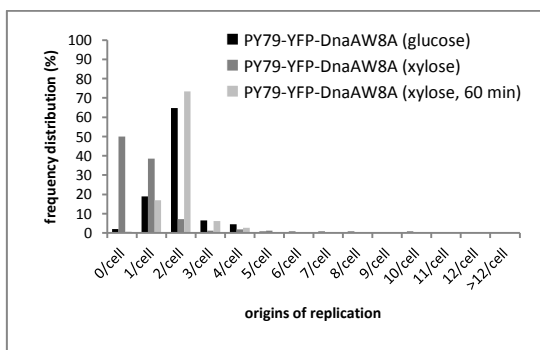
3.9.6. *B. subtilis* PY79-YFP-DnaAW8A does not assemble distinct YFP-DnaAW8A foci *in vivo*

*B. subtilis* strain PY79-YFP-DnaAW8A [*spo0J::(mIs lacO<sub>256</sub>, spo0J), thrC::(cm p<sub>pen</sub>-lacI-cfp), amyE::(spec p<sub>xyI</sub>-yfp-dnaAW8A)*] did not show any significant differences in cell length, nucleoid distribution, initiation frequency or occurrence of YFP-DnaAW8A foci compared to PY79-YFP-wtDnaA when grown in glucose containing medium, i.e. ~15% of all cells were smaller than 2  $\mu\text{m}$ , ~50% were 2-3  $\mu\text{m}$  long, ~20% were 3-4  $\mu\text{m}$  long, ~80% contained one nucleoid, ~65% had two *oriC*-CFP and ~20% one focus per cell and no YFP-DnaAW8A focus could be detected (Figs. 3.9.6.1.A/B/C/D, 3.9.6.2.A/B/D/E).

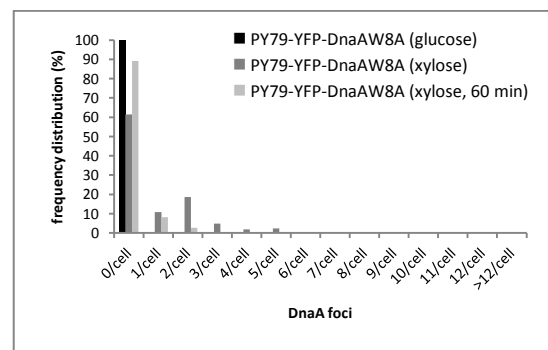
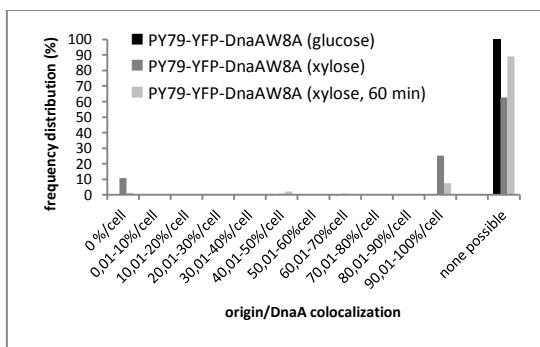
[A] Cell length distribution



[B] Nucleoid distribution

[C] *oriC*-CFP distribution

[D] YFP-DnaAW8A distribution

[E] *oriC*-CFP/YFP-DnaAW8A colocalization

**Fig. 3.9.6.1:** Charts displaying the distribution of several live cell parameters of *B. subtilis* strain PY79-YFP-DnaAW8A grown in S750 minimal medium (supplemented as indicated below) at 30°C until exponential growth. Black columns: glucose (5 mg/ml) [cells analyzed: 153]. Dark grey columns: xylose (5 mg/ml) [cells analyzed: 166]. Light grey columns: xylose (5 mg/ml, 60 min) [cells analyzed: 147]. A, frequency distribution of cell length. B, frequency distribution of number of chromosomes per cell. C, frequency distribution of number of origins of replication (*oriC*-CFP) per cell. D, frequency distribution of number of YFP-DnaAW8A foci per cell. E, frequency distribution of *oriC*-CFP/YFP-DnaAW8A colocalization events.

Moderate ectopic expression of YFP-DnaAW8A, except for a slightly reduced initiation frequency, did not lead to any significant differences of the observed parameters compared to maximal repression, including the lack of YFP-DnaAW8A foci (~90% of all cells) (Figs. 3.9.6.1.A/B/C/D, 3.9.6.4.A/B/D/E). Full induction of the construct consequently down regulated *dnaA-dnaN* transcription (see chapter 3.8.2.), resulting in blocked replication. The effects on PY79-YFP-DnaAW8A were similar to PY79-YFP-DnaAD214N and PY79-YFP-DnaAR260A (see chapters 3.9.4. and 3.9.5.) and appeared to be more severe than in PY79-YFP-wtDnaA. Blocked replication resulted in elongated cells (~40% of all cells were longer than 3  $\mu\text{m}$ ), out of which ~50% were anucleate, while the other fraction of cells mostly contained one condensed nucleoid (~40%), one *oriC*-CFP focus (~40%) and either no YFP-DnaAW8A focus (~60%), one focus (~10%) or two foci (~20%) per cell, which appeared to be rather diffuse since the fluorescence was dispersed within the cytoplasm (Figs. 3.9.6.1.A/B/C/D, 3.9.6.3.A/B/D/E).

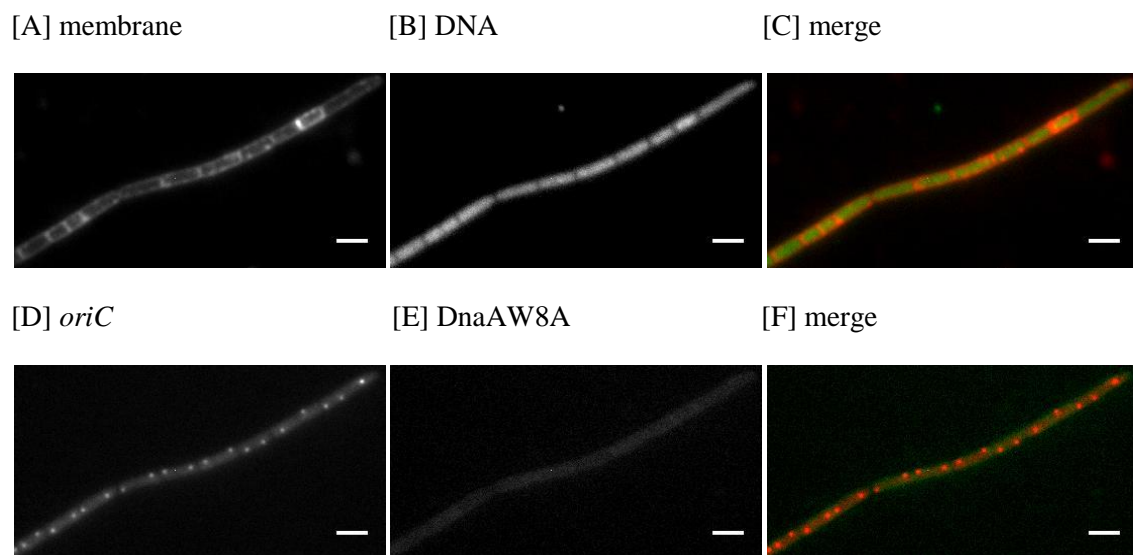


**Fig. 3.9.6.2.:** Fluorescence microscopy of *B. subtilis* strain PY79-YFP-DnaAW8A grown in S750 minimal medium (supplemented with glucose) until exponential growth at 30°C. A, membrane. B, DNA (nucleoids). C, overlay of membrane (red) and DNA (green). D, origins of replication (*oriC*-CFP). E, YFP-DnaAW8A. F, overlay of *oriC*-CFP (red) and YFP-DnaAW8A (green). White bar: 2  $\mu\text{m}$ .

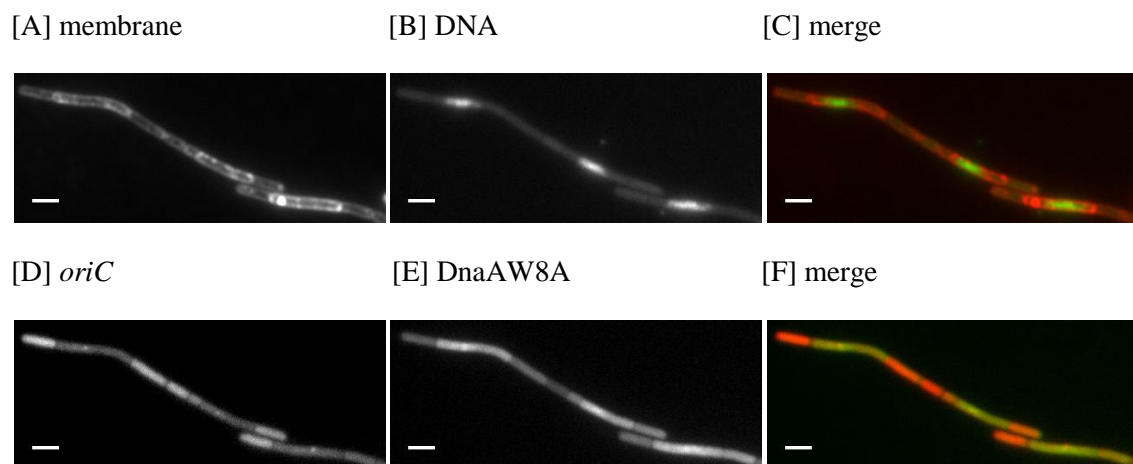


**Fig. 3.9.6.3.:** Fluorescence microscopy of *B. subtilis* strain PY79-YFP-DnaAW8A grown in S750 minimal medium (supplemented with xylose) until exponential growth at 30°C. A, membrane. B, DNA (nucleoids). C, overlay of membrane (red) and DNA (green). D, origins of replication (*oriC*-CFP). E, YFP-DnaAW8A. F, overlay of *oriC*-CFP (red) and YFP-DnaAW8A (green). White bar: 2  $\mu\text{m}$ .

[A] mem. [B] DNA [C] merge [D] *oriC* [E] W8A [F] merge

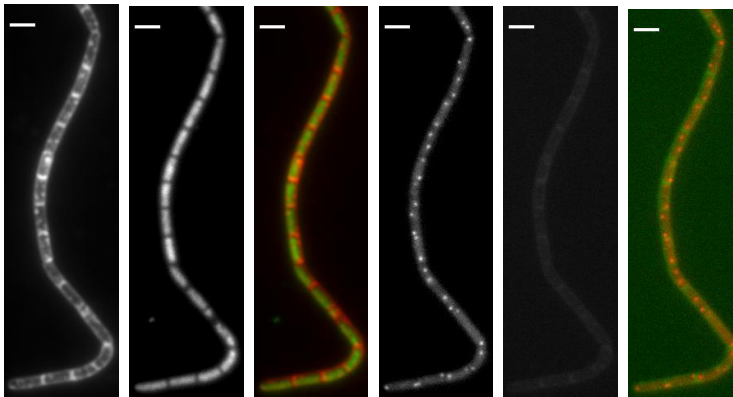
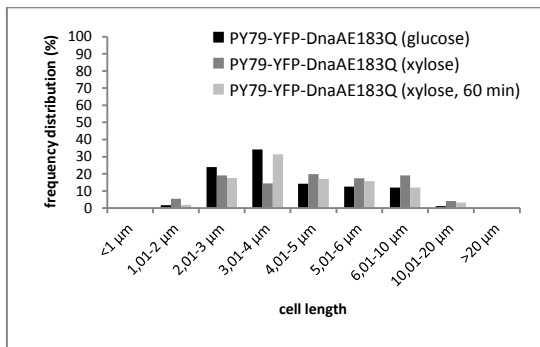


**Fig. 3.9.6.4:** Fluorescence microscopy of *B. subtilis* strain PY79-YFP-DnaAW8A grown in S750 minimal medium (supplemented with xylose for 60 min after entering exponential growth phase) at 30°C. A, membrane. B, DNA (nucleoids). C, overlay of membrane (red) and DNA (green). D, origins of replication (*oriC*-CFP). E, YFP-DnaAW8A. F, overlay of *oriC*-CFP (red) and YFP-DnaAW8A (green). White bar: 2  $\mu$ m.

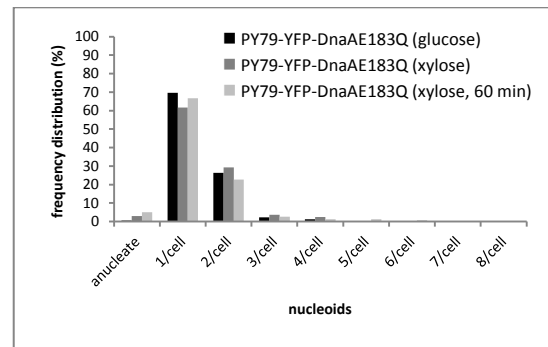
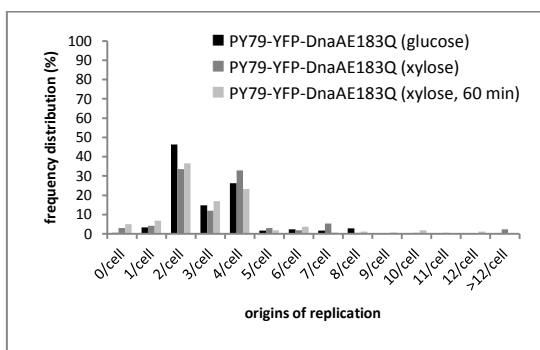
### 3.9.7. *B. subtilis* PY79-YFP-DnaAE183Q cells are significantly elongated *in vivo*

*B. subtilis* strain PY79-YFP-DnaAE183Q [*spo0J*::(*mls lacO*<sub>256</sub>, *spo0J*), *thrC*::(*cm p<sub>pen</sub>-lacI-cfp*), *amyE*::(*spec p<sub>xyI</sub>-yfp-dnaAE183Q*)] displayed a strong phenotypic effect in cell morphology, i.e. cells were significantly elongated. The fact that cells were already abnormally elongated (~75% of all cells were longer than 3  $\mu$ m) in glucose containing minimal medium, suggest that YFP-DnaAE183Q is dominant negative over chromosomally encoded DnaA (Figs. 3.9.7.1.A, 3.9.7.2.A). In support of this conclusion, the investigated parameters of moderate ectopic expression or maximal expression of YFP-DnaAE183Q did not significantly differ from non-induced conditions (~60-70% of the cells contained one nucleoid and ~20-30% two nucleoids, ~35-45% contained two *oriC*-CFP foci, ~15% three foci and ~25-35% four foci), except for a slightly increased number of YFP-DnaAE183Q foci that did not colocalize with *oriC*-CFP foci in most of the cases (Figs. 3.9.7.1.A/B/C/D/E, 3.9.7.2.A/B/D/E, 3.9.7.3.A/B/D/E/F, 3.9.7.4.A/B/D/E/F). PY79-YFP-DnaAE183Q showed an enhanced initiation frequency, but this could be attributed to a greater DNA-content in the elongated cells. Maximal induction of YFP-DnaAE183Q did not lead to strong cell cycle malfunctions and replication blocks.

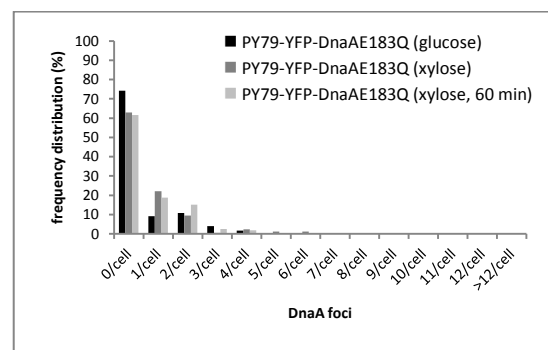
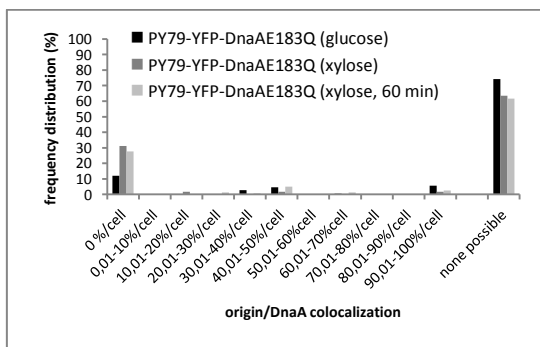
[A] Cell length distribution



[B] Nucleoid distribution

[C] *oriC*-CFP distribution

[D] YFP-DnaAE183Q distribution

[E] *oriC*-CFP/YFP-DnaAE183Q colocalization

**Fig. 3.9.7.1.:** Charts displaying the distribution of several live cell parameters of *B. subtilis* strain PY79-YFP-DnaAE183Q grown in S750 minimal medium (supplemented as indicated below) at 30°C until exponential growth. Black columns: glucose (5 mg/ml) [cells analyzed: 175]. Dark grey columns: xylose (5 mg/ml) [cells analyzed: 167]. Light grey columns: xylose (5 mg/ml, 60 min) [cells analyzed: 159]. A, frequency distribution of cell length. B, frequency distribution of number of chromosomes per cell. C, frequency distribution of number of origins of replication (*oriC*-CFP) per cell. D, frequency distribution of number of YFP-DnaAE183Q foci per cell. E, frequency distribution of *oriC*-CFP/YFP-DnaAE183Q colocalization events.

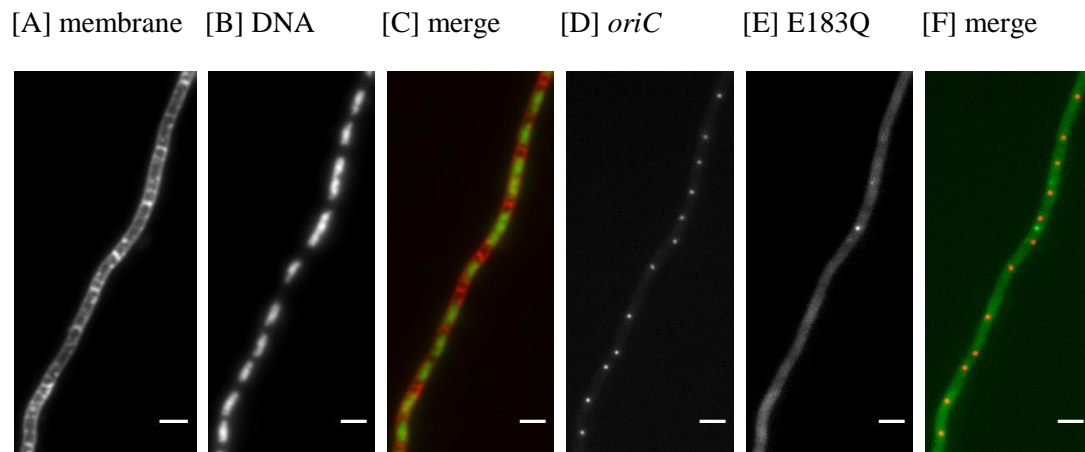


**Fig. 3.9.7.2.:** Fluorescence microscopy of *B. subtilis* strain PY79-YFP-DnaAE183Q grown in S750 minimal medium (supplemented with glucose) until exponential growth at 30°C. A, membrane. B, DNA (nucleoids). C, overlay of membrane (red) and DNA (green). D, origins of replication (*oriC*-CFP). E, YFP-DnaAE183Q. F, overlay of *oriC*-CFP (red) and YFP-DnaAE183Q (green). White bar: 2  $\mu$ m.

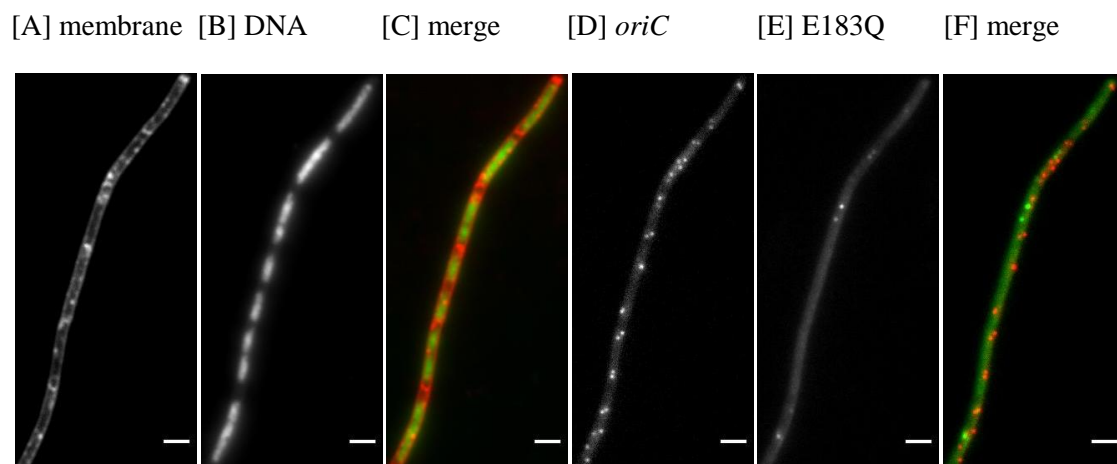


**Fig. 3.9.7.3.:** Fluorescence microscopy of *B. subtilis* strain PY79-YFP-DnaAE183Q grown in S750 minimal medium (supplemented with xylose) until exponential growth at 30°C. A, membrane. B, DNA (nucleoids). C, overlay of membrane (red) and DNA (green). D, origins of replication (*oriC*-CFP). E, YFP-DnaAE183Q. F, overlay of *oriC*-CFP (red) and YFP-DnaAE183Q (green). White bar: 2  $\mu$ m.

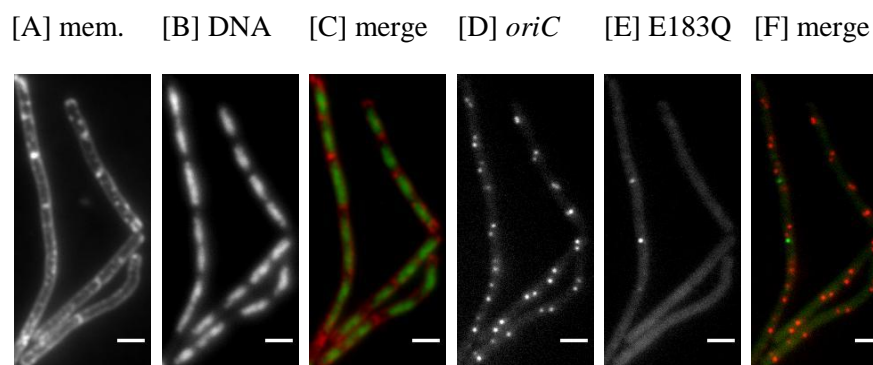
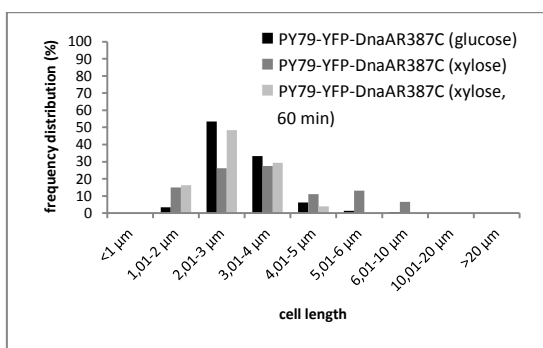


**Fig. 3.9.7.4.:** Fluorescence microscopy of *B. subtilis* strain PY79-YFP-DnaAE183Q grown in S750 minimal medium (supplemented with xylose for 60 min after entering exponential growth phase) at 30°C. A, membrane. B, DNA (nucleoids). C, overlay of membrane (red) and DNA (green). D, origins of replication (*oriC*-CFP). E, YFP-DnaAE183Q. F, overlay of *oriC*-CFP (red) and YFP-DnaAE183Q (green). White bar: 2  $\mu$ m.

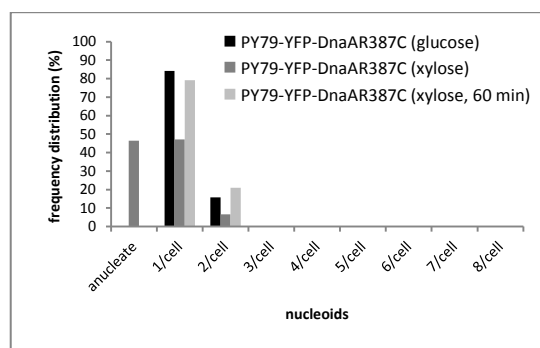
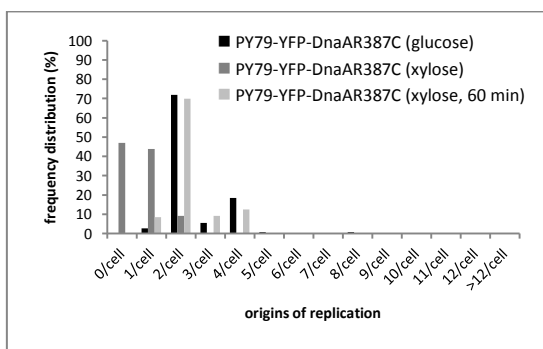
### 3.9.8. *B. subtilis* PY79-YFP-DnaAR387C does not assemble distinct YFP-DnaAR387C foci *in vivo*

*B. subtilis* strain PY79-YFP-DnaAR387C [*spo0J::(mIs lacO<sub>256</sub>, spo0J)*, *thrC::(cm p<sub>pen</sub>-lacI-cfp)*, *amyE::(spec p<sub>xyI</sub>-yfp-dnaAR387C)*] did not show any significant differences in cell length, nucleoid distribution, initiation frequency or occurrence of YFP-DnaAR387C foci compared to PY79-YFP-wtDnaA when grown in glucose containing medium, i.e. ~50% of all cells were 2-3  $\mu\text{m}$  long and ~30% were 3-4  $\mu\text{m}$  long, ~80% contained one nucleoid, ~70% contained two *oriC*-CFP foci per cell and no YFP-DnaAR387C focus could be detected (Figs. 3.9.8.1.A/B/C/D, 3.9.8.2.A/B/D/E).

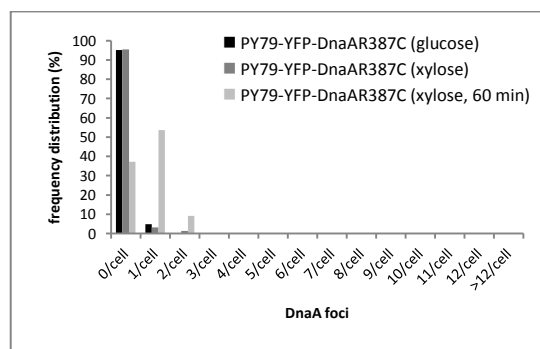
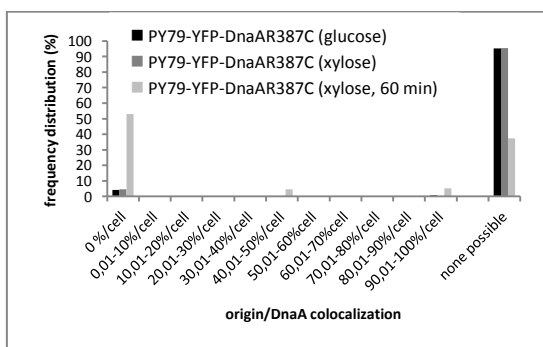
[A] Cell length distribution



[B] Nucleoid distribution

[C] *oriC*-CFP distribution

[D] YFP-DnaAR387C distribution

[E] *oriC*-CFP/YFP-DnaAR387C colocalization

**Fig. 3.9.8.1.:** Charts displaying the distribution of several live cell parameters of *B. subtilis* strain PY79-YFP-DnaAR387C grown in S750 minimal medium (supplemented as indicated below) at 30°C until exponential growth. Black columns: glucose (5 mg/ml) [cells analyzed: 146]. Dark grey columns: xylose (5 mg/ml) [cells analyzed: 153]. Light grey columns: xylose (5 mg/ml, 60 min) [cells analyzed: 153]. A, frequency distribution of cell length. B, frequency distribution of number of chromosomes per cell. C, frequency distribution of number of origins of replication (*oriC*-CFP) per cell. D, frequency distribution of number of YFP-DnaAR387C foci per cell. E, frequency distribution of *oriC*-CFP/YFP-DnaAR387C colocalization events.

Moderate ectopic expression of YFP-DnaAR387C did not lead to any significant differences of the observed parameters compared to maximal repression of the construct, except for an increased number of YFP-DnaAR387C foci (~50% of all cells contained one focus and ~10% two foci) that did not colocalize with *oriC*-CFP foci (Figs. 3.9.8.1.A/B/C/D, 3.9.8.4.A/B/D/E/F). Full induction of the DNA-binding deficient construct did not down regulate *dnaA-dnaN* transcription (see chapter 3.8.4.). Nevertheless, blocked replication was observed and resulted in elongated cells (~60% of all cells were longer than 3  $\mu\text{m}$ ), out of which ~45% were anucleate, while the other fraction of cells mostly contained one nucleoid (~45%), one *oriC*-CFP focus (~40%) and no YFP-DnaAR387C focus (~95%), since the fluorescence was distributed mainly all over the cytoplasm (Figs. 3.9.8.1.A/B/C/D, 3.9.8.3.A/B/D/E).

[A] mem. [B] DNA [C] merge [D] *oriC* [E] R387C [F] merge

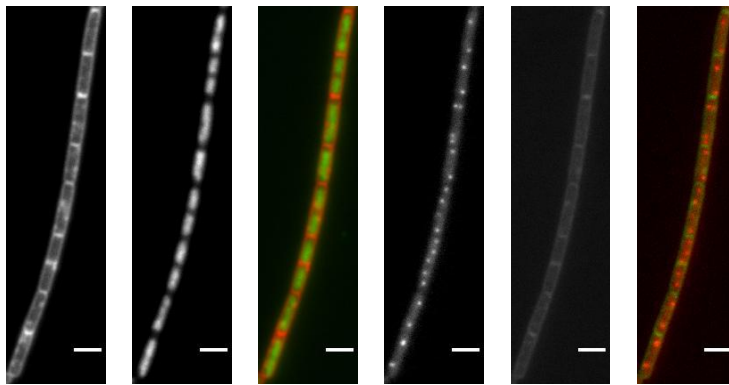
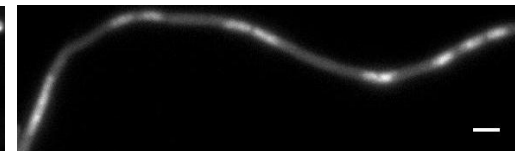
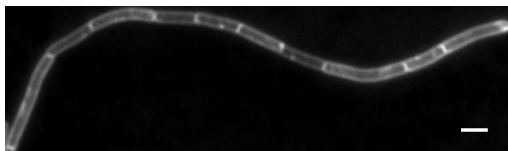


**Fig. 3.9.8.2.:** Fluorescence microscopy of *B. subtilis* strain PY79-YFP-DnaAR387C grown in S750 minimal medium (supplemented with glucose) until exponential growth at 30°C. A, membrane. B, DNA (nucleoids). C, overlay of membrane (red) and DNA (green). D, origins of replication (*oriC*-CFP). E, YFP-DnaAR387C. F, overlay of *oriC*-CFP (red) and YFP-DnaAR387C (green). White bar: 2  $\mu\text{m}$ .

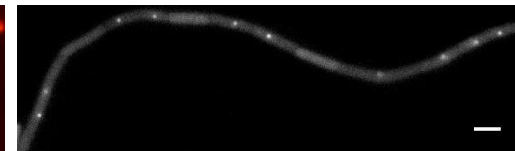
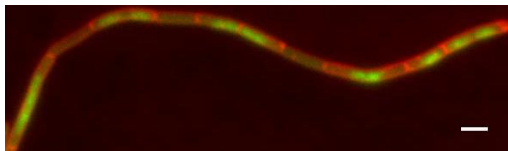
[A] membrane

[B] DNA



[C] merge

[D] *oriC*



[E] DnaAR387C

[F] merge

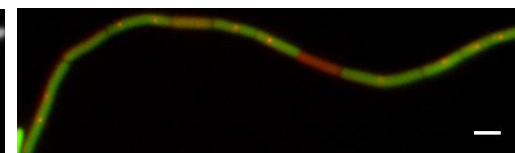


**Fig. 3.9.8.3.:** Fluorescence microscopy of *B. subtilis* strain PY79-YFP-DnaAR387C grown in S750 minimal medium (supplemented with xylose) until exponential growth at 30°C. A, membrane. B, DNA (nucleoids). C, overlay of membrane (red) and DNA (green). D, origins of replication (*oriC*-CFP). E, YFP-DnaAR387C. F, overlay of *oriC*-CFP (red) and YFP-DnaAR387C (green). White bar: 2  $\mu\text{m}$ .

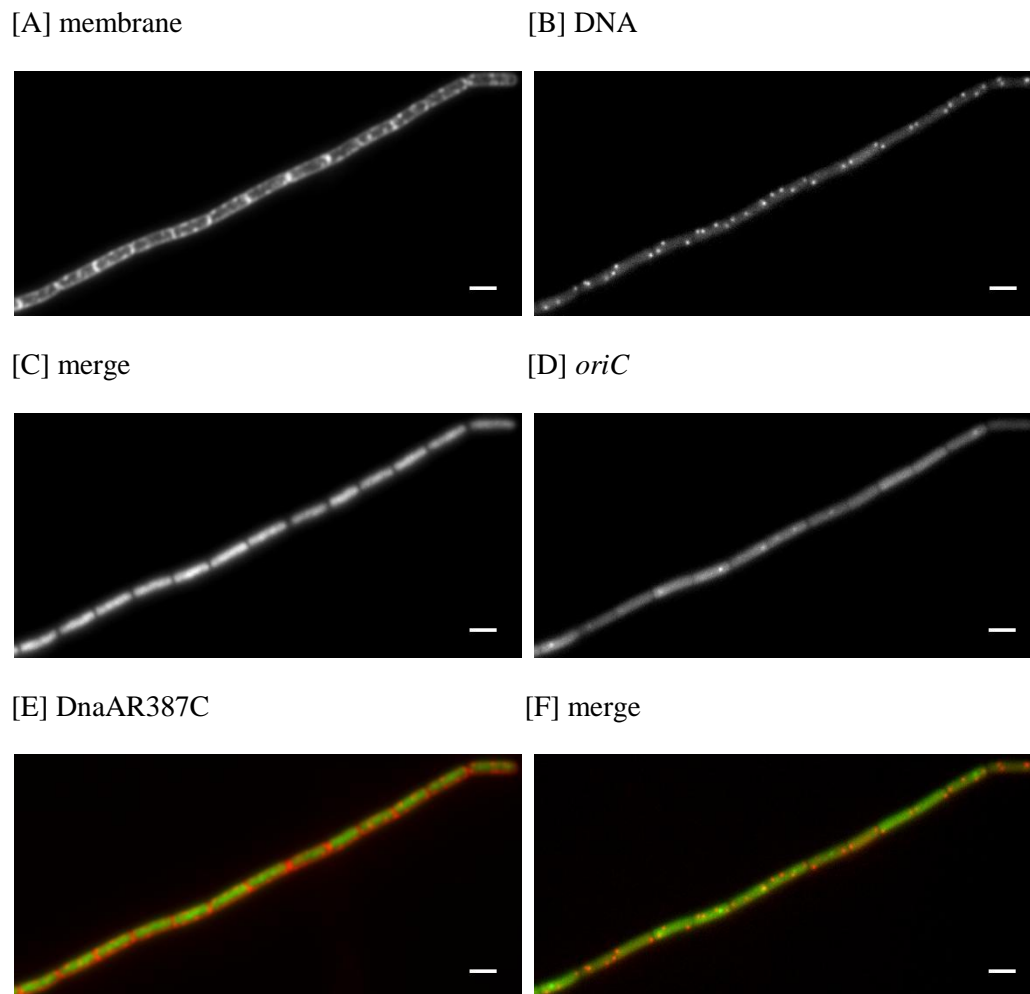


**Fig. 3.9.8.4.:** Fluorescence microscopy of *B. subtilis* strain PY79-YFP-DnaAR387C grown in S750 minimal medium (supplemented with xylose for 60 min after entering exponential growth phase) at 30°C. A, membrane. B, DNA (nucleoids). C, overlay of membrane (red) and DNA (green). D, origins of replication (*oriC*-CFP). E, YFP-DnaAR387C. F, overlay of *oriC*-CFP (red) and YFP-DnaAR387C (green). White bar: 2  $\mu$ m.

## DISCUSSION

---

## 4. Discussion

Specific DnaA activities, such as ATP-binding and hydrolysis, oligomerization and DNA-binding, their implications and interdependencies in the initiation of replication of *Bacillus subtilis* were investigated both *in vitro* and *in vivo* by generating several DnaA mutants, each carrying single substitutions of highly conserved amino acids. It was of particular interest to understand how ATP-binding and ATP-hydrolysis are involved in pre-RC assembly in *B. subtilis*. The principal hypothesis of this work was the functional requirement of ATP-hydrolysis for cooperative multimerization of DnaA protomers in order to efficiently bind to *oriC* prior to duplex unwinding. This would contrast the mode of operation of DnaA in *E. coli* where ATP-hydrolysis is induced to disassemble an established multimer and would indeed support the assumption according to which the initiation of replication occurs differently in Gram positive and Gram negative bacteria [1, 4, 33-34].

### 4.1. Recapitulatory overview

|   | wtDnaA   | DnaAD214N   | DnaAE183Q  | DnaAR260A  | DnaAW8A  | DnaAR387C   | DnaAA163V   |
|---|--|---|--|--|--|---|---|
| <b>ATP-binding activity</b>   | very strong temperature independent ATP-binding activity | 10-fold reduced ATP-binding activity                          | 2-fold reduced ATP-binding activity  | 1,5-fold reduced ATP-binding activity  | very strong temperature independent ATP-binding activity         | very strong temperature independent ATP-binding activity  | ATP-binding deficient                                 |
| <b>ATPase activity</b>  | weak temperature dependent ATPase activity               | ATPase deficient  | 6-7-fold reduced ATPase activity   | 2-fold reduced ATPase activity   | weak temperature dependent ATPase activity                       | weak temperature dependent ATPase activity                | ATPase deficient                                      |
| <b>DNA-binding activity</b>   | ATP-dependent differential DNA-binding activity          | ATP-independent DNA-binding activity                          | ATP-independent DNA-binding activity   | ATP-dependent differential DNA-binding activity                                | ATP-dependent differential DNA-binding activity                  | DNA-binding deficient                                     | ATP-independent DNA-binding activity                  |
| <b>Native constitution</b>  | dimer/trimer   | dimer/trimer  | dimer/trimer   | dimer/trimer   | monomer  | dimer/trimer  | constitutive multimer (> 600 kDa)                     |
| <b>Oligomerization capacity</b>   | ATP-dependent oligomerization (HMWC, > 300 kDa)          | reduced oligomerization capacity                              | reduced oligomerization capacity   | ATP-dependent oligomerization (HMWC, > 300 kDa)                                | ATP-dependent oligomerization (HMWC, > 300 kDa)                  | ATP-dependent oligomerization (HMWC, > 300 kDa)           | constitutive multimer (> 600 kDa)                     |
| <b>DNA-binding proficient multimers</b>   | DNA-binding proficient multimers                         | reduced multimeric DNA-binding                                | reduced multimeric DNA-binding   | DNA-binding proficient multimers   | DNA-binding deficient multimers                                  | DNA-binding deficient multimers                           | DNA-binding proficient multimers                      |
| <b><i>dnaA-dnaN</i> (transcriptional regulation)</b>                                | active transcriptional regulation of <i>dnaA-dnaN</i>    | active transcriptional regulation of <i>dnaA-dnaN</i>         | could not clearly be demonstrated  | active transcriptional regulation of <i>dnaA-dnaN</i>                          | active transcriptional regulation of <i>dnaA-dnaN</i>            | inactive transcriptional regulation of <i>dnaA-dnaN</i>   | active transcriptional regulation of <i>dnaA-dnaN</i> |
| <b>Morphology/ cell length (moderate ectopic expression in S750 minimal medium)</b> | normal<br>2-3µm (~60%)<br>1-2 µm (~20%)<br>> 3 µm (~20%) | slightly elongated<br>> 3 µm (~70%)<br>≤ 3 µm (~30%)          | elongated<br>> 3 µm (~80%)<br>≤ 3 µm (~20%)  | small<br>1-2 µm (~60%)<br>2-3 µm (~40%)  | normal<br>2-3µm (~60%)<br>1-2 µm (~30%)<br>> 3 µm (~10%)         | normal<br>2-3 µm (~50%)<br>1-2 µm (~15%)<br>> 3 µm (~35%) | elongated<br>> 3 µm (~80%)<br>≤ 3 µm (~20%)           |
| <b>Frequency of initiation (moderate ectopic expression in S750 minimal medium)</b> | normal<br>2 <i>oriC</i> (~70%)<br>4 <i>oriC</i> (~10%)   | increased<br>≥ 4 <i>oriC</i> (~60%)<br>< 4 <i>oriC</i> (~40%) | slightly increased<br>2 <i>oriC</i> (~35%)<br>4 <i>oriC</i> (~25%)<br>3 <i>oriC</i> (~20%) | normal<br>2 <i>oriC</i> (~60%)<br>3 <i>oriC</i> (~15%)<br>4 <i>oriC</i> (~10%) | slightly reduced<br>2 <i>oriC</i> (~70%)<br>1 <i>oriC</i> (~15%) | normal<br>2 <i>oriC</i> (~70%)<br>4 <i>oriC</i> (~15%)    | strongly increased<br>≥ 4 <i>oriC</i> (~90%)          |

**Table 4.1.:** Overview of the properties of *B. subtilis* wt/mutDnaA investigated in this work.

#### 4.2. *B. subtilis* wild type DnaA characteristics

*B. subtilis* (His)<sub>6</sub>-wtDnaA displays a very strong temperature independent ATP-binding activity, but a rather weak intrinsic ATPase activity (see chapters 3.3.1. and 3.4.1.). Furthermore, (His)<sub>6</sub>-wtDnaA binds sequence specifically to DnaA-box containing double-stranded DNA with a cofactor (ATP) dependent affinity and capacity (see chapter 3.5.1.). DSS crosslinking assays indicated that (His)<sub>6</sub>-wtDnaA multimerizes in the presence of ATP constituting high-molecular weight complexes far bigger than 300 kDa, whereas ATP-free conditions lead to homo-dimer and homo-trimer formation (see chapter 3.6.1.). Nonetheless, self-multimerization of (His)<sub>6</sub>-wtDnaA seems to be slightly stimulated by *oriC*-DNA. *In vivo* experiments with ectopically encoded N-terminal YFP-fusions of wild type DnaA in *B. subtilis* domestic strain PY79 clearly showed that strong ectopic expression of this construct leads to a significant growth delay, which is probably due to stopped replication as a consequence of a lack of DnaN (see chapters 3.7. and 3.8.1.). This is consistent with previously published results according to which increasing DnaA levels lead to blocked replication and induction of the SOS response, suggesting that the ectopically encoded construct is fully functional [9]. Since *dnaA-dnaN* transcription is regulated by DnaA protein, overexpressed (YFP-)DnaA down regulates the expression of the operon, which results in highly decreased DnaN levels [8-9]. DnaN is essential for replication elongation, since it represents the sliding-clamp of DNA-polymerase III [8-9]. Moderate ectopic expression of YFP-wtDnaA (~3-fold) *in vivo* does not interfere with the transcriptional regulation of *dnaA-dnaN*, since equal amounts, compared to non-induced conditions, of the original wild type DnaA were still measurable. On the contrary, maximal expression of YFP-wtDnaA (~6-fold) consequently represses *dnaA-dnaN* transcription, since no signal of DnaA was detectable any longer. In addition to this, under conditions of maximal repression or moderate ectopic expression of YFP-wtDnaA, microscopically monitored parameters, such as cell length, number of nucleoids and origins per cell of *B. subtilis* strain PY79-YFP-wtDnaA were similar to PY79-*oriC*-CFP (see chapters 3.9.1. and 3.9.2.). Maximal induction of the ectopically encoded construct severely interferes with the regulation of the cell cycle, similar to the previously published data [9]. Cells showed a strongly filamentous phenotype without replicating their chromosomes. Most of the cells contained only one nucleoid (~70%) and an important number of cells were anucleate (~20%). The reduction of the frequency of initiation of replication was confirmed by a significant decrease of the number of *oriC*-CFP foci per cell. Nevertheless, the distribution of YFP-wtDnaA foci was similar to moderate expression levels, though beyond, high protein accumulation could be detected as diffuse fluorescence distributed in the cytoplasm.

### 4.3. ATP-binding and ATPase deficient DnaAD214N

In agreement to *E. coli* DnaAD235N, its *B. subtilis* analogue (His)<sub>6</sub>-DnaAD214N binds very poorly to ATP and has a fully abrogated ATPase activity (see chapters 3.3.2. and 3.4.2.) [95]. As a consequence, (His)<sub>6</sub>-DnaAD214N displays a strongly reduced cofactor (ATP) dependent differential affinity to *oriC*-DNA (see chapter 3.5.5.). SPR experiments showed that binding of (His)<sub>6</sub>-DnaAD214N to *oriC*-DNA reaches a maximal response corresponding to 1.3-fold (without ATP) and 2-fold (with ATP) higher values than for (His)<sub>6</sub>-wtDnaA in the absence of ATP. Though, it seemed contradictory that the DNA-binding capacity of an ATP-binding mutant was modified by ATP, but this effect might result from the very weak residual ATP-binding capacity of (His)<sub>6</sub>-DnaAD214N at 25°C. However, (His)<sub>6</sub>-DnaAD214N has a reduced capacity in constituting stable higher-order multimers (see chapter 3.6.4.). Since (His)<sub>6</sub>-wtDnaA establishes high-molecular weight complexes only in the presence of ATP, it was not surprising that the self-multimerization of (His)<sub>6</sub>-DnaAD214N was affected. (His)<sub>6</sub>-DnaAD214N forms dimeric and trimeric structures in the absence of ATP, which are more pronounced in the presence of ATP, but higher-order structures were evident in only low amounts. These results are highly consistent with the specific DNA-binding activity of (His)<sub>6</sub>-DnaAD214N, according to which (His)<sub>6</sub>-DnaAD214N displays a slightly increased capacity to bind *oriC*-DNA in the presence of ATP, probably as a result of residual ATP-binding. Moreover, EMSA experiments indicated that binding to linear *oriC*-DNA occurs in multimeric constitutions, but very high protein concentrations were required to detect DNA-binding competent high-molecular weight complexes of (His)<sub>6</sub>-DnaAD214N, suggesting that the low amount of established multimers were still functional. In support of this, overexpression of YFP-DnaAD214N outcompeted DnaA in regulating *dnaA-dnaN* transcription *in vivo* (see chapter 3.8.2.). In addition to this, under non-induced conditions, PY79-YFP-DnaAD214N displayed a significant reduction of growth, which was furthermore strongly reduced when fully expressed (see chapter 3.7.). Intriguingly, this growth defect was more pronounced than the effect of overexpressed YFP-wtDnaA, but can probably again be attributed to stopped replication due to repressed DnaN expression, indicating that transcriptional regulation could still be maintained. Microscopical analyses revealed, that *B. subtilis* PY79-YFP-DnaAD214N displays an increased replication initiation frequency (see chapter 3.9.4.). Under conditions of maximal repression or moderate ectopic expression of YFP-DnaAD214N cells were slightly elongated compared to PY79-YFP-wtDnaA with generally one nucleoid. Maximal induction of the construct led to repression of the *dnaA-dnaN* operon, but strikingly had more severe consequences than overexpression of YFP-wtDnaA. Blocked replication in PY79-YFP-DnaAD214N resulted in ~50% anucleate cells. This massive effect could be explained by an additional control defect at the level of transcriptional regulation of genes containing *dnaA*-boxes in their promoter. It is probable that the activity of DnaA as a transcription factor is regulated through binding to differentially

organized DnaA-boxes in the promoter regions of the respective genes. Thus, ATP-binding deficient YFP-DnaAD214N could bind to very abundant high-affinity boxes in the promoter region of the *dnaA-dnaN* operon, but could fail to respond to others lacking those high-affinity boxes, since YFP-DnaAD214N would be insensitive for low-affinity sites, such that those genes would not be properly transcribed. The increased initiation frequency provoked by moderately expressed YFP-DnaAD214N could result from the inability to respond to regulation mechanisms. However, YFP-DnaAD214N has been shown to display a very low capacity to multimerize and, thus, to bind efficiently to *oriC*-DNA *in vitro*. Hence, it cannot be excluded that this incompatibility of limited initiation potential and observed overinitiation could also be due to spontaneous suppressor mutations bypassing a possibly lethal phenotype.

#### 4.4. ATPase deficient DnaAE183Q

(His)<sub>6</sub>-DnaAE183Q shows an approximately 2-fold reduced ATP-binding capacity, whereas its ATPase activity is decreased between 6-7-fold compared to (His)<sub>6</sub>-wtDnaA levels (see chapter 3.3.3. and 3.4.3.). Furthermore, (His)<sub>6</sub>-DnaAE183Q displays a strongly reduced cofactor-dependent differential DNA-binding capacity similar to (His)<sub>6</sub>-DnaAD214N (see chapter 3.5.4.). Intriguingly, in sharp contrast to (His)<sub>6</sub>-wtDnaA the DNA-shifting of (His)<sub>6</sub>-DnaAE183Q in EMSA experiments occurred in two phases whereby a considerable amount of the DNA was retained by an intermediate complex in the middle of the gel within a broad range of protein concentrations, while the remaining DNA was further shifted, suggesting that (His)<sub>6</sub>-DnaAE183Q constitutes two different major DNA-binding competent complexes. Another difference when compared to (His)<sub>6</sub>-wtDnaA was the capacity of (His)<sub>6</sub>-DnaAE183Q to shift DNA as a high-molecular weight complex only at very high protein concentrations. Together with the observation that the apparent binding constant of (His)<sub>6</sub>-DnaAE183Q was rather similar to the respective  $K_{app}$  of (His)<sub>6</sub>-wtDnaA, this suggests that not DNA-affinity but the DNA-binding stability of (His)<sub>6</sub>-DnaAE183Q through affected cooperative multimerization is rather low. SPR experiments of (His)<sub>6</sub>-DnaAE183Q clearly showed that the binding characteristics to *oriC*-DNA in the absence of ATP, including affinity, saturation levels and dissociation rates were similar to those of (His)<sub>6</sub>-wtDnaA. But strikingly, in the presence of ATP the response was nearly identical. Intermediate and high-molecular weight complex formation, as observed in EMSA, probably occurred during the rather long incubation time of protein and DNA, but was not detectable in real-time SPR measurements. Given the fact that the ATP-binding capacity of (His)<sub>6</sub>-DnaAE183Q is approximately 2-fold reduced compared to (His)<sub>6</sub>-wtDnaA, a certain reduction in the response to *oriC*-DNA could be explained, but it seemed rather unlikely to assign the abrogated cofactor-dependent differential *oriC*-DNA-binding activity to a reduction of the ATP-binding capacity. One could speculate that the reason for this unexpected DNA-

binding response is due to the strongly reduced ATPase activity. If one would assume, unlike in *E. coli* where ATP-hydrolysis is induced to disassemble an established multimer, that cooperative multimerization, essential for efficient DNA-binding, requires individual ATP-hydrolysis events of the protomers, the ATPase activity would play a key role in providing initiation potential in *B. subtilis* cells. In support of this hypothesis, (His)<sub>6</sub>-DnaAE183Q does not constitute stable higher-order multimers (see chapter 3.6.3.). The multimeric structure of (His)<sub>6</sub>-DnaAE183Q is indistinguishable from (His)<sub>6</sub>-wtDnaA in ATP-free conditions. Hence, (His)<sub>6</sub>-DnaAE183Q adopts dimeric and trimeric constitutions and homo-pentamer formation could slightly be stimulated by linear *oriC*-DNA. This is consistent with the similar DNA-binding behavior of both proteins measured with SPR. Remarkably, in the presence of ATP the self-multimerization capacity of (His)<sub>6</sub>-DnaAE183Q was drastically reduced, i.e. no higher-molecular weight complexes bigger than 300 kDa were detectable. Moreover, mostly in all experiments, signals detected above 200 kDa (approximately corresponding to (His)<sub>6</sub>-DnaAE183Q tetramers) appeared as a pronounced smear, suggesting unstable multimeric structures, an indication for a decreased self-multimerization capacity of (His)<sub>6</sub>-DnaAE183Q. *B. subtilis* strain PY79-YFP-DnaAE183Q has a strong growth defect and does not enter exponential growth (see chapter 3.7.). The maximal doubling time of approximately 90 minutes was achieved independently of the presence of glucose or xylose in the medium. This effect suggests a dominant negative effect of equal amounts of YFP-DnaAE183Q over DnaA in the presence of glucose. In addition to this, either the amount of ectopically expressed YFP-DnaAE183Q is not sufficient or the protein itself is mechanistically inactive to repress transcription of the *dnaA-dnaN* operon (see chapter 3.8.3.). The expression level of YFP-DnaAE183Q *in vivo* suggests that only a certain amount of this protein is tolerated. The quantities of YFP-DnaAE183Q of cells grown in xylose and those induced with xylose for only 60 minutes were rather similar, indicating that higher protein levels would be lethal. Furthermore, PY79-YFP-DnaAE183Q displayed a strong phenotypic effect in cell morphology, i.e. cells were notably filamentous (see chapter 3.9.7.). It was not surprising that maximal induction of YFP-DnaAE183Q did not lead to strong cell cycle malfunctions and replication blocks, which could be indicative as an important increase of anucleate cells, since PY79-YFP-DnaAE183Q did not tolerate high cellular levels of YFP-DnaAE183Q that would result in the repression of the *dnaA-dnaN* operon. These results are strongly supportive to the theory that the mode of operation of the initiation of replication in Gram positive bacteria indeed differs from that in Gram negative bacteria, such as in *E. coli*. In agreement to this, it has previously been published that pre-RC formation in *Mycobacterium tuberculosis*, and not inactivation of a functional pre-RC, requires ATP-hydrolysis [76-77]. More detailed, these studies suggest an implication of both ATP-binding and ATP-hydrolysis in efficient cooperative binding and multimerization of DnaA at the origin [76]. A DnaA mutant protein unable to hydrolyze ATP

does not associate on *oriC* as fast as wild type DnaA *in vitro* and its expression is lethal for replicating cells [76]. The ATPase activity is stimulated by supercoiled DNA-templates independently of the presence of specific DnaA binding sites [77]. Moreover, DnaA bound to the non-hydrolyzable ATP analogue ATP $\gamma$ S is deficient in open complex formation *in vitro* [77]. Thus, ATP-hydrolysis is mechanistically required for pre-RC formation in *M. tuberculosis* which lies in sharp contrast to the molecular mode of operation of *E. coli* DnaA that can still assemble a functional pre-RC when associated with ATP $\gamma$ S [24, 77]. Nevertheless, it has very recently been shown that an ATPase deficient mutant of the Gram negative *Caulobacter crescentus* provoked overinitiation and exceptional cell filamentation due to blocked cell division [100]. Thus, the overinitiation phenotype resulted from the inability of inactivation of this mutant protein, indicating a similar functionality like *E. coli* DnaA [100]. However, it could be demonstrated that strong cell elongation was an indirect consequence of misregulation of the activity of DnaA as a transcription factor, i.e. the authors proposed that DnaA activity is not only controlled in its function of an initiation factor but also of a transcription factor on the level of ATP-hydrolysis [100].

#### 4.5. Prematurely initiating DnaAR260A

(His)<sub>6</sub>-DnaAR260A displays a 2-fold decreased ATPase activity and a reduced ATP-binding capacity that varies between 1.3-fold and 1.7-fold lower (dependent on the type of assay) compared to (His)<sub>6</sub>-wtDnaA (see chapter 3.3.3. and 3.4.3.). This effect can be explained with the local position of the amino acid substitution that resides within DnaA domain III, which is predicted to contain all AAA+ motifs including Walker type motifs, the ATP-sensor and arginine finger for ATP-dependent self-oligomerization of DnaA [7, 74, 98]. However, a reduced binding affinity or capacity has not been reported for its *E. coli* analogue mutant DnaAR281A [74, 98]. Furthermore, (His)<sub>6</sub>-DnaAR260A exhibits a cofactor-dependent DNA-binding activity (see chapter 3.5.6.). SPR analyses showed that (His)<sub>6</sub>-DnaAR260A binds in the absence of ATP to surface bound *oriC*-DNA in a (His)<sub>6</sub>-DnaAD214N like manner. Though, in the presence of ATP (His)<sub>6</sub>-DnaAR260A reached maximum binding values that are 1.5-fold reduced compared to (His)<sub>6</sub>-wtDnaA. Since (His)<sub>6</sub>-DnaAR260A has an approximately 1.5-fold reduced ATP-binding capacity and 2-fold reduced ATPase activity, whereas (His)<sub>6</sub>-DnaAD214N displays a strongly reduced ATP-binding and ATPase activity one could assume, that the respective differences of both proteins in their DNA-binding characteristics might result either from their differing ATP-binding or ATPase capacities. In addition to this, the self-multimerization activity of (His)<sub>6</sub>-DnaAR260A is not affected, i.e. the ATP-dependent formation of multimers, both low- and high-molecular weight structures occurred in a (His)<sub>6</sub>-wtDnaA-like manner (see chapter 3.6.5.). Moreover, linear *oriC*-DNA stimulated

pentamerization of (His)<sub>6</sub>-DnaAR260A. Strikingly, *E. coli* DnaAR281A is proposed to be initiation deficient, both *in vivo* and *in vitro* due to failure of establishing stable multimers on *oriC* [74]. It was shown that DnaAR281A was proficient in open complex formation, but it has been postulated that the nucleoprotein-complex on *oriC* failed to recruit DnaB helicase [74]. Nevertheless, if this assumption is correct, this would lead to an altered DNA-binding activity of DnaAR281A to *oriC*-DNA. Since no such defects could be observed by EMSA, the authors argued that the proposed unstable protein-DNA complex would be stabilized by the caging effect of polyacrylamide gels [74]. However, exponential growth of PY79-YFP-DnaAR260A appeared to be unaffected under non-induced conditions (see chapter 3.7.). Shortly after reaching stationary phase, when grown in glucose supplemented LB-medium, the optical density decayed, suggesting that the constitutively expressed low amounts of YFP-DnaAR260A interfere with the regulation of replication with severe consequences for stationary phase conditions. Moreover, maximal induction of the construct led to a strong growth defect, which was more pronounced than the effect of overexpressed YFP-wtDnaA. Under these conditions, the abundance of YFP-DnaAR260A outcompeted DnaA in regulating *dnaA-dnaN* transcription *in vivo*, suggesting that the reduced DNA-binding activity *in vitro* does not affect the cellular interaction of YFP-DnaAR260A with double-stranded genomic DNA (see chapter 3.8.2.). Fluorescence microscopy data indicate that *B. subtilis* strain PY79-YFP-DnaAR260A does not show any significant differences compared to PY79-YFP-wtDnaA when grown in glucose containing minimal medium (see chapter 3.9.5.). Under conditions of moderate ectopic expression of YFP-DnaAR260A the observed cells were considerably smaller (~60% of all cells were 1-2  $\mu\text{m}$  long), suggesting premature initiation of replication and/or cell division. However, the frequency distribution of the number of nucleoids and origins was nearly identical to non-induced conditions. Maximal induction of the construct led to repression of the *dnaA-dnaN* operon, which had severe consequences on the cell cycle similar to PY79-YFP-DnaAD214N. Blocked replication resulted in elongated cells, out of which ~60% were anucleate, while the other fraction of cells mostly contained one condensed nucleoid, one *oriC*-CFP focus per cell and a highly variable number of YFP-DnaAR260A foci, which in some cases localized as an arranged helical pattern in the cell membrane. Since principally all biochemically analyzed properties of (His)<sub>6</sub>-DnaAR260A were similar to (His)<sub>6</sub>-wtDnaA, except for a reduction in its DNA-binding activity in the presence of ATP, one might speculate that premature initiation results from a deficiency in responding to a yet unknown cell cycle regulating factor that connects the initiation of replication and cell division. Unpublished data suggest that this function could be exerted by YabA. YabA has been shown to negatively regulate initiation during replication by inhibiting DnaA multimerization at *oriC* that would lead to pre-RC formation [10, 40, 52]. Furthermore, YabA is able to titrate an important number of DnaA molecules to the replication machinery at midcell during ongoing replication, since YabA

defective mutants lead to diffuse YFP-DnaA signals that are distributed all over the cytoplasm [10, 52]. Tandem affinity purification experiments with YabA performed to determine interaction partners led to the identification of the ATPase MinD (data not shown). MinD acts together with MinC (MinCD complex) in order to inhibit cell division by blocking FtsZ-ring formation [101]. If one would assume that YabA negatively influences MinCD, the disassembly of the replication machinery after terminated chromosomal replication would lead to the dissociation of previously complexed YabA, which could allow to negatively regulate MinCD, thus derepressing FtsZ polymerization. Premature initiation as a consequence of moderate YFP-DnaAR260A expression could therefore result from a labile interaction with YabA. Wild type DnaA is diluted out by the expression of YFP-DnaAR260A, because the ectopically expressed mutant DnaA represses the original *dnaA* promoter. The strikingly severe effect of YFP-DnaAR260A overexpression, similar to YFP-DnaAD214N, could again be explained by a possible deficiency at the level of transcriptional regulation of genes containing low-affinity *dnaA*-boxes in their promoter.

#### 4.6. Conditionally dimerization deficient DnaAW8A

(His)<sub>6</sub>-DnaAW8A is not significantly affected either in its ATP-binding nor its ATPase activity (see chapters 3.3.4. and 3.4.4.). This was perfectly consistent, since this point mutation is located in DnaA domain I, which does not contain any specific motifs responsible for ATP-binding or hydrolysis [70]. EMSA experiments with (His)<sub>6</sub>-DnaAW8A showed that the protein was still able to bind double-stranded linear *oriC*-DNA, both in the presence and absence of ATP (see chapter 3.5.7.). Strikingly, the detected protein-DNA complexes had a significantly lower molecular weight than those constituted with (His)<sub>6</sub>-wtDnaA. This suggests that the presumed dimerization deficiency of (His)<sub>6</sub>-DnaAW8A affects severely the cooperative multimerization capacity of DnaA that is predicted to be located in the AAA+ domain III, which in turn seems to be required for efficient sequence specific DNA interaction with DnaA domain IV. In agreement to this assumption, SPR data of (His)<sub>6</sub>-DnaAW8A binding to *oriC*-DNA clearly showed a strongly reduced response, both in the presence and absence of ATP when compared to (His)<sub>6</sub>-wtDnaA. This effect could not be attributed to a limited ability of binding or hydrolyzing ATP since both activities were fully functional. In spite of a significant increase of the affinity to *oriC*-DNA and a more efficient dissociation from the DNA in the presence of ATP, (His)<sub>6</sub>-DnaAW8A seems to be importantly affected in its self-multimerization dependent specific DNA-binding activity. This is consistent with the observation that (His)<sub>6</sub>-DnaAW8A displays a conditional dimerization deficiency in the absence of ATP (see chapter 3.6.6.). Under ATP-free conditions, (His)<sub>6</sub>-DnaAW8A could be detected almost exclusively as a monomer, whereas (His)<sub>6</sub>-wtDnaA adopted dimeric and trimeric forms. A very small protein fraction of

(His)<sub>6</sub>-DnaAW8A was detectable as homo-dimers and homo-trimers. However, dimerization and formation of high-molecular weight complexes could be maintained in the presence of ATP. Surprisingly, linear *oriC*-DNA might stimulate both dimerization and self-multimerization, even at high salt concentrations, but these established multimers were not competent in efficiently binding to *oriC*-DNA, suggesting that domain I mediated dimerization of two *B. subtilis* DnaA protomers is required for coordinated domain III interactions leading to functionally initiation proficient multimers. Nevertheless, overexpression of YFP-DnaAW8A could still outcompete DnaA in regulating *dnaA-dnaN* transcription, which indicates that DNA interaction with promoter regions does not require self-multimerization of DnaA in *B. subtilis* (see chapter 3.8.2.). It is interesting to notice, that in contrast to *B. subtilis*, *E. coli* DnaA autoregulation requires multimeric structures for interactions with the DnaA promoter region [69, 102]. In addition to this, a competition assay between DnaAW6A (*E. coli* analogue of DnaAW8A) and DnaA revealed that the mutant protein was unable to interact with DnaA, and finally did not lead to a significant reduction in initiation [70]. Fluorescence microscopy revealed that *B. subtilis* strain PY79-YFP-DnaAW8A did not show any significant differences in cell length, nucleoid distribution and initiation frequency compared to PY79-YFP-wtDnaA when grown in glucose containing minimal medium (see chapter 3.9.6.). Moderate ectopic expression of YFP-DnaAW8A, except for a slightly reduced initiation frequency, did not lead to any significant differences of the observed parameters compared to maximal repression of the construct, but strikingly no YFP-DnaAW8A foci could be observed, indicating that no stable multimers can be established *in vivo*. Full induction of the construct consequently down regulates *dnaA-dnaN* transcription, resulting in blocked replication. The effects on PY79-YFP-DnaAW8A were similar to PY79-YFP-DnaAD214N and appeared to be more severe than in PY79-YFP-wtDnaA. Blocked replication resulted in elongated cells, out of which ~50% were anucleate, while the other fraction of cells mostly contained one condensed nucleoid and one *oriC*-CFP focus and either no YFP-DnaAW8A focus (~60%), one focus (~10%) or two foci (~20%) per cell, which appeared to be rather diffuse since the fluorescence was distributed mainly all over the cytoplasm, probably as a consequence of the inability to establish initiation competent multimeric structures at *oriC*. Its *E. coli* analogue DnaAW6A has also been shown to be defective in the interaction of two DnaA-protomers via their respective domain I [6, 70]. Additionally, tryptophane 6 plays a key role in helicase recruitment to the open complex [6, 70]. Nevertheless, it was also shown that DnaAW6A was not principally affected in DnaB loading or sequence-specific binding to DnaA-box containing DNA, since both activities were functional in the presence of single-stranded DNA, but abrogated with supercoiled duplex *oriC*-DNA [70].

## 4.7. DNA-binding deficient DnaAR387C

(His)<sub>6</sub>-DnaAR387C is neither significantly affected in its ATP-binding nor its ATPase activity (see chapter 3.3.4 and 3.4.4.). Nevertheless, (His)<sub>6</sub>-DnaAR387C displays a strongly reduced DNA-binding activity (see chapter 3.5.2.). This binding activity to specific *oriC*-DNA resembled strongly to that one of (His)<sub>6</sub>-wtDnaA incubated with nonspecific DNA. Similar to this protein-DNA interaction a weak shifting of *oriC*-DNA by (His)<sub>6</sub>-DnaAR387C in EMSA experiments could be observed, suggesting that a small amount of unstable transient binding events occurred. This indicates that probably only monomeric or dimeric, but not multimeric (His)<sub>6</sub>-DnaAR387C can still bind *oriC*-DNA, but with a strongly reduced affinity to DNA. SPR experiments, performed in order to study the low affinity and the real-time binding events of (His)<sub>6</sub>-DnaAR387C did not show any interaction of the protein to the sensor chip bound DNA beyond background levels, independently of the presence or absence of ATP. Furthermore, DSS crosslinking assays indicate that multimer formation of (His)<sub>6</sub>-DnaAR387C is irresponsive to linear *oriC*-DNA (see chapter 3.6.7.). (His)<sub>6</sub>-DnaAR387C self-multimerizes in an ATP-dependent manner similar to (His)<sub>6</sub>-wtDnaA. In the absence of ATP (His)<sub>6</sub>-DnaAR387C dimerized or adopted trimeric structures, whereas ATP availability immediately led to the formation of multimeric structures. Strikingly, in contrast to (His)<sub>6</sub>-wtDnaA, *oriC*-DNA did not stimulate self-multimerization of (His)<sub>6</sub>-DnaAR387C. The constituted multimers in the presence of ATP, analogous to (His)<sub>6</sub>-DnaAW8A, did not bind to *oriC*-DNA. Hence, high-molecular weight complexes of (His)<sub>6</sub>-DnaAR387C would fail to initiate chromosomal replication *in vivo*, since only lower-multimeric constitutions are somewhat DNA-binding proficient, but which in turn would be insufficient for a functional pre-RC assembly. Nevertheless, under non-induced conditions, growth of *B. subtilis* strain PY79-YFP-DnaAR387C were nearly similar with PY79, whereas continuous induction resulted in slightly reduced growth, suggesting that *B. subtilis* is not severely affected by the presence of high quantities of this ectopically expressed mutant protein (see chapter 3.7.). As expected, overexpression of YFP-DnaAR387C did not interfere with the transcriptional regulation of *dnaA-dnaN* by DnaA (see chapter 3.8.4.). YFP-DnaAR387C cellular protein levels could be tolerated to a much higher degree than all other mutant DnaA proteins tested, and than YFP-wtDnaA itself, without leading to repression of *dnaA-dnaN* transcription. Fluorescence microscopy revealed that PY79-YFP-DnaAR387C did not show any significant differences in cell length, nucleoid distribution and initiation frequency compared to PY79-YFP-wtDnaA when grown in glucose containing medium. Moderate ectopic expression of YFP-DnaAR387C did not lead to any significant differences of the observed parameters compared to maximal repression of the construct, except for an increased number of YFP-DnaAR387C foci that did not colocalize with *oriC*-CFP foci. Full induction of the DNA-binding deficient construct did not down regulate *dnaA-dnaN* transcription, but, nevertheless, blocked replication was observed and resulted in elongated cells, out of which ~45% were

anucleate, while the other fraction of cells mostly contained one nucleoid, one *oriC*-CFP focus and no YFP-DnaAR387C focus, since the fluorescence was distributed mainly all over the cytoplasm. This replication block might be the consequence of titration of DnaA by YFP-DnaAR387C, since its multimerization capacity is not affected. If this assumption is correct, initiation competent DnaA-molecules would be complexed by the mutant protein and thereby restrained from interacting with *oriC*. Notably, YFP-DnaAR387C foci rarely colocalized with *oriC* *in vivo* confirming the biochemically demonstrated DNA-binding deficiency.

#### 4.8. Specific *B. subtilis* mutant DnaAA163V (“DnaAcos”)

*B. subtilis* (His)<sub>6</sub>-DnaAA163V neither binds nor hydrolyzes ATP (see chapters 3.3.2. and 3.4.2.), which is consistent with the fact that its *E. coli* DnaA counterpart DnaAA184V also does not show any significant ATP-binding or ATPase activity [79, 82]. In addition to this, (His)<sub>6</sub>-DnaAA163V exhibits an extremely stable cofactor (ATP) independent DNA-binding activity (see chapter 3.5.2.). SPR experiments revealed that (His)<sub>6</sub>-DnaAA163V strongly binds *oriC*-DNA, irrespective of the presence or absence of ATP, which is perfectly conclusive with its ATP-binding deficiency. Furthermore, no significant dissociation from the DNA could be observed once loading terminated, suggesting that the established protein-DNA interaction was highly stable. The fact that binding of (His)<sub>6</sub>-DnaAA163V to *oriC*-DNA occurred in a non-stepwise manner in EMSA (only one DNA-binding type of complex was formed) and the very strong protein accumulation measured by SPR in the absence of ATP highly indicates that high-molecular weight complexes of (His)<sub>6</sub>-DnaAA163V represent the only DNA-binding competent constitution of this mutant protein, whereas EMSA experiments showed that (His)<sub>6</sub>-wtDnaA binds *oriC*-DNA substrates in different multimeric constitutions (see chapter 3.5.1.). In support of this theory, DSS crosslinking assays in ATP-free conditions, but independently of specific DNA, revealed that (His)<sub>6</sub>-DnaAA163V constitutively forms stable high-molecular weight complexes (see chapter 3.6.2.). This was confirmed by size-exclusion chromatography and would explain why, even in the absence of ATP (His)<sub>6</sub>-DnaAA163V binds strongly to *oriC*-DNA. Surprisingly, ATP seems to interfere with the intrinsic capacity to form these high-molecular structures, so that monomeric, dimeric and trimeric structures could be detected by immunoblotting. Considering these crosslinking properties of (His)<sub>6</sub>-DnaAA163V one would have expected that binding or affinity to *oriC*-DNA is affected under ATP-containing conditions. But EMSA experiments and SPR measurements indicate that (His)<sub>6</sub>-DnaAA163V binds strongly and with similar affinities to *oriC*-DNA both in the presence and absence of ATP. Despite an obvious reduction in the capacity to establish high-molecular weight complexes, the detected smear suggests that even in the presence of ATP higher-order multimers are still formed, but with a strongly decreased efficiency. Since only a certain fraction

of (His)<sub>6</sub>-wtDnaA multimerized in the presence of ATP, this could partly explain, why no considerable change in the DNA-binding response of (His)<sub>6</sub>-DnaAA163V was measurable. Nevertheless, a constitutive multimeric constitution has previously been shown *in vitro* for DnaAA184V, the analogous *E. coli* mutant protein of (His)<sub>6</sub>-DnaAA163V, and thus the present results indeed support these propositions [79-80]. Moreover, *in vivo* experiments further strengthened the hypothesis according to which *B. subtilis* mutant DnaAA163V exhibit similar properties like *E. coli* DnaAA184V. PY79-YFP-DnaAA163V displayed a significant but slight decrease in growth with doubling times in exponential phase of approximately 60 minutes, both for induced and non-induced cells (see chapter 3.7.). This effect could be explained by a functionally partial dominant negative effect of equal amounts of YFP-DnaAA163V over DnaA in the presence of glucose, i.e. the mutant protein would mainly govern replication without interfering with the transcriptional regulation of the *dnaA-dnaN* operon by DnaA. However, overexpression of YFP-DnaAA163V outcompeted DnaA in regulating *dnaA-dnaN* transcription (see chapter 3.8.2.). Strikingly, *B. subtilis* strain PY79-YFP-DnaAA163V displayed a strong phenotypic effect in the frequency of initiation of replication (see chapter 3.9.3.). The observation that under conditions of maximal repression, hence growth in glucose containing medium, cells were already abnormally elongated, mostly contained one highly decondensed nucleoid and exhibited a strongly increased number of origins, suggest that YFP-DnaAA163V is dominant negative over chromosomally encoded DnaA. Moreover, this would explain why the observed effects of moderate ectopic expression or maximal expression of YFP-DnaAA163V did not significantly differ from non-induced conditions, except for a strongly increased number of YFP-DnaAA163V foci that mostly colocalized with *oriC*-CFP. It was surprising that the highly increased amount of YFP-DnaAA163V (under maximally induced conditions), which led to repression of the *dnaA-dnaN* operon, did not result in blocked replication as would have been expected as a consequence of reduced DnaN levels. On the contrary, PY79-YFP-DnaAA163V displayed a strong overinitiation phenotype, which is consistent with the fact that *E. coli* DnaAA184V also leads to hyperinitiation *in vivo* [79-80, 82]. However, it has been shown that the *E. coli* phenotype is due to DnaAA184V that is irresponsive to regulation mechanisms inactivating or titrating DnaA from *oriC* in order to prevent reinitiation of replication, such as RIDA and *datA* [80]. Nonetheless, these mechanisms do not exist in *B. subtilis*, which involves a different molecular basis for the effect of this mutation [1, 4]. Hence, this DnaA mutant strain is a perfect tool to investigate initiation control mechanisms in *B. subtilis*. Moreover, studies on Soj-mediated DnaA regulation revealed that the inhibition of replication initiation by a DNA-binding deficient Soj mutant (SojG12V) can be suppressed by spontaneous point mutations in *dnaA* leading to overinitiation. Among those, amino acid substitution H162Y has been identified, which lies adjacent to the corresponding

*dnaAcos* phenotype determining residue substitution A163V, but it remains to be investigated if this specific mutation indeed does also provoke hyperinitiation *in vivo* [53].

#### 4.9. Functional dissection and mechanistic implications of DnaA in the initiation of replication in *B. subtilis*

Taken together, the results of this work and their integration into the postulated theories about initiation of replication in *B. subtilis* led to the following model. An initiation competent cell needs to accumulate a threshold level of ATP-bound DnaA molecules, which is primarily achieved by *de novo* DnaA synthesis [4, 8-9, 38]. The expression of DnaA is autoregulated by a negative feedback loop, i.e. high DnaA levels repress *dnaA* transcription and low levels derepress *dnaA* transcription [8-9]. This control mechanism does not seem to require ATP-bound DnaA, since both ATP-binding defective mutant proteins (YFP-DnaAA163V, YFP-DnaAD214N) could still efficiently repress *dnaA* transcription *in vivo*. Nevertheless, the fact that ATPase mutant YFP-DnaAE183Q does not efficiently inhibit DnaA synthesis might result from the incapacity to bear up against high intracellular levels of this protein or from a blocked intramolecular switch in its transcriptional activity similar to a mechanism in *Caulobacter crescentus* [100]. Subsequently, DnaA molecules interact via their respective domain I to form native dimeric or trimeric constitutions, which has been shown for (His)<sub>6</sub>-wtDnaA and all other mutant forms, except (His)<sub>6</sub>-DnaAA163V and (His)<sub>6</sub>-DnaAW8A that imperatively establish constitutive multimers or monomers, respectively. Presumably, most of the DnaA protomers are present in a cofactor-bound state since they have an extremely high affinity to ATP [1, 11-12]. *B. subtilis oriC* contains several high-affinity boxes allowing ATP-DnaA interaction, which leads to the constitution of the bacterial ORC prior to self-multimerization dependent pre-RC formation [1, 8, 11-15]. It was clearly demonstrated that (His)<sub>6</sub>-DnaAW8A, despite its unaffected ATP-binding and ATPase activity, was unable to form DNA-binding proficient high-molecular weight complexes. Thus, it seems that domain I mediated dimerization of two *B. subtilis* DnaA protomers is required for coordinated AAA+ domain III interactions leading to functionally initiation competent multimers. Furthermore, it was shown that the abrogated cofactor-dependent differential *oriC*-DNA-binding activity of (His)<sub>6</sub>-DnaAE183Q could mainly be attributed to its strongly reduced ATPase activity. This led to the hypothesis that unlike in *E. coli* where ATP-hydrolysis is induced to disassemble an established multimer, cooperative multimerization, essential for efficient DNA-binding, requires individual ATP-hydrolysis events of the DnaA protomers. Hence, the ATPase activity would play a key role in providing initiation potential in *B. subtilis* cells. In support of this assumption, (His)<sub>6</sub>-DnaAE183Q does not constitute stable higher-order multimers and PY79 does not seem to tolerate high amounts of

YFP-DnaAE183Q *in vivo*. However, it has recently been shown that cooperative binding of DnaA to *oriC*-DNA is only partly affected in the presence of a non-hydrolyzable ATP analogue *in vitro* [40]. These results differ from the data presented above, but might be due to different experimental setups. Nevertheless, these suggestions imply possible regulation pathways of DnaA initiated chromosomal replication in *B. subtilis*. If the proposed mechanism of ATPase dependent multimerization indeed triggers pre-RC assembly, one could assume that both stimulatory and inhibitory factors would target the ATP-hydrolysis activity of DnaA. In agreement to this, Soj has been shown to be able to enhance or to repress DnaA activity [53-54]. Unpublished data indicate that Soj interacts with the AAA+ domain of DnaA and regulates its oligomerization capacity and consequently its active or inactive conformation. If the postulated mode of operation is correct, Soj interacts with the AAA+ domain of DnaA, blocks ATP-hydrolysis and consequently inhibits initiation proficient multimer formation.

## BIBLIOGRAPHY

---

## 5. Bibliography

1. Messer, W., *The bacterial replication initiator DnaA. DnaA and oriC, the bacterial mode to initiate DNA replication.* FEMS Microbiol Rev, 2002. **26**(4): p. 355-74.
2. Duderstadt, K.E., et al., *Origin remodeling and opening in bacteria rely on distinct assembly states of the DnaA initiator.* J Biol Chem, 2010. **285**(36): p. 28229-39.
3. Rozgaja, T.A., et al., *Two oppositely-oriented arrays of low affinity recognition sites in oriC guide progressive binding of DnaA during E. coli pre-RC assembly.* Mol Microbiol, 2011. **82**(2): p. 475-88.
4. Katayama, T., et al., *Regulation of the replication cycle: conserved and diverse regulatory systems for DnaA and oriC.* Nat Rev Microbiol, 2010. **8**(3): p. 163-70.
5. Berkmen, M.B. and A.D. Grossman, *Subcellular positioning of the origin region of the Bacillus subtilis chromosome is independent of sequences within oriC, the site of replication initiation, and the replication initiator DnaA.* Mol Microbiol, 2007. **63**(1): p. 150-65.
6. Ozaki, S. and T. Katayama, *DnaA structure, function, and dynamics in the initiation at the chromosomal origin.* Plasmid, 2009. **62**(2): p. 71-82.
7. Mott, M.L. and J.M. Berger, *DNA replication initiation: mechanisms and regulation in bacteria.* Nat Rev Microbiol, 2007. **5**(5): p. 343-54.
8. Moriya, S., et al., *Regulation of initiation of Bacillus subtilis chromosome replication.* Plasmid, 1999. **41**(1): p. 17-29.
9. Ogura, Y., et al., *Autoregulation of the dnaA-dnaN operon and effects of DnaA protein levels on replication initiation in Bacillus subtilis.* J Bacteriol, 2001. **183**(13): p. 3833-41.
10. Soufo, C.D., et al., *Cell-cycle-dependent spatial sequestration of the DnaA replication initiator protein in Bacillus subtilis.* Dev Cell, 2008. **15**(6): p. 935-41.
11. Fukuoka, T., et al., *Purification and characterization of an initiation protein for chromosomal replication, DnaA, in Bacillus subtilis.* J Biochem, 1990. **107**(5): p. 732-9.
12. Messer, W., et al., *Bacterial replication initiator DnaA. Rules for DnaA binding and roles of DnaA in origin unwinding and helicase loading.* Biochimie, 2001. **83**(1): p. 5-12.
13. Krause, M., et al., *Complexes at the replication origin of Bacillus subtilis with homologous and heterologous DnaA protein.* J Mol Biol, 1997. **274**(3): p. 365-80.
14. Moriya, S., et al., *Replication of a Bacillus subtilis oriC plasmid in vitro.* Mol Microbiol, 1994. **12**(3): p. 469-78.
15. Moriya, S., et al., *Regulation of initiation of the chromosomal replication by DnaA-boxes in the origin region of the Bacillus subtilis chromosome.* EMBO J, 1988. **7**(9): p. 2911-7.
16. Graumann, P., *Bacillus : cellular and molecular biology.* 2007, Wymondham, Norfolk: Caister Academic Press. xv, 454 p.
17. Scholefield, G., J.W. Veening, and H. Murray, *DnaA and ORC: more than DNA replication initiators.* Trends Cell Biol, 2011. **21**(3): p. 188-94.
18. Ryan, V.T., et al., *Escherichia coli prereplication complex assembly is regulated by dynamic interplay among Fis, IHF and DnaA.* Mol Microbiol, 2004. **51**(5): p. 1347-59.
19. Nievera, C., et al., *SeqA blocking of DnaA-oriC interactions ensures staged assembly of the E. coli pre-RC.* Mol Cell, 2006. **24**(4): p. 581-92.
20. Miller, D.T., et al., *Bacterial origin recognition complexes direct assembly of higher-order DnaA oligomeric structures.* Proc Natl Acad Sci U S A, 2009. **106**(44): p. 18479-84.
21. Cassler, M.R., J.E. Grimwade, and A.C. Leonard, *Cell cycle-specific changes in nucleoprotein complexes at a chromosomal replication origin.* EMBO J, 1995. **14**(23): p. 5833-41.

22. McGarry, K.C., et al., *Two discriminatory binding sites in the Escherichia coli replication origin are required for DNA strand opening by initiator DnaA-ATP*. Proc Natl Acad Sci U S A, 2004. **101**(9): p. 2811-6.
23. Erzberger, J.P., M.L. Mott, and J.M. Berger, *Structural basis for ATP-dependent DnaA assembly and replication-origin remodeling*. Nat Struct Mol Biol, 2006. **13**(8): p. 676-83.
24. Bramhill, D. and A. Kornberg, *Duplex opening by dnaA protein at novel sequences in initiation of replication at the origin of the E. coli chromosome*. Cell, 1988. **52**(5): p. 743-55.
25. Leonard, A.C. and J.E. Grimwade, *Regulation of DnaA Assembly and Activity: Taking Directions from the Genome*. Annu Rev Microbiol, 2010.
26. Kaguni, J.M., *Replication initiation at the Escherichia coli chromosomal origin*. Curr Opin Chem Biol, 2011.
27. Speck, C. and W. Messer, *Mechanism of origin unwinding: sequential binding of DnaA to double- and single-stranded DNA*. EMBO J, 2001. **20**(6): p. 1469-76.
28. Makowska-Grzyska, M. and J.M. Kaguni, *Primase directs the release of DnaC from DnaB*. Mol Cell, 2010. **37**(1): p. 90-101.
29. Kurokawa, K., et al., *Replication cycle-coordinated change of the adenine nucleotide-bound forms of DnaA protein in Escherichia coli*. EMBO J, 1999. **18**(23): p. 6642-52.
30. Leonard, A.C. and J.E. Grimwade, *Building a bacterial orisome: emergence of new regulatory features for replication origin unwinding*. Mol Microbiol, 2005. **55**(4): p. 978-85.
31. Grimwade, J.E., et al., *Mutational analysis reveals Escherichia coli oriC interacts with both DnaA-ATP and DnaA-ADP during pre-RC assembly*. Mol Microbiol, 2007. **66**(2): p. 428-39.
32. Fujimitsu, K., T. Senriuchi, and T. Katayama, *Specific genomic sequences of E. coli promote replicational initiation by directly reactivating ADP-DnaA*. Genes Dev, 2009. **23**(10): p. 1221-33.
33. Su'etsugu, M., et al., *Protein associations in DnaA-ATP hydrolysis mediated by the Hda-replicase clamp complex*. J Biol Chem, 2005. **280**(8): p. 6528-36.
34. Xu, Q., et al., *A structural basis for the regulatory inactivation of DnaA*. J Mol Biol, 2009. **385**(2): p. 368-80.
35. Messer, W. and C. Weigel, *DnaA initiator--also a transcription factor*. Mol Microbiol, 1997. **24**(1): p. 1-6.
36. Braun, R.E., K. O'Day, and A. Wright, *Autoregulation of the DNA replication gene dnaA in E. coli K-12*. Cell, 1985. **40**(1): p. 159-69.
37. Atlung, T., A. Lobner-Olesen, and F.G. Hansen, *Overproduction of DnaA protein stimulates initiation of chromosome and minichromosome replication in Escherichia coli*. Mol Gen Genet, 1987. **206**(1): p. 51-9.
38. Herrick, J., et al., *The initiation mess?* Mol Microbiol, 1996. **19**(4): p. 659-66.
39. Hansen, F.G., et al., *Titration of DnaA protein by oriC DnaA-boxes increases dnaA gene expression in Escherichia coli*. EMBO J, 1987. **6**(1): p. 255-8.
40. Merrikkh, H. and A.D. Grossman, *Control of the replication initiator DnaA by an anti-cooperativity factor*. Mol Microbiol, 2011. **82**(2): p. 434-46.
41. Kaguni, J.M., *DnaA: controlling the initiation of bacterial DNA replication and more*. Annu Rev Microbiol, 2006. **60**: p. 351-75.
42. Lu, M., et al., *SeqA: a negative modulator of replication initiation in E. coli*. Cell, 1994. **77**(3): p. 413-26.
43. Slater, S., et al., *E. coli SeqA protein binds oriC in two different methyl-modulated reactions appropriate to its roles in DNA replication initiation and origin sequestration*. Cell, 1995. **82**(6): p. 927-36.
44. Okumura, H., et al., *Regulation of chromosomal replication initiation by oriC-proximal DnaA-box clusters in Bacillus subtilis*. Nucleic Acids Res, 2011.
45. Bogan, J.A. and C.E. Helmstetter, *DNA sequestration and transcription in the oriC region of Escherichia coli*. Mol Microbiol, 1997. **26**(5): p. 889-96.

46. Braun, R.E. and A. Wright, *DNA methylation differentially enhances the expression of one of the two E. coli dnaA promoters in vivo and in vitro*. Mol Gen Genet, 1986. **202**(2): p. 246-50.
47. Crooke, E., et al., *Replicatively active complexes of DnaA protein and the Escherichia coli chromosomal origin observed in the electron microscope*. J Mol Biol, 1993. **233**(1): p. 16-24.
48. Sekimizu, K., B.Y. Yung, and A. Kornberg, *The dnaA protein of Escherichia coli. Abundance, improved purification, and membrane binding*. J Biol Chem, 1988. **263**(15): p. 7136-40.
49. Kitagawa, R., et al., *Negative control of replication initiation by a novel chromosomal locus exhibiting exceptional affinity for Escherichia coli DnaA protein*. Genes Dev, 1998. **12**(19): p. 3032-43.
50. Ogawa, T., et al., *The datA locus predominantly contributes to the initiator titration mechanism in the control of replication initiation in Escherichia coli*. Mol Microbiol, 2002. **44**(5): p. 1367-75.
51. Kitagawa, R., et al., *A novel DnaA protein-binding site at 94.7 min on the Escherichia coli chromosome*. Mol Microbiol, 1996. **19**(5): p. 1137-47.
52. Noirot-Gros, M.F., et al., *Functional dissection of YabA, a negative regulator of DNA replication initiation in Bacillus subtilis*. Proc Natl Acad Sci U S A, 2006. **103**(7): p. 2368-73.
53. Murray, H. and J. Errington, *Dynamic control of the DNA replication initiation protein DnaA by Soj/ParA*. Cell, 2008. **135**(1): p. 74-84.
54. Scholefield, G., et al., *Spo0J regulates the oligomeric state of Soj to trigger its switch from an activator to an inhibitor of DNA replication initiation*. Mol Microbiol, 2011. **79**(4): p. 1089-100.
55. Castilla-Llorente, V., et al., *Spo0A, the key transcriptional regulator for entrance into sporulation, is an inhibitor of DNA replication*. EMBO J, 2006. **25**(16): p. 3890-9.
56. Rahn-Lee, L., et al., *The conserved sporulation protein YneE inhibits DNA replication in Bacillus subtilis*. J Bacteriol, 2009. **191**(11): p. 3736-9.
57. Wagner, J.K., K.A. Marquis, and D.Z. Rudner, *SirA enforces diploidy by inhibiting the replication initiator DnaA during spore formation in Bacillus subtilis*. Mol Microbiol, 2009. **73**(5): p. 963-74.
58. Moriya, S., et al., *Effects of oriC relocation on control of replication initiation in Bacillus subtilis*. Microbiology, 2009. **155**(Pt 9): p. 3070-82.
59. Donachie, W.D., *Relationship between cell size and time of initiation of DNA replication*. Nature, 1968. **219**(5158): p. 1077-9.
60. Murakami, S., et al., *Initiation of DNA replication in Bacillus subtilis. III. Analysis of molecular events involved in the initiation using a temperature-sensitive dna mutant*. J Mol Biol, 1976. **108**(4): p. 683-704.
61. Ogasawara, N., et al., *Conservation of genes and their organization in the chromosomal replication origin region of Bacillus subtilis and Escherichia coli*. EMBO J, 1985. **4**(12): p. 3345-50.
62. Ozaki, S., et al., *A common mechanism for the ATP-DnaA-dependent formation of open complexes at the replication origin*. J Biol Chem, 2008. **283**(13): p. 8351-62.
63. Grimwade, J.E., V.T. Ryan, and A.C. Leonard, *IHF redistributes bound initiator protein, DnaA, on supercoiled oriC of Escherichia coli*. Mol Microbiol, 2000. **35**(4): p. 835-44.
64. Kawakami, H., K. Keyamura, and T. Katayama, *Formation of an ATP-DnaA-specific initiation complex requires DnaA Arginine 285, a conserved motif in the AAA+ protein family*. J Biol Chem, 2005. **280**(29): p. 27420-30.
65. Moriya, S., et al., *Cloning of an autonomously replicating sequence (ars) from the Bacillus subtilis chromosome*. Mol Microbiol, 1992. **6**(3): p. 309-15.
66. Ishikawa, S., et al., *Distribution of stable DnaA-binding sites on the Bacillus subtilis genome detected using a modified ChIP-chip method*. DNA Res, 2007. **14**(4): p. 155-68.

67. Kadoya, R., et al., *Two separate DNA sequences within oriC participate in accurate chromosome segregation in Bacillus subtilis*. Mol Microbiol, 2002. **45**(1): p. 73-87.
68. Berkmen, M.B. and A.D. Grossman, *Spatial and temporal organization of the Bacillus subtilis replication cycle*. Mol Microbiol, 2006. **62**(1): p. 57-71.
69. Sutton, M.D. and J.M. Kaguni, *The Escherichia coli dnaA gene: four functional domains*. J Mol Biol, 1997. **274**(4): p. 546-61.
70. Felczak, M.M., L.A. Simmons, and J.M. Kaguni, *An essential tryptophan of Escherichia coli DnaA protein functions in oligomerization at the E. coli replication origin*. J Biol Chem, 2005. **280**(26): p. 24627-33.
71. Sutton, M.D., et al., *Escherichia coli DnaA protein. The N-terminal domain and loading of DnaB helicase at the E. coli chromosomal origin*. J Biol Chem, 1998. **273**(51): p. 34255-62.
72. Abe, Y., et al., *Structure and function of DnaA N-terminal domains: specific sites and mechanisms in inter-DnaA interaction and in DnaB helicase loading on oriC*. J Biol Chem, 2007. **282**(24): p. 17816-27.
73. Ishida, T., et al., *DiaA, a novel DnaA-binding protein, ensures the timely initiation of Escherichia coli chromosome replication*. J Biol Chem, 2004. **279**(44): p. 45546-55.
74. Felczak, M.M. and J.M. Kaguni, *The box VII motif of Escherichia coli DnaA protein is required for DnaA oligomerization at the E. coli replication origin*. J Biol Chem, 2004. **279**(49): p. 51156-62.
75. Erzberger, J.P., M.M. Pirruccello, and J.M. Berger, *The structure of bacterial DnaA: implications for general mechanisms underlying DNA replication initiation*. EMBO J, 2002. **21**(18): p. 4763-73.
76. Madiraju, M.V., et al., *The intrinsic ATPase activity of Mycobacterium tuberculosis DnaA promotes rapid oligomerization of DnaA on oriC*. Mol Microbiol, 2006. **59**(6): p. 1876-90.
77. Kumar, S., A. Farhana, and S.E. Hasnain, *In-vitro helix opening of M. tuberculosis oriC by DnaA occurs at precise location and is inhibited by IciA like protein*. PLoS One, 2009. **4**(1): p. e4139.
78. Nyborg, M., et al., *Two types of cold sensitivity associated with the A184-->V change in the DnaA protein*. Mol Microbiol, 2000. **35**(5): p. 1202-10.
79. Simmons, L.A. and J.M. Kaguni, *The DnaAcos allele of Escherichia coli: hyperactive initiation is caused by substitution of A184V and Y271H, resulting in defective ATP binding and aberrant DNA replication control*. Mol Microbiol, 2003. **47**(3): p. 755-65.
80. Felczak, M.M. and J.M. Kaguni, *DnaAcos hyperinitiates by circumventing regulatory pathways that control the frequency of initiation in Escherichia coli*. Mol Microbiol, 2009. **72**(6): p. 1348-63.
81. Kellenberger-Gujer, G., A.J. Podhajska, and L. Caro, *A cold sensitive dnaA mutant of E. coli which overinitiates chromosome replication at low temperature*. Mol Gen Genet, 1978. **162**(1): p. 9-16.
82. Carr, K.M. and J.M. Kaguni, *The A184V missense mutation of the dnaA5 and dnaA46 alleles confers a defect in ATP binding and thermolability in initiation of Escherichia coli DNA replication*. Mol Microbiol, 1996. **20**(6): p. 1307-18.
83. Imai, Y., et al., *Subcellular localization of DnaA-initiation proteins of Bacillus subtilis: evidence that chromosome replication begins at either edge of the nucleoids*. Mol Microbiol, 2000. **36**(5): p. 1037-48.
84. Youngman, P., J.B. Perkins, and R. Losick, *Construction of a cloning site near one end of Tn917 into which foreign DNA may be inserted without affecting transposition in Bacillus subtilis or expression of the transposon-borne erm gene*. Plasmid, 1984. **12**(1): p. 1-9.
85. Dubnau, D. and R. Davidoff-Abelson, *Fate of transforming DNA following uptake by competent Bacillus subtilis. I. Formation and properties of the donor-recipient complex*. J Mol Biol, 1971. **56**(2): p. 209-21.
86. Wilson, G.A. and K.F. Bott, *Nutritional factors influencing the development of competence in the Bacillus subtilis transformation system*. J Bacteriol, 1968. **95**(4): p. 1439-49.

87. Harwood, C., S.M. Cutting, and R. Chambert, *Molecular biological methods for bacillus*. 1990: Wiley. 1 v.
88. Birnboim, H.C. and J. Doly, *A rapid alkaline extraction procedure for screening recombinant plasmid DNA*. *Nucleic Acids Res*, 1979. **7**(6): p. 1513-23.
89. Feucht, A. and P.J. Lewis, *Improved plasmid vectors for the production of multiple fluorescent protein fusions in Bacillus subtilis*. *Gene*, 2001. **264**(2): p. 289-97.
90. Lewis, P.J. and A.L. Marston, *GFP vectors for controlled expression and dual labelling of protein fusions in Bacillus subtilis*. *Gene*, 1999. **227**(1): p. 101-10.
91. Laemmli, U.K., *Cleavage of structural proteins during the assembly of the head of bacteriophage T4*. *Nature*, 1970. **227**(5259): p. 680-5.
92. Nguyen, B., F.A. Tanius, and W.D. Wilson, *Biosensor-surface plasmon resonance: quantitative analysis of small molecule-nucleic acid interactions*. *Methods*, 2007. **42**(2): p. 150-61.
93. Tsien, R.Y., *The green fluorescent protein*. *Annu Rev Biochem*, 1998. **67**: p. 509-44.
94. Sakamoto, K., et al., *Effect of environmental factors on the dominant lethality caused by expression of a mutated DnaA protein with decreased intrinsic ATPase activity*. *FEMS Microbiol Lett*, 1998. **159**(1): p. 93-7.
95. Mizushima, T., et al., *Site-directed mutational analysis for the ATP binding of DnaA protein. Functions of two conserved amino acids (Lys-178 and Asp-235) located in the ATP-binding domain of DnaA protein in vitro and in vivo*. *J Biol Chem*, 1998. **273**(33): p. 20847-51.
96. Nishida, S., et al., *A nucleotide switch in the Escherichia coli DnaA protein initiates chromosomal replication: evidence from a mutant DnaA protein defective in regulatory ATP hydrolysis in vitro and in vivo*. *J Biol Chem*, 2002. **277**(17): p. 14986-95.
97. Blaesing, F., et al., *Analysis of the DNA-binding domain of Escherichia coli DnaA protein*. *Mol Microbiol*, 2000. **36**(3): p. 557-69.
98. Mizushima, T., et al., *Negative control of DNA replication by hydrolysis of ATP bound to DnaA protein, the initiator of chromosomal DNA replication in Escherichia coli*. *EMBO J*, 1997. **16**(12): p. 3724-30.
99. Sekimizu, K., D. Bramhill, and A. Kornberg, *Sequential early stages in the in vitro initiation of replication at the origin of the Escherichia coli chromosome*. *J Biol Chem*, 1988. **263**(15): p. 7124-30.
100. Fernandez-Fernandez, C., D. Gonzalez, and J. Collier, *Regulation of the activity of the dual-function DnaA protein in Caulobacter crescentus*. *PLoS One*, 2011. **6**(10): p. e26028.
101. Gregory, J.A., E.C. Becker, and K. Pogliano, *Bacillus subtilis MinC destabilizes FtsZ-rings at new cell poles and contributes to the timing of cell division*. *Genes Dev*, 2008. **22**(24): p. 3475-88.
102. Lee, Y.S. and D.S. Hwang, *Occlusion of RNA polymerase by oligomerization of DnaA protein over the dnaA promoter of Escherichia coli*. *J Biol Chem*, 1997. **272**(1): p. 83-8.

# ACKNOWLEDGEMENTS

---

## 6. Acknowledgements

In the first place, I want to thank my supervisor Prof. Dr. Peter L. Graumann for his encouragement, support and his cordiality during this work. Furthermore, I am very grateful for the collaborations with Dr. Friedel Drepper (Department of Biochemistry, University of Freiburg) and Prof. Dr. Gudula Schmidt (Institute of Experimental and Clinical Pharmacology and Toxicology, University of Freiburg) who introduced me into surface plasmon resonance and the work with radio-isotopes, respectively. In particular, I want to thank Dr. Joël Defeu Soufo, Dr. Tobias Knust and Dr. Esther Garcia Tirado for intensive discussions and support, both in technical and scientific issues. Moreover, I thank Julia Rugor who was involved with incredible verve in some experiments during her Erasmus stage and Katharina Herr who helped a lot with protein purification during the last six months. Especially, I want to thank Astrid Steindorf who always did more than she had to! Besides, I thank all my colleagues for a working atmosphere that allowed the accomplishment of this work. In particular, I thank Tommy and Wlad for sharing the bench, the stress, the chaos and the fun. I thank Luise, Katrin and Steffi, for their straightness, humor and comprehension. And thanks to all who provided plates, gels and chemicals in emergency situations.

Ich möchte mich auch bei meinen Freunden bedanken, die mich nicht vergessen haben lassen, dass es ein Leben neben der Arbeit gibt. Danke Sonja, Johann, Babou, Alex, Robb, Bina und die TriKo-connection Kirk, Kirsten, Dimi, Ramon, Sarah, Jan und Katinka für die unglaublich vielen fantastischen und lustigen Abende.

A Esther, quiero darte las gracias por tu afectuosidad, tu sentido de humor, tu pasión en todo lo que haces y tu creatividad en apoyarme durante este tiempo. Tu también, has cambiado todo.

Ganz besonders danke ich meinen Eltern! Ihr seid die wichtigsten Menschen in meinem Leben, ihr seid immer für mich da, habt meine Krisen und Frustrationen ertragen, mich aber dennoch fortwährend unterstützt und an mich geglaubt! Danke für Eure Kraft, Euer Verständnis, Euer Vertrauen und Eure Liebe!